Copyright

by

Edward Kelly Merritt, Jr.

2009

The Dissertation Committee for Edward Kelly Merritt, Jr. Certifies that this is the approved version of the following dissertation:

REPAIR OF SKELETAL MUSCLE TRANSECTION INJURY WITH TISSUE LOSS

Committee:

Roger Farrar, Supervisor

Martin Adamo

John Ivy

Laura Suggs

Thomas Walters

REPAIR OF SKELETAL MUSCLE TRANSECTION INJURY WITH TISSUE LOSS

by

Edward Kelly Merritt, Jr. B.S., M.A.

Dissertation

Presented to the Faculty of the Graduate School of

The University of Texas at Austin

in Partial Fulfillment

of the Requirements

for the Degree of

Doctor of Philosophy

The University of Texas at Austin

August, 2009

Dedication

Numerous people throughout the years have had a profound influence on my life. All of my family and friends obviously deserve to be recognized for everything that they have done for me, but I would like to dedicate this dissertation to all of my past teachers. I have been lucky to have received an incredible education from incredible educators starting with my kindergarten teacher Ms. Dinjar to my doctoral advisor Dr. Roger Farrar and everyone in between. Without the guidance, support, and advice given to me at every step along the way, this dissertation would not have been possible. My teachers' devotion to education is truly appreciated. I hope to have the same influence on my future students.

Acknowledgements

I am grateful to Dr. Roger Farrar for overseeing my education, research, and employment at The University. Dr. Tom Walters and others at the U.S. Army Institute of Surgical Research have been instrumental in helping me to develop this research and in helping to find outside financial support for myself as well as my studies. Special thanks to my committee members; Dr. Laura Suggs, Dr. Martin Adamo, and Dr. John Ivy for guiding me in the right direction. Thanks also to David Hammers, Matt Tierney, Rohit Gokhale, Long Le, Rosemary French, and Apurva Sarathy, and a host of great undergraduate lab assistants for the countless hours of technical assistance. Finally, thank you to Patty Coffman, Tan Thai, and the rest of the Department of Kinesiology & Health Education for helping me with anything and everything during my time at The University.

REPAIR OF SKELETAL MUSCLE TRANSECTION INJURY WITH TISSUE LOSS

Edward Kelly Merritt, Jr. Ph.D.

The University of Texas at Austin, 2009

Supervisor: Roger Farrar

A traumatic skeletal muscle injury that involves the loss of a substantial portion of tissue will not regenerate on its own. Little is understood about the ability of the muscle to recover function after such a defect injury, and few research models exist to further elucidate the repair and regeneration processes of defected skeletal muscle. In the current research, a model of muscle injury was developed in the lateral gastrocnemius (LGAS) of the rat. In this model, the muscle gradually remodels but functional recovery does not occur over 42 days. Repair of the defect with muscle-derived extracellular matrix (ECM), improves the morphology of the LGAS. Blood vessels and myofibers grow into the ECM implant *in vivo*, but functional recovery does not occur. Addition of bone marrow-derived mesenchymal stem cells (MSCs) to the implanted ECM in the LGAS increases the number of blood vessels and regenerating myofibers within the ECM. Following 42 days of recovery, the cell-seeded ECM implanted LGAS produces significantly higher isometric force than the non-repaired and non-cell seeded ECM muscles. These results suggest that the LGAS muscle defect is a suitable model for the study of traumatic skeletal muscle injury with tissue loss. Additionally, MSCs seeded on an implanted ECM lead to functional restoration of the defected LGAS.

Table of Contents

List of Tables

List of Figures

Chapter I: General Introduction

Injuries to the soft tissue of the extremities comprise the largest number of wounds received by United States military personnel in war-time activities [1]. Operations performed on the extremities make up the greatest percentage of surgical procedures due to battlefield injuries [2, 3]. Some injuries are so traumatic that the only possible treatment for the victim is to amputate the entire limb [3]. However, even when the limb can be saved, the initial damage done to the skeletal muscle and the further debridement of muscle and surrounding tissue will leave the soldier with a physical handicap despite the fact that the limb is still predominantly intact. Ultimately, the functionality of the limb will depend on the remaining skeletal muscle. While skeletal muscle is capable of regeneration to a limited capacity, it is not able to fully repair itself after the loss of a significant amount of tissue. The current standard of care for these injuries attempts to repair the damaged area by autologous tissue transfer (muscle flaps) using donor tissue from other areas of the victim's body. Recent reports describe functional free muscle transplantation in the forearm [4] and elbow [5], but these procedures are associated with significant donor site morbidity and are not yet applicable to large muscle defects. Individuals who have lost significant portions of muscle can expect to live the rest of their lives with a physical handicap. As such, addressing the need for a suitable treatment to better return function to limbs that have lost large portions of skeletal muscle is important.

The development of a muscle defect model in a load bearing muscle is important to understanding the potential for regenerating large segments of muscle and restoring

function. Currently, several skeletal muscle defect models have been established [6-9]. These models, however, are limited in their application to regeneration of large segments of muscle necessary for restoration of normal function.

OBJECTIVES

The overall objective of this study was to develop a defect model of skeletal muscle injury, repair it surgically, and characterize the regenerated muscle functionally and morphologically. To accomplish this, the specific aims for the study were as follows:

1. Develop a skeletal muscle defect injury model that results in a permanent deficit in function and also allows for implantation of tissue engineered constructs and long term functional analysis of the constructs.
2. Functionally characterize the defect injury model in a load bearing muscle that is critical for mobility such as the lateral gastrocnemius (LGAS) muscle.
3. Develop a biocompatible, extracellular matrix (ECM) implant that can be used to repair missing tissue in injured skeletal muscle, which will transmit mechanical force between the remnants of damaged muscle and also serve as a platform for muscle progenitor cells to proliferate and differentiate into functional muscle.
4. Both functionally and morphologically, assess muscle regeneration in the muscle repaired with an ECM.
5. Functionally and histologically characterize the skeletal muscle defect repaired with an ECM seeded with bone marrow-derived mesenchymal stem cells.

HYPOTHESES

1. Removal of a large portion of the LGAS will prevent regenerating myofibers from spanning the gap and the area will be left permanently devoid of tissue. The remaining segments of the muscle will remodel, but permanent loss of function will be related to the loss of muscle mass.
2. The ECM implant groups will maintain structure and function better than non-repaired defect groups.
3. Complete muscle regeneration in the defect area will be limited by fibrosis which will limit vascular supply to the regenerating area.
4. Bone marrow derived mesenchymal stem cell-seeded ECM groups will regenerate muscular structure and function better than ECM repair alone due to the regenerative stimulus provided by mesenchymal stem cells.

SIGNIFICANCE

The prevalence of injuries to skeletal muscle that result in loss of muscle tissue and concomitant loss of function demonstrates the importance for research that identifies useful surgical and therapeutic mechanisms to improve muscle regeneration. Current treatment methods do little to combat the permanent loss of muscle function which results from these injuries.

Research is needed to better understand the regenerative process after loss of a large volume of muscular tissue. Limited data exists on muscle repair mechanisms utilizing implantable, acellular, skeletal muscle ECM with stem cells in order to regenerate myofibers and restore function following injury. The available literature on repair of lost skeletal muscle tissue is limited to repair of abdominal wall defects with

ECM and unipotent progenitor cells. Studies that directly measure the function of muscles with cell-seeded ECM implants are virtually nonexistent. The findings from this study will help determine the effectiveness of muscle repair with ECM and multipotent cells with regard to restoration of function and morphology. Ideally the findings will identify promising routes for research that will ultimately lead to clinical applications. The techniques established should serve as a path forward for the restoration of function for patients with traumatic muscle injuries. While a person who is injured today might have a permanent disability, in several years a person with the same injury might have no noticeable impairment due in part to findings established by this study.

DELIMITATIONS AND LIMITATIONS

This study was performed on 5-9 month old male Sprague-Dawley and Lewis rats. The portion of muscle removed from the LGAS accounted for nearly 20% of the total mass in this model, but this creates only a one centimeter wide defect. Regeneration of skeletal muscle after the removal of 20% of the muscle mass in the muscle of a human might be limited by diffusion distances, extent of neural regeneration, and degree of fibrosis in a larger muscle mass. Therefore, the animal subject pool limits applicability to human beings, but can be used to theorize the process of skeletal muscle regeneration.

During the recovery period, animals were confined to their home cages, but the activity levels of the animals was not controlled or monitored. Activation and mobilization of skeletal muscle following injury can have dramatic effects on the muscle's ability to regenerate; however, there is no reason to believe that animals in any group of this study had significantly different activity levels. Skeletal muscle function

was only measured during isometric contractions. Generally isometric function is a good measure of overall function, but care should be taken when interpreting the results in regards to dynamic muscle function. Lastly, the injected bone marrow derived cells were not labeled or tracked, so their exact contribution to regeneration cannot be determined.

Chapter II: Review of the Literature

SKELETAL MUSCLE INJURY

The plasticity of skeletal muscle is well known. It has a remarkable capacity to regenerate in response to damaging stimuli. A skeletal muscle can be completely removed, minced into small bits, and placed back into its compartment, and it will regenerate enough to contract and produce force [10]. But even in less severe injuries, the repair process takes time and is not always 100% efficient. The ability of a muscle to recover following damage depends on the type and severity of the injury, but once the damage has occurred, the regeneration process proceeds in the same manner no matter what the type of injury. The healing process can be divided into three main phases which exist in an overlapping continuum and begin immediately after an injury has occurred: the destruction/ inflammatory phase; the repair phase; and the remodeling phase.

The Destruction/Inflammatory Phase

Immediately following an injury to skeletal myofibers, such as a laceration/transection injury, myofibers are sheared and torn apart allowing the contents of the cell to interact with the extracellular environment. Single myofibers are often many centimeters long and following transection, run the risk of being necrotized completely. The death of the full myofiber is normally prevented by a structure known as the contraction band. Cytoskeletal materials flow to the edge of the injury and form a barrier to seal off the cell from the outside environment [11]. Due to their elastic nature, the torn fibers will retract and a gap will form between the two ends.

Due to skeletal muscle's high vascularity, the capillaries that surround each fiber will also be damaged. Damage to the vessels will allow for blood to leak out creating a hematoma in the recently formed gap. The hematoma is comprised of blood components including clot forming proteins, which will form the beginnings of the connective tissue scar, as well as various types of white blood cells. The white blood cells will digest the necrotic tissue and activate other cell types to start the regeneration process. Neutrophils are typically the first inflammatory cell to the site [12]. These cells begin the process of digesting the necrotic myofibers and cellular debris by phagocytosis. They also release cytokines which further amplify the inflammation process by signaling other cells. These cytokines also play a role in repair by stimulating muscle satellite cells, which are a group of normally quiescent muscle progenitor cells found beneath the basal lamina [13] The satellite cells proliferate and move to the damaged area [14]. Monocytes attracted to the injured area are converted into macrophages. The macrophages are the dominant cell type present during the later phases of the inflammatory reaction and continue the process of proteolysis and phagocytosis of damaged tissue [12]. They are selective in the breakdown of tissue and the basement membrane is generally left intact [15]. Satellite cells also receive signaling factors from the macrophages that will insure their continued survival [16]. More signals are triggered by the disruption of the integrity of the extracellular matrix (ECM). Several growth factors are known to reside in inactivated forms on the ECM, but upon mechanical disruption of the ECM, these factors are activated and act on surrounding cells to enhance the repair response [17].

Repair Phase

While damaged tissue is being removed, the repair process has already been started by the growth factors and signals coming from the macrophages, ECM, and activated satellite cells. Nerves, blood vessels, and muscle begin to infiltrate the wound area [17]. The process is characterized by the activity of satellite cells. Upon activation, the satellite cells will migrate to the injured area, become myoblasts and proliferate, differentiate, and fuse to existing myofibers or with each other to form myotubes to replace damaged fibers [15, 18]. Specific markers are expressed by quiescent satellite cells (Pax 7, cMET-R). Once they become activated, they differentially express other markers (MyoD, myf5, myogenin, MRF4, etc) such that the sequence leading to addition of nuclei to existing fibers or the formation of new fibers altogether can be tracked throughout the repair process [19].

While satellite cells are the predominant cell used for repair of skeletal muscle following injury, they are not the only group of progenitor cells capable of contributing to regeneration. Other groups of muscle derived cells known as muscle derived stem cells, as well as cells from other tissues like bone marrow can contribute nuclei to the injured area [20, 21]. The cells can arrive from remote locations and contribute to the healing process by undergoing myogenic differentiation or by releasing paracrine growth factors that act on the surrounding cells [22, 23].

Another aspect of the repair phase is the formation of a connective tissue scar. The scar acts to bridge the gap between the ends of the myofibers. This bridge allows for the transduction of force along the muscle length and also acts as a conduit for regenerating myofibers [17]. The scar is initially composed of fibrin and fibronectin from the blood, and as time progresses the area is infiltrated by fibroblasts which, under the

control of the growth factor TGF-β, help produce the ECM for the rebuilding phase [11, 24, 25]. While the connective tissue scar initially serves the purpose of holding the ends of the myofibers together and preventing further damage from occurring, the scar formed in more severe injury cases can actually become a barrier to complete regeneration of the muscle by blocking the fibers from bridging the gap and connecting to regenerating fibers on the other side [26, 27]. The scar ultimately forms another myotendinous-type junction to bridge the cut ends of the muscle, effectively creating two muscles in series [28, 29].

Critical to the survival of the regenerating area of muscle is the reintroduction of a sufficient blood and nerve supply. Since skeletal muscle is highly vascularized, the cut ends of blood vessels are in close proximity to the regenerating area. After only several days, new capillaries have sprouted into the damaged area [30]. While regeneration of the myofibers will proceed for a period of time without innervation, reinnervation of the fibers (especially those distal portions of the transected fibers) is necessary for them to survive; otherwise they will atrophy and ultimately die [31]. If the transected ends of the fibers remain in close proximity, nerve outgrowths from nearby surviving neuromuscular junctions (NMJ) will normally reinnervate the fibers after only fifteen days [32, 33].

Remodeling Phase

The remodeling phase is essentially a continuation of the repair phase. This process is characterized by the appearance of centrally nucleated myofibers created when satellite cells convert to myotubes and fuse with each other or existing myofibers. The fibers grow and begin to penetrate the scar and form adhesions with the ECM [11, 28]. Approximately ten days after injury, the connective tissue scar is stronger than the surrounding myofibers and is not likely to be pulled apart by muscle contractions [34].

As the myofibers grow and penetrate into the scar they form adhesions with the connective tissue, and the scar gradually shrinks [28, 34]. Depending on the size of the gap, the fibers from each end ultimately reach each other, interlace with the ECM and possibly re-fuse [29, 35]. The myofibers continue to mature, and the expression of proteins in the reorganizing muscles, such as myosin heavy chain (MHC), transition from developmental isoforms to mature isoforms until they are phenotypically similar to normal myofibers [36].

The regeneration process is sufficient for complete recovery much of the time and no permanent loss of function will result. However, traumatic muscle injuries caused by extraordinary events such as car accidents, gun shots, and explosive devices often require more than the body is capable of by itself. The remainder of this review will focus on muscle injuries unlikely to fully heal on their own.

TRANSECTION INJURY

Skeletal muscle transection injuries that also involve loss of significant portions of muscle tissue are often irreparable. But until the last several years, most of the research regarding traumatic muscle injury did not involve any actual loss of tissue. Most studies focused on severe injuries that left the muscle mass predominantly intact such as contusion and ischemia/ reperfusion injuries. Most of the research that involved myofiber transection used various types of laceration models where the tissue was severely damaged, but the full mass of the muscle was still present. The laceration model research, however, does prove to be a good starting point for the more serious injuries that include tissue loss.

The functional outcome of a muscle laceration depends on where the muscle is located, where it is lacerated, the depth and length of the laceration, as well as whether or not the lacerated muscle has synergists. Comparison between functional studies can be difficult because no single muscle laceration model is used by all researchers. Some researchers use a partial laceration model, while some use a full laceration model and cut the muscle into two separate pieces. A complete transection of a muscle will obviously lead to loss of normal function, but in many cases both parts of the muscle will survive and even contract with nervous input, although if they are not connected, the ends will simply contract and pull away from each other with no external work done [37]. The connective tissue scar might bridge the gap between transected segments, but full functional recovery is nearly impossible even if the muscle has been repaired by suturing the transected ends together [38].

Repair is critical to functional recovery in laceration injuries of significant depth and length, even if the muscle has not been fully transected. A skeletal muscle is normally under passive tension even at rest, and it is this tension that will cause the ends of myofibers to retract when there is a break in the continuity due to a laceration injury. The larger the gap between the two ends, the larger the subsequent scar, and the less functional recovery [35, 39]. To decrease the size of the gap and connective tissue scar, the ends of the muscle can be sutured together [40]. Significant improvements in muscle function occur if the ends can be brought together with suturing techniques soon after injury [37, 38, 41]. Even though repair will improve the recovery of transected skeletal muscle, severely damaged muscle does not normally regain full functionality. To address this problem, other treatments have been developed which aim to increase the regrowth

of myofibers through the connective tissue scar by decreasing the size of the scar and inducing fibers to grow into the area.

Much of the focus to improve muscle regeneration following transection has been to decrease the connective tissue scar formation and fibrosis that occurs. Early after laceration injury, the formation of the connective tissue scar is important to help prevent the injury from recurring and creating more damage [17]. However, with the most severe laceration injuries, the scar formation becomes excessive and creates a barrier that impedes regenerating myofibers and decreases functional improvements [27]. Formation of the connective tissue scar and excessive fibrosis is closely associated with an increase in TGF-β signaling, and controlling this growth factor can play a part in modulating the amount of fibrosis that occurs after injury [25]. Multiple studies have been performed using compounds capable of inhibiting or upregulating TGF-β. Inhibition of TGF-β by compounds such as relaxin, suramin, and decorin, can, depending on the time of injection, significantly decrease the amount of fibrosis seen in regenerating muscles. With less fibrosis, functional improvement is observed in the regenerating muscles as well [42-45]. Upregulation of TGF-β has the opposite effect. It increases fibrosis and delays functional recovery [36].

Another method to promote the growth of myofibers across the lacerated area and prevent the scar tissue from impeding the regeneration process is to help the myofibers regrow with factors that promote their regeneration. A multitude of growth factors act on skeletal muscle as mitogens and can be used in a therapeutic manner to enhance healing following injury. Normally growth factors are released by inflammatory cells, satellite cells, and other nearby cells. Basic fibroblast growth factor (bFGF), insulin-like growth

factor-1 (IGF-1), and nerve growth factor (NGF) are some of the signals that can improve muscle healing and function after strain injuries [46]. When injected directly into the laceration site in mice, each is individually capable of improving functional measures significantly [22, 47]. The mechanism by which some growth factors, such as IGF-1 act, is through the stimulation of satellite cell proliferation and differentiation [48]. If the growth factors can help to stimulate more growth from nearby satellite cells, the lacerated muscle stands a better chance of healing completely. The potential therapeutic effect of being able to turn on mitogenic signals and activate muscle progenitor cells has great implications in healing skeletal muscle injuries.

LACERATION AND TISSUE LOSS

A unique challenge arises when the skeletal muscle is injured such that muscle tissue is actually lost from the injured area. This type of injury is similar to the laceration injury, because the myofibers are transected. But with an injury that creates a defect in the muscle, suturing the ends back together and promoting regeneration is not always possible. A defect that creates a gap of significant size will be too large for skeletal myofibers or even scar tissue to bridge across and repair [39]. Without the ability to regrow across the defect and reconnect the transected fibers, the muscle will not function properly. The surgical repair of a skeletal muscle defect is dependent on the ability of an implant to bridge the gap between the transected muscle segments and allow transmission of force between the two ends, as it is necessary for the proper orientation of regenerating myofibers and subsequent return of function [10]. The tension developed in the regenerating muscle also stimulates autocrine/paracrine release of growth factors that will

further enhance regeneration [49]. Ideally, the implant should also serve as a scaffold which will allow the incorporation of blood vessels and regenerating muscle, connective, and nervous tissue.

DEFECT REPAIR

Surgeons and tissue engineers have long used various materials both natural and synthetic to patch injuries with sizeable defects when the body's natural mechanisms are unable to repair them. Synthetic materials, both permanent and absorbable, have been in clinical use for decades. Clinically available materials such as Dacron, Silastic, Marlex, Vicryl and others are often used to repair large muscular defects of the abdominal wall, but the success of these grafts varies due to issues with biocompatibility [50]. The grafts are considered successful when they contain the bowels and look aesthetically normal, but most do not allow for the full incorporation of the original tissue that they replace. Natural materials for repair are theoretically better for biocompatibility and host cell incorporation, but as with all implants, the issue of tissue rejection due to a hyper-immune response is always a possibility. Natural grafts such as skin grafts have been used to repair wounds for centuries, and recent evidence suggests that a variety of tissue types including skeletal muscle could benefit from similar types of surgeries as well.

One natural material that could be used to create the proper environment for the regeneration of a large portion of tissue is ECM. The ECM is the structural framework that supports tissues in the body and also has important roles in growth and wound healing. Evidence that the ECM is important in skeletal muscle formation has been determined by several different methods. If ECM synthesis is blocked, cultured skeletal

muscle cells will not differentiate [51], but will differentiate normally after the addition of exogenous ECM. Myogenic cells plated on ECM- coated culture dishes proliferate and differentiate more readily than those same cells cultured under normal conditions [52]. Furthermore, addition of an ECM coating to tissue engineered scaffolds, such as poly L-lactic acid fibers, increases the attachment of myoblasts to the scaffold [53]. An important role also exists for the ECM in muscle regeneration. During the regeneration process, the ECM degrades and remodels. The degradation process releases molecules that recruit progenitor cells to the area and also increase the proliferation of these cells [54] [55]. Evidence also exists that these degradation products possess antimicrobial properties and can therefore help to prevent wound infection during regeneration [56].

To obtain a 3-dimensional ECM suitable for implant, removal of all cellular components from the tissue is necessary so that only the ECM in its natural shape remains. The ECM of decellularized tissue can be advantageous for a number of reasons. The implanted ECM will have physical properties similar to those seen by cells in vivo, and the ECM will naturally direct cells to align in the proper orientation. This is important for cells such as muscle progenitor cells activated during the repair process, because they develop best on substances that are most similar to muscle tissue [57]. Skeletal myofibers are only useful functionally if they are aligned correctly and the ECM's orientation should be conducive to that alignment. A properly derived ECM scaffold is also non-immunogenic. When implanted, the ECM will not elicit an immune response that would otherwise lead to its rejection because the decellularization process also removes immune reactive antigens on the cells. [58]. *In vitro,* ECM constructs are capable of supporting the growth of myofibers [59]. Borschel et al. were even able to

produce skeletal muscle capable of contraction by seeding myoblasts on a decellularized ECM *in vitro*.

Decellularized ECM constructs have been successfully used as a patch to repair defects in a number of tissues other than skeletal muscle including tendons and cardiac muscle. Implanted ECM scaffolds are effective at repairing tendon injuries of the rotator cuff and Achilles tendon [60, 61]. The ECM scaffold is not only effective at bridging the gaps in the tendon, but it also allows incorporation of cells from the native tissue. Similar results have been observed in cardiac muscle with ECM repair. A myocardial ventricular wall defect patched with ECM incorporated more myocardial tissue into the defected area than a synthetic expanded polytetrafluoroethylene patch used clinically [62] Better functional improvement is observed in ventricular wall defects repaired with ECM when compared to another clinically available synthetic material known as DACRON [63].

With the promising results in myocardial tissue, decellularized ECM has recently been used as a patch to repair skeletal muscle defects. A 3 x 3 cm abdominal wall defect was created and a piece of decellularized skeletal muscle ECM was sutured into its place [7]. The ECM maintained the structural integrity of the defect area and some evidence of vascularization and new collagen growth was observed, but ingrowth of myofibers after ninety days was not evident. A similar defect model was created in the rabbit vastus lateralis [8]. An acellular collagen scaffold was surgically fitted to repair the 1 x 1 cm defect and the muscle was evaluated histologically over the course of 24 weeks. The macroscopic morphology of the vastus lateralis was well maintained in the repaired defect group compared to the untreated group. Some ingrowth of myofibers into the

middle of the defect was seen, but the fibers were unable to fully regrow to fill the entire defect area. Functional analysis was not performed.

The results from the above studies prove that the repair of a muscle defect with decellularized ECM alone is preferred to nothing, but the ability to regenerate new myofibers into the area is very limited. While it is known that skeletal muscle capable of contraction can be grown on decellularized ECM *in vitro*, it appears that this only happens to a limited extent *in vivo* when ECM is implanted into a defect [58]. A method to improve the regeneration of an ECM-repaired defect is to seed the ECM with cells capable of enhancing the regeneration process and growing to replace the missing tissue. Stem cells and other muscle progenitor cells are obvious candidates.

CELL THERAPY

The potential for cell-based therapies to aid in the regeneration of muscle is tremendous. Early research has shown the ability of myoblasts to partially restore the dystrophin protein absent from skeletal muscles of dystrophic mice and even humans [64, 65]. Injection of myoblasts into muscles prior to transplant improves the functional capacity and morphology of the muscles and enhances regeneration compared to non-seeded control transplant muscles [66, 67]. Satellite cells and muscle-derived stem cells, which are distinct from satellite cells, are also capable of aiding in the regeneration process when given exogenously to compromised skeletal muscle [21, 68-70]. Cell-seeded ECM constructs used to repair defects in skeletal muscle are a very recent research endeavor, however, and only a handful of studies have been undertaken in the area. The most researched model is a defect in the skeletal muscle of the abdominal wall.

This model mimics congenital abdominal wall defects that occur in infants during prenatal development. Several groups have attempted to reconstruct the abdominal wall muscle by using acellularized ECM seeded with autologous myoblasts [9, 71-73]. Implanted acellularized ECM alone showed signs of contracture and was replaced with fibrous scar tissue after only one month [71, 73]. However, with the addition of the cultured myoblasts into the ECM, less contracture occurred and vessel ingrowth was detected [73]. Myoblasts were still present in the ECM after one month in a study by Conconi et al., but after ninety days the number of surviving myoblasts was less than at thirty days [71]. Evidence for the long term survival of myoblasts in the ECM implant has been observed though. Male, XY-karyotyped satellite cell-derived myoblasts were seeded on an ECM implanted into female rats and the male myoblasts were still present nine months post-defect injury [72]. Increased myofiber regeneration occurs in the defect area when surrounding tissue is damaged with Marcaine to stimulate regeneration [9]. The damage to the muscle bordering the implant is hypothesized to stimulate the proliferation, differentiation, and migration of satellite into the implant.

In addition to cells already committed to the myogenic lineage and found within the muscle, other cell types could theoretically be used to enhance muscle regeneration in a defect area. Due to their omnipotency, embryonic stem cells (ESCs) are an obvious candidate for many cell-based therapies, including those involving muscle. When implanted on a polyglycolic acid patch, green fluorescent protein (GFP) labeled ESCs improved functional parameters of the infracted left ventricle [74]. GFP- positive cells were also seen in the defect area indicating that the stem cells might have been incorporated into the regenerating tissue. Limitations exist with ESCs, however. They

are difficult to obtain and ethical issues prevent many researchers from using these cells. Other cells with myogenic potential are found within the body though. One group of cells with myogenic potential is found in the bone marrow.

Interestingly, bone marrow-derived cells partake in muscle regeneration naturally. In the MDX mouse model of muscular dystrophy, desmin and GFP-positive myofibers incorporated into skeletal muscle in mice that received bone marrow transplants, and GFP positive fibers were found occupying the satellite cell niche as well [23]. LaBarge and Blau further elucidated the mechanism and showed that in response to injury, bone marrow cells progressed to functioning muscle satellite cells prior to becoming differentiated myofibers [20]. Using parabiotically joined mice, Palermo et al. has shown that bone marrow cells can even incorporate into muscle in response to normal physiologic stressors such as exercise [75].

Bone marrow contains a population of cells known as mesenchymal stem cells (MSCs) that are multipotent. MSCs could be advantageous compared to ESCs, because no ethical issues exist with obtaining them and they are relatively easy to culture and expand *in vitro.* MSCs adhere to culture plates or flasks and will proliferate for multiple population doublings, which gives them great clinical potential [76]. *In vitro* MSCs are capable of differentiating into mesenchymal tissues including bone, cartilage, tendon, adipose tissue, and muscle [77-79] [80]. Evidence also exists that they can differentiate into hepatocytes and neurons which are of the endodermal and ectodermal lineages respectively [81-83]. These multipotent cells could be advantageous to an injury involving significant loss of tissue, because multiple types of cells including; muscle, connective tissue, and nerve might need to be replaced.

Research has determined that exogenous bone marrow-derived cells can partake in muscle repair as well. Ferrari et al. injected bone marrow-derived cells into the damaged muscles of mice and they were found to have incorporated into the newly formed myofibers of the regenerating skeletal muscles [84]. Dezawa et al. cultured MSCs, differentiated them into myocytes using Notch1, and implanted them into degenerating muscles of immunodeficient mice and MDX mice [85]. The myocytes incorporated into the muscles with some differentiating into multinucleated fibers and others remaining in the satellite cell domain. Muguruma et al. has shown that bone marrow derived progenitor cells can differentiate into myocytes without the use of demethylation agents or gene transfers, and still participate in regeneration of skeletal muscle [86]. Contractile force is restored more effectively with the implantation of bone marrow derived cells following crush injury [87]. Evidence even exists that some stem cell based muscle therapies using bone marrow derived stem cells will improve muscle regeneration after laceration injury without the stem cells even incorporating into myofibers [88]. The stem cells are hypothesized to release growth factors and other compounds which may facilitate regeneration of existing fibers and satellite cells.

Limited research has been performed using bone marrow-derived cells in defected skeletal muscle, but in the myocardium, BrdU labeled MSCs were implanted in an acellular pericardial ECM [89]. While function between the ECM alone and the cell-seeded ECM was no different, cells positive for BrdU and a specific muscle protein, α-sarcomeric actin, were located in the implanted ECM. The stem cells might have become cardiomyocytes and contributed to the partial regeneration of the defect area. These

studies indicate the tremendous potential for bone marrow-derived cell therapy for replacement of lost muscle tissue and regeneration of damaged muscle tissue. Taken together, the work proving bone marrow derived multipotent progenitor cells are capable of aiding in muscle regeneration establishes these cells as a suitable cell type for research into the repair of a skeletal muscle injury with tissue loss.

SUMMARY

As the literature currently stands, a limited but useful amount of knowledge can be gained regarding the regeneration of defected muscle. The ECM is advantageous to synthetic materials because of its ability to incorporate the host tissue and become a functioning component, while most synthetic materials just serve to fill a tissue void. Many synthetic materials also run the risk of immune rejection, which is less likely to be the case with acellular ECM since its reactive components were stripped off during decellularization. Undoubtedly, different methods of ECM isolation will lead to different ECM environments, so it is necessary to understand what the differences might be and how they can be corrected to more closely mimic a muscle progenitor cell's natural environment. Cell seeding of ECMs is a technique which is proven to be better than simply filling the defect, but further research to determine the optimal cell type and number for seeding is necessary. Since a number of tissues will need to repopulate the defect area, cells which are unipotent might be of limited use, whereas a multipotent stem cell, such as those found in bone marrow, could possibly give rise to more tissue types needed for complete regeneration. Ultimately the main goal of these types of treatments will be to return function to traumatic skeletal muscle injuries, but research regarding the

contractile properties of damaged muscles undergoing treatment with ECM and stem cells is lacking. The potential to treat genetic skeletal muscle diseases as well as muscle injuries with stem cells is immense but further study is required.

Chapter III: Functional Assessment of Skeletal Muscle Regeneration Utilizing Homologous Extracellular Matrix as Scaffolding

ABSTRACT

The loss of a portion of skeletal muscle poses a unique challenge for the normal regeneration of muscle tissue. A transection injury with tissue loss will not heal due to the gap between muscle segments. A damage model was developed by removing a portion of the lateral gastrocnemius (LGAS) of Sprague-Dawley rats. Maximal isometric tetanic tension (P_o) was measured following the removal of either a small, 0.5cm x 1.0cm, defect (SDEF) or a large 1.0cm x 1.0cm (LDEF) piece of the GAS. I*n situ* P_o immediately after creation of the defect was 88.3 ± 2.0% of the non-operated contralateral GAS force for SDEF and 76.9 ± 3.2% of control for LDEF. No functional recovery occurred in either group over the course of 28 days. To enhance recovery, a homologous, decellularized, muscle extracellular matrix (ECM) was implanted into the 1 x 1 cm defect of the LGAS of Lewis rats. After 42 days, growth of blood vessels and myofibers into the ECM was apparent, but no restoration of P_o occurred. These data demonstrate the ability of the ECM to support muscle and blood vessel regeneration, but full recovery of function does not occur after 42 days.

INTRODUCTION

Skeletal muscle injuries including strains, contusions, and lacerations are well documented (For review see [17, 19]). Most of these injuries, if given sufficient time, will repair themselves with partial or total restoration of function [17]. The repair of the muscular tissue is largely the result of proliferation of resident satellite cells, muscle progenitor cells, and even bone-marrow mesenchymal stem cells (MSCs), which are capable of migrating to the area and differentiating into muscle, connective, and vascular tissues [20, 75].

Severe skeletal muscle injuries, such as those involving the loss of a substantial portion of muscle, connective tissue, and blood vessels, however, are not capable of full regeneration on their own. These types of injuries are seen in military personnel wounded-in-action, car accident and gun shot victims, and patients having undergone surgeries where the debridement of muscle tissue was necessary [90]. The remnants of the muscle remaining do not have an ECM scaffolding and connective tissue to transmit force between the remaining muscle segments.

Surgical repair of a skeletal muscle defect is dependent on the ability of an implant to bridge the gap between the transected muscle segments and allow transmission of force between the two ends as it is necessary for the proper orientation of regenerating myofibers and subsequent return of function [10]. The tension developed in the regenerating muscle also stimulates autocrine/paracrine release of growth factors that will further enhance regeneration [49]. The implant should also serve as a scaffold which will

allow the incorporation of regenerating muscle, connective, nerve, and blood vessel tissues.

Several types of constructs suitable for skeletal muscle repair are commercially available. Materials such as Dacron, Silastic, Marlex, Vicryl and others are often used to repair congenital muscular defects of the abdominal wall, but the success of these grafts varies due to issues with biocompatibility [50] and inability to allow for cell ingrowth [91]. The grafts are considered successful when they contain the bowels and look aesthetically normal, but most do not allow for the full incorporation of the original tissue they replace. Natural materials for repair can be better for biocompatibility, host cell incorporation, and for reducing infection risks. These have been used successfully for repair of abdominal wall defects and may well be applied to load-bearing muscle grafts in the future.

In skeletal muscle the ECM is an important structural component for the development of myofibers [51], providing the proper mechanical and chemical environment for the proliferation and differentiation of myogenic progenitor cells [52, 57, 92] as well as releasing chemical signals to the surrounding environment that attract macrophages and progenitor cells that aid in the repair process [54, 55, 93]. Allografts and xenografts of ECM from the integument, urinary bladder and small intestine have been employed in research to repair tissues in the clinical setting (For review See [94]).

This study was designed to evaluate whether a homologous graft of ECM from skeletal muscle could be cut to the size, shape, and orientation of a large muscle defect, and provide the tensile strength for muscular force transmission, as well as the proper environment for growth and differentiation of regenerating muscle tissue. While some

researchers have studied ECM implantation into non-load bearing, defected muscles such as those of the abdominal wall [7, 71, 72], functional analysis and implantation of ECM into a skeletal muscle defect of an active, load bearing muscle has not been attempted. Therefore, the purpose of this study was to develop a model to study the regeneration of a skeletal muscle defect involving replacement of lost tissue with a decellularized ECM that could be readily assessed functionally, morphologically, and histologically.

METHODS

Animals

The study was done in two stages. The first stage consisted of establishing the muscle defect model in male, Sprague Dawley (S-D) rats. Initial work in isolating the ECM through decellularization, as well as development of the *in vivo* model of assessment of muscular function was established in the S-D rat strain. In order to be consistent, the laceration model and defect model were established in this same strain. The second phase was conducted in Lewis rats, an inbred strain, bred for transplantation experiments.

Both male, S-D rats from colonies provided by the University of Texas at Austin Animal Resource Center and male, Lewis rats obtained from Charles River Laboratories (Wilmington, MA) 6-9 mo. of age were used in this study. Rats were housed individually and maintained on a 12-hour light/dark cycle. Rats were allowed ad libitum access to food (Rodent Chow, Harlan Teklad) and water. Rats were randomly assigned to experimental groups. All experimental procedures were approved and conducted in

accordance with guidelines set by the University of Texas at Austin Institutional Animal Care and Use Committee.

Experimental Groups

S-D rats were divided into one of four groups; sham operated (SHAM), laceration only (LAC), small defect (SDEF), and large defect (LDEF). Surgeries were performed under aseptic conditions and the rats anesthetized with IP injections of sodium pentobarbital (65 mg/kg). Rats in the LAC group had a 2 cm incision made on the lateral side of the lower limb parallel to the tibia. The biceps femoris muscle was separated from the tibia to expose the lateral side of the LGAS muscle. The muscle was lacerated with a #9 scalpel blade distal to the neuromuscular junction in line with the tibial tuberosity. The incision was 1 cm in length through the lateral side of the LGAS and through the full thickness of the muscle. The two contiguous portions of the LGAS were not sutured together. To close the wound, the biceps femoris muscle was reattached to the tibia using simple, interrupted, polypropylene suture (Prolene 5-0; Ethicon), and the incision in the skin was closed with silk suture (Ethicon 4-0). Rats in the LAC groups were placed back in their home cages and allowed to recover for 42 days.

Rats in the SDEF and LDEF groups underwent the same procedure as those rats in the LAC groups; however, instead of a laceration, a full thickness defect was created with two #9 scalpel blades separated by 0.5 cm (SDEF) or 1.0 cm (LDEF). The result is two lacerations each 1 cm in length and 0.5 cm or 1.0 cm apart. The tissue between the lacerations was excised with fine surgical scissors, and the free section of muscle removed and weighed. The wound was closed as in the LAC group. Rats in the SDEF groups were immediately subjected to functional analysis (n = 6) or recovered for 14 days

(n = 6). Rats in the LDEF groups were immediately subjected to functional analysis (n = 8) or allowed to recover for 14 days (n = 7), or 28 days (n = 6).

The surgery for the SHAM group (n =6) was identical to that of the defect groups except no incision or defect was created in the LGAS. An incision in the skin and the biceps femoris was made and the LGAS exposed and separated from the soleus. The biceps femoris and skin incisions were sutured as in the other groups, returned to their cages, and allowed to recover for 14 days.

Following development of the model in the S-D rats, further experiments were conducted using the exact same defect model in Lewis rats, because they are better suited for transplantation experiments. The previously described defect surgery was performed on 48 Lewis rats and 1 x 1 cm piece of the LGAS was removed. The average mass of the muscle defect removed from the Lewis rats was 238 ± 6 mg and 224 ± 6 mg for the DEF ONLY and DEF/REP groups respectively. The difference was not statistically significant. The defect removed accounted for approximately 20% of the total mass of the LGAS. No repair surgery was performed on 24 rats (DEF ONLY), but the other 24 rats were subjected to a repair of the defect (DEF/REP) with a homologous ECM cut to the dimensions of the injury as described below. Six rats from each group were evaluated functionally and histologically at each of the following days of recovery; 7, 14, 28, and 42.

ECM Isolation

GAS muscles were removed from a separate group of male Lewis rats and decellularized using a method similar to Borschel et al. [58], but with several modifications. Upon extraction the muscles were placed in deionized water at 4° C for

one day to cause cell swelling and membrane rupture. The muscle was placed in chloroform and continuously agitated for four to five days depending on its size. The muscle was rinsed with water and submerged in 2% sodium dodecyl sulfate (SDS) and agitated continuously. The SDS solution was changed twice per week until the cellular components were washed out. The remaining ECM was rinsed in a large volume of deionized water (10:1 v/w) over several days with solution changes each day to rid the ECM of SDS. To completely insure removal of SDS, the ECMs were rinsed for 4 hours in a 0.1 M tris buffer solution of pH 9.0. The ECM was then submerged in phosphate buffered saline with 1% penicillin/streptomycin (Sigma-Aldrich; St. Louis, MO), exposed to ultraviolet light for at least twelve hours, and stored at 4°C until ready for implantation. To insure complete decellularization, samples of prepared ECM were stained with hematoxylin and eosin. Samples were run on an SDS-PAGE gel and stained with Coomassie Blue to determine whether all soluble proteins were removed. Additionally, mass spectrophotometer analysis (Maldi TOF Voyager DE STR) was used to identify the components of the ECM, and a scanning electron microscope (Zeiss Supra BP at UT-Austin ICMB Core Facility) was used to obtain high magnification images of the ECM (Figure 3.1). A colorimetric assay described by Arand et al. [95] to measure the content of SDS was performed to insure complete removal of SDS from the ECM.

The ECM was implanted in the muscle with the defect using a modified Kessler stitch (5-0 Prolene; Ethicon) with simple interrupted sutures on each of the three borders to hold the cut ends together and serve as markers for later analysis. The modified Kessler stitch was used because it has been shown to be the most effective way to suture the transected muscle segments back together [96].

Force Measurements

After the designated recovery time, the GAS muscles were isolated and subjected to functional measurements. A skin incision was made down the midline of the posterior portion of the lower limb from the popliteal area to the calcaneus. The skin was reflected to expose the biceps femoris which inserts along the distal portion of the tibia in rats. The biceps femoris was cut and reflected to expose the medial and lateral GAS. With care to minimize bleeding and damage to surrounding tissues, the GAS was isolated from the superficial skin and biceps femoris as well as the deep soleus and plantaris. In order to attach the GAS to the muscle lever for force measurements, the Achilles tendon with an attached portion of the calcaneus was cut and tied to the lever arm of a dual-mode servomotor (model 310 B, Aurora Scientific). The muscle was stimulated to contract utilizing a stimulator (Model 2100, A-M Systems) with leads applied to the tibial nerve 1 cm proximal to its insertion into the GAS. The muscle was kept wet in mineral oil, and the temperature maintained at 36°C with a radiant heat lamp and monitored on the muscle surface with a thermometer. The muscle length was adjusted to the length that produced the highest twitch force, and maximal twitch tension determined using stimulation at 0.5 Hz and 7V. The muscle was stimulated at 150 Hz and 20V for peak tetanic tension (P_o). Each contraction was followed by two minutes of rest. The servomotor was interfaced with the computer and equipped with a National Instruments A/D board. The data were stored and analyzed using LabView software. After the completion of contractile measurements, the muscle was dissected free and weighed.

Lateral Gastrocnemius in situ Force Measurements

Functional analysis of the DEF ONLY and DEF/REP was identical to the analysis done to the S-D rat muscle samples except that the medial GAS of the Lewis rats was denervated, so that only the LGAS was contributing to force production.

Histology and Immunohistochemistry

DEF ONLY and DEF/REP muscles were removed, weighed, and placed in 10% neutral buffered Formalin (Protocol, Fisher Scientific; Waltham, MA) for 24 hours, and stored in 70% ethanol until further analysis. Samples were embedded in a Tissue Tech paraffin embedding system prior to sectioning on a Reichert-Jung microtome. Within the defect area, at least six, 5 μm sections per muscle were subjected to histologic and immunohistochemical treatment. Hematoxylin and eosin staining was performed, as was Masson's trichrome (Sigma-Aldrich; St. Louis, MO) staining to identify regions of collagen-containing ECM, myofibers and other cytoplasmic cells, and nuclei. To visualize blood vessels, the rabbit anti-human von Willebrand Factor (vWF) polyclonal antibody (1:300: Dako; Carpinteria, CA) was used to identify endothelial cells. The signal was enhanced with biotinylated polyclonal goat-anti-rabbit IgG with streptavidin-HRP. Color was developed after incubation with 3,3-diaminobenzidine (DAB). Muscular infiltration into the ECM was further confirmed by immunofluorescent staining for the muscle specific cytoskeleton protein, desmin. Sections were exposed to mouse monoclonal anti-desmin antibody (1:500: Sigma-Aldrich; St. Louis, MO). Sections were then incubated with $F(ab')_2$ Goat Anti-Mouse IgG Fluorescein (1:100, $\lambda = 495$nm: Thermoscientific; Waltham, MA) and counterstained with Hoescht 33258 ($\lambda = 395$ nm: AnaSpec; San Jose, CA) to identify nuclei. H&E, trichrome, and vWF sections were visualized with a Nikon Diaphot microscope mounted with an Optronix Microfire digital

camera interfaced with a Dell 8250 computer for storage and analysis of images. Immunofluorescent desmin was visualized with a fluorescence microscope (Leica DM LB2) and photographed with a digital camera *(*Leica DFC340FX).

Statistical Analysis

Means of all measurements were analyzed utilizing Student's t-tests for comparison between samples sets or ANOVA with Tukey's post hoc analysis for analysis of groups of samples. Data are represented as mean ± SEM. Significance is defined as $p < 0.05$.

RESULTS

Immediately upon laceration, the transected myofibers retracted to form a small gap. In LAC, no sign of laceration was apparent macroscopically after 42 days of recovery. No difference in isometric tetanic force or muscle weight was apparent between lacerated and control muscles following 42 days of recovery (Table 3.1).

The average mass of the removed muscle defect from the S-D rats was 152 ± 10 mg and 306 ± 10 mg for the SDEF and LDEF groups respectively and was statistically significant. The mass of the small defect was approximately 5% of the total mass of the GAS, and the mass of the large defect was approximately 10% of the total mass of the GAS. Immediately upon removal of the muscle defect, the remaining portions of the transected myofibers retracted forming a gap larger than the original defect (Figure 3.2a). A gradual remodeling of the LGAS occurred such that at 28 days post-defect injury, little if any of the original defect wound was recognizable (Figure 3.2b). Wet muscle weight of

the defected LGAS was significantly decreased at all time points relative to the non-operated contralateral LGAS (Table 3.2).

Maximal isometric, tetanic tension (P_o) of the whole GAS immediately following the defect injury was 88.3 ± 2.0 % and 76.9 ± 3.2% of the contralateral limb for SDEF and LDEF respectively. After 14 days of recovery P_o was 88.1 ± 5.6% (SDEF) and 80.7 ± 3.5% (LDEF) of the contralateral limb. Twenty-eight days post-injury P_o of LDEF was 79.4 ± 4.0% (Figure 3.3). The P_o of the SDEF group was significantly higher than that of the LDEF group at all recovery time points ($p < 0.05$). No significant difference was found at the different recovery time points within each group.

The average mass of the muscle defect removed from the Lewis rats was 238 ± 6 mg and 224 ± 6 mg for the DEF ONLY and DEF/REP groups respectively. The difference was not statistically significant. The defect removed accounted for approximately 20% of the total mass of the LGAS. As seen in the S-D rats, immediately upon removal of the defect, the transected myofibers retracted, and if the defect was not repaired, a gradual remodeling took place such that the original defect area was hard to define by 42 days. However, repair with the ECM maintained the overall morphology of the LGAS (Figure 3.2d).

Prior to implant, mass spectrophometric analysis of samples of decellularized ECM demonstrated that it was composed of approximately 99% collagen. No nuclei or cytoplasm were evident within the decellularized ECMs used for implant as evidenced by Masson's trichrome staining. The decellularization protocol removed all soluble proteins as determined by the Bradford Assay and Coomassie Blue staining. Preparation of the

ECM for implantation also completely removed any residual SDS as determined by Arand's colorimetric assay.

Functionally, the maximal, isometric, tetanic tension produced by the LGAS of the DEF ONLY group was significantly lower than that of the non-operated, contralateral limb at all recovery time points, and no recovery of force occurred as recovery time increased (Table 3.3; Figure 3.4). The tetanic tension of the ECM-repaired LGAS did not significantly recover over the course of 42 days (Table 3.4; Figure 3.4). A statistically significant difference between the DEF ONLY and DEF/REP groups was seen at 7 days post injury, but not at any subsequent time point. As shown in Tables 3.3 and 3.4, the average mass of the defected LGAS with the exception of one were significantly lower than the non-operated, contralateral LGAS. While the mass of the DEF/REP LGAS tended to be higher relative to the contralateral limb than the mass of the DEF ONLY LGAS, the difference was not statistically significant.

Histological analysis of the defect area with ECM at 7, 14, 28, and 42 days shows a progression of regeneration from inflammation to the appearance of small blood vessels and central-nucleated myofibers that increase in number at each time point (Figure 3.5). Immunohistochemistry confirmed the presence of vWF positive endothelial cells and desmin positive myofibers (Figure 3.6). Myofibers and blood vessels were found deeper in the ECM as recovery time increased. The area of ECM closest to the border with the transected myofibers appeared most dense with regenerating fibers and blood vessels indicating approximately 1 mm of growth (Figure 3.7a). Fewer fibers and blood vessels were seen in the areas deeper into the ECM that were 2-3 mm from the cut muscle surface (Figure 3.7b).

DISCUSSION

Little to no regeneration occurs in skeletal muscle following a transection of the myofibers when a substantial amount of the tissue is lost. Regrowth across the muscle defect gap does not occur over the course of 42 days following injury. The remodeling process that takes place during this time makes it unlikely that the muscle would ever return to its original size and shape. Since the maximal, isometric, tetanic force immediately post-defect injury is the same regardless of the recovery time allowed, it is likely that permanent functional damage was incurred. Without any significant functional recovery of the muscle and the morphological changes it undergoes, this muscle defect model is a suitable model for use in further investigations into skeletal muscle's regenerative capacity. Since the laceration-only injury showed no functional deficit after 42 days, and the defect injury had not recovered function after 42 days, the defect model presented here could be a better model for the study of skeletal muscle regeneration, and surgical and tissue engineering interventions aimed at regenerating significant amounts of skeletal muscle than a laceration injury model.

Researchers have used GAS laceration models that resulted in a more severe loss of function which, if left unrepaired, persisted for weeks [38, 41, 97]. Others, however, have seen functional recovery after only 25 days even in full transection laceration models of the soleus [35]. The lack of an apparent functional deficit in this LGAS model after 42 days is likely due to the size and location of the laceration. The laceration occurred only on the LGAS and did not transect the medial GAS. Additionally, nerve and major blood vessels in the area were left intact which likely explains the full functional recovery and return of muscle mass that occurs in this model, but does not occur in other

models where a complete transection of the muscle is performed [38, 97]. However, in the context of our work, we were only attempting to create a laceration as a control injury that was at the same site and to the same depth as the muscle defect. The lack of a functional deficit 42 days post-laceration injury underscores the importance of a defect model that has no functional improvement over the same timeframe.

During development of the muscle defect model, two different defect sizes were utilized to determine the critical size for establishing significance of our treatment techniques. The 0.5 cm x 1.0 cm (~ 150 mg) defect was not large enough to allow for easy determination of the effectiveness of surgical repair. Although there was a decrease in function that did not begin to return to normal by 14 days**,** it was not a significant enough functional deficit to allow for definitive evaluation of different repair techniques. The decrease in mass in the SDEF from 92% of contralateral weight to 82% of contralateral weight at day 14 might be explained by the potential for atrophy of the remaining transected myofibers in SDEF. A larger portion of the transected fibers remained in the SDEF and could subsequently experience more atrophy, whereas more mass was initially removed in the LDEF so smaller portions of transected fibers remained and less mass might be lost due to atrophy. The superior and inferior portions of the LGAS (above and below the defect) were not assessed, however. The 1.0 cm x 1.0 cm (~ 306 mg) defect was the maximum size allowed by the rat's anatomy without cutting nerve or major blood vessels and the function did not change from 0 to 28 days of recovery. This larger defect allowed for a thorough evaluation of the subsequent repair technique.

Following the development of the defect injury model in the S-D rats, further experiments were performed on the Lewis rat, an inbred-strain of rat more suited for surgical implantation research. Another set of defect surgeries was performed to confirm the lack of functional recovery seen in the S-D rats. Due to minor anatomical differences of the Lewis rat, the 300+ mg defect removed from the S-D rats could not be achieved, and the Lewis rat defect mass was approximately 230 mg. To better isolate the functional effect of the defect on the LGAS, the medial GAS was denervated in the Lewis rats immediately prior to force analysis, so that only the LGAS was contributing to force production.

To repair the muscle defect, an implantable material was needed that could bridge the gap between the transected ends of the myofibers and allow mechanical transduction of force. The material also needed to be capable of supporting the growth of myofibers and other muscle associated cell types. Skeletal muscle ECM was chosen for this reason. The process of decellularizing skeletal muscle to obtain an ECM is possible. The decellularization process removes all cellular components from the tissue so that only the ECM scaffold is left. Acellular tissue is advantageous for a number of reasons; the implanted ECM scaffold has physical properties similar to those seen by cells *in vivo*, and the ECM should naturally direct cells to orient in the proper direction. This is important for cells such as muscle progenitor cells activated in the repair process, because they develop best on substances that are most like muscle tissue [57]. Proper alignment of the scaffolding is also important for the transmission of force. A properly derived ECM scaffold is also non-immunogenic. When implanted, the tissue did not elicit an immune

response that would otherwise reject the implant and render it ineffective, because its immune reactive antigens were stripped off with the cells [58].

Borschel et al. have had success growing viable muscle tissue *in vitro* on an ECM derived from decellularized skeletal muscle [58]. Implantation of acellularized skeletal muscle into muscle defects of the abdominal wall has been performed by several groups with varying levels of success, although the functional outcome has not been assessed [9]. Evidence that the ECM is infiltrated by blood vessels is apparent and some researchers have seen infiltration of skeletal myofibers as well [9], but more successful repair with ECM of non-load bearing muscles occurs when myoblasts or satellite cells are seeded onto the ECM prior to implantation [71-73]. Acellular ECM has been successfully employed as a patch to repair defects in a number of tissues including tendons and cardiac muscle. Implanted ECM scaffolds implanted with no other treatment are effective at repairing tendon injuries of the rotator cuff and Achilles tendon [60, 61]. The ECM scaffold is not only effective at bridging the gaps in the tendon, but it also allows incorporation of cells from the native tissue. Similar positive results have been shown in cardiac muscle with ECM repair. A myocardial ventricular wall defect patched with ECM incorporated more myocardial tissue into the defected area than a synthetic, ePTFE patch used clinically [62]. Defects of the ventricular wall repaired with ECM also lead to increased functional improvements compared to DACRON [63].

As evidenced by this study and others, the muscle-derived ECM used here to repair skeletal muscle tissue lost due to injury is capable of supporting the growth of blood vessels and myofibers, and is a promising model for the study of muscle regeneration [58]. As recovery time increased, an increase in the number of blood vessels

and myofibers was apparent in the ECM at progressively deeper levels, suggesting that the fibers and vessels are growing into the ECM from the transected ends of the surviving myofibers. After 42 days, however, the middle of the ECM was not yet populated with myofibers or blood vessels. The ingrowth of blood vessels seen in the ECMs used in this study has been seen in studies performed on the repair of abdominal wall musculature with similarly derived ECMs [7, 9]. Limited ingrowth of myofibers has been confirmed in some of the abdominal wall defect ECM implants [9], but not all [7, 71, 73]. The myofiber ingrowth observed in the present study might be due to the difference of the muscles chosen. Functionally, the LGAS is very active and is subjected to a relatively high amount of mechanical stress during normal activity, while the abdominal wall musculature does not see the same demands. An increase in the activity level of an injured muscle can expedite the healing process [98]. Functionally, the matrix-repaired muscle was not different from the unrepaired muscle up to 42 days post-injury, although longer recovery times were not studied. The lack of functional recovery could be due to the small size and limited number of fibers growing into the ECM, insufficient vasculogenesis throughout the ECM, and possibly incomplete nerve reinnervation of fibers.

In conclusion, the LGAS defect injury model allows for a uniform standard for the study of the regeneration potential following traumatic skeletal muscle injury. This model has tremendous potential to aid researchers in the best treatments to restore function and aesthetics to severely damaged skeletal muscle. The muscle defect area could easily be replaced with any of a number of natural or engineered replacement tissues, and their growth and function could be monitored in the *in vivo* environment as

was done with the ECM in this case. The morphology of the repaired LGAS and aesthetic appearance were well maintained over 42 days despite the fact that functional recovery did not occur. However, it is evident that the ECM was a suitable environment for blood vessel and myofiber ingrowth indicating a promising future as an implant material. Further research should focus on increasing the number and size of myofibers in and throughout the ECM and improving the functional outcome.

LAC 42 Day Recovery	
Force (LAC % of Control)	103.5 ± 6.3%
Control GAS Mass	2883 ± 88 mg
LAC GAS Mass	2950 ± 108 mg

Table 3.1 – Laceration

DEF LGAS Mass (% of Control)

	0 days	14 days	28 days
SDEF	92%	82%	-
LDEF	85%	84%	81%

Table 3.2 – Small v. Large Defect

Days Recovery	Force (% of Con)	Defect Force (N)	Control Force (N)	Defect LGAS Wt (mg)	Contralateral LGAS Wt (mg)	Def SP_o (N/cm^2)	Con SP_o (N/cm^2)
7	70.4 ± 3.4	15.6 ± 0.7	22.2 ± 0.4	1054.2 ± 23.9	1271.3 ± 19.8	17.5 ± 0.9	21.7 ± 0.4
14	72.9 ± 2.3	16.1 ± 0.6	22.1 ± 0.5	1066.1 ± 29.5	1264.4 ± 20.8	18.6 ± 0.5	21.1 ± 0.7
28	77 ± 0.8	17.2 ± 0.4	22.4 ± 0.6	1115.5 ± 40.3	1302.8 ± 35.0	19.7 ± 0.4	21.5 ± 0.4
42	74.1 ± 4.4	16.4 ± 1.6	21.9 ± 0.8	1054.7 ± 74.1	1283.8 ± 65.9	19.5 ± 0.9	21.1 ± 0.6

Table 3.3 – DEF-ONLY

Days Recovery	Force (% of Con)	Defect Force (N)	Control Force (N)	Defect LGAS Wt (mg)	Contralateral LGAS Wt (mg)	Def SP_o (N/cm^2)	Con SP_o (N/cm^2)
7	75.7 ± 5.8	16.5 ± 1.4	21.8 ± 0.6	1377 ± 129	1164 ± 67	17.4 ± 1.0	24.2 ± 0.9
14	75.6 ± 2.6	15.7 ± 0.3	20.9 ± 0.6	1125 ± 43.4	1242 ± 18	18.1 ± 0.7	21.7 ± 0.8
28	77.3 ± 2.7	15.7 ± 0.4	20.4 ± 0.3	1073 ± 14.9	1279 ± 18	18.3 ± 0.6	20.1 ± 0.5
42	74.7 ± 2.2	17.0 ± 0.6	22.7 ± 0.5	1137 ± 33.3	1277 ± 30.7	18.9 ± 0.9	22.4 ± 0.6

Table 3.4 – DEF/REP

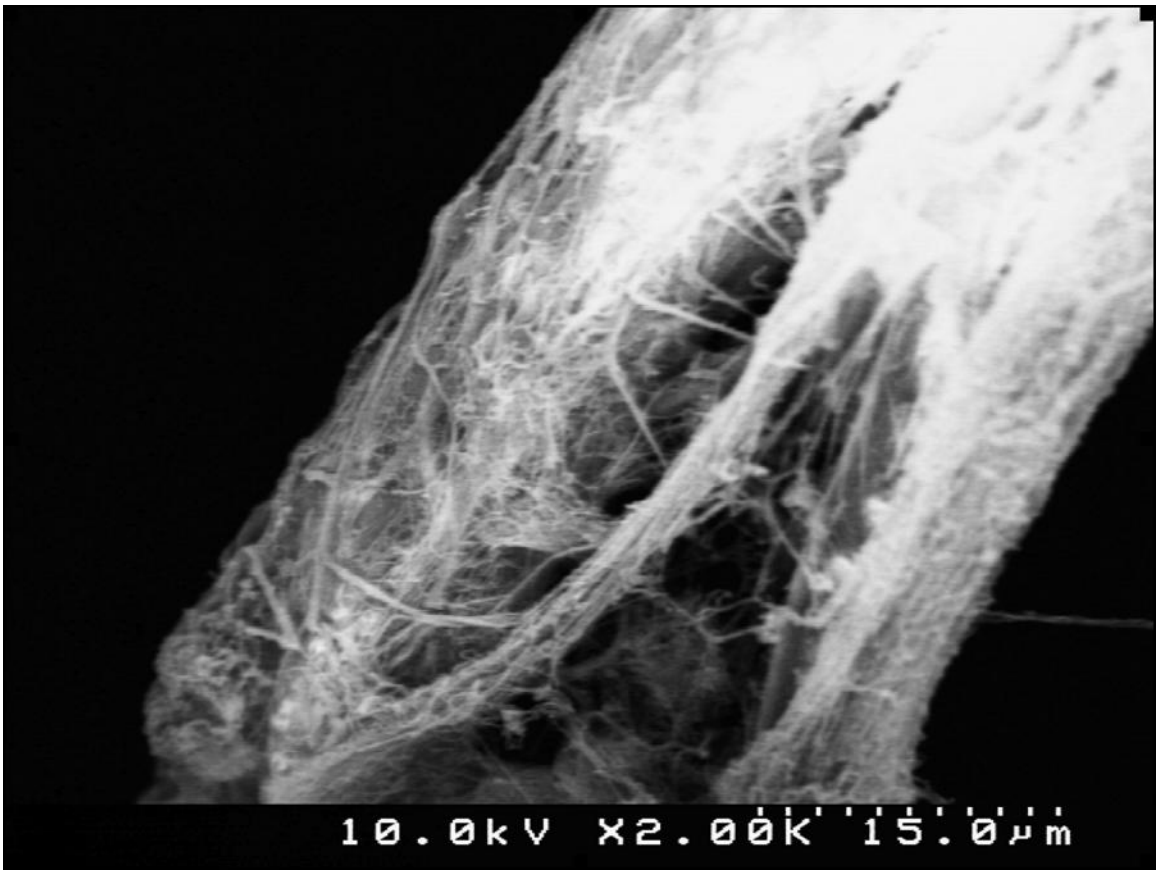

FIGURE 3.1: SCANNING EM OF ECM

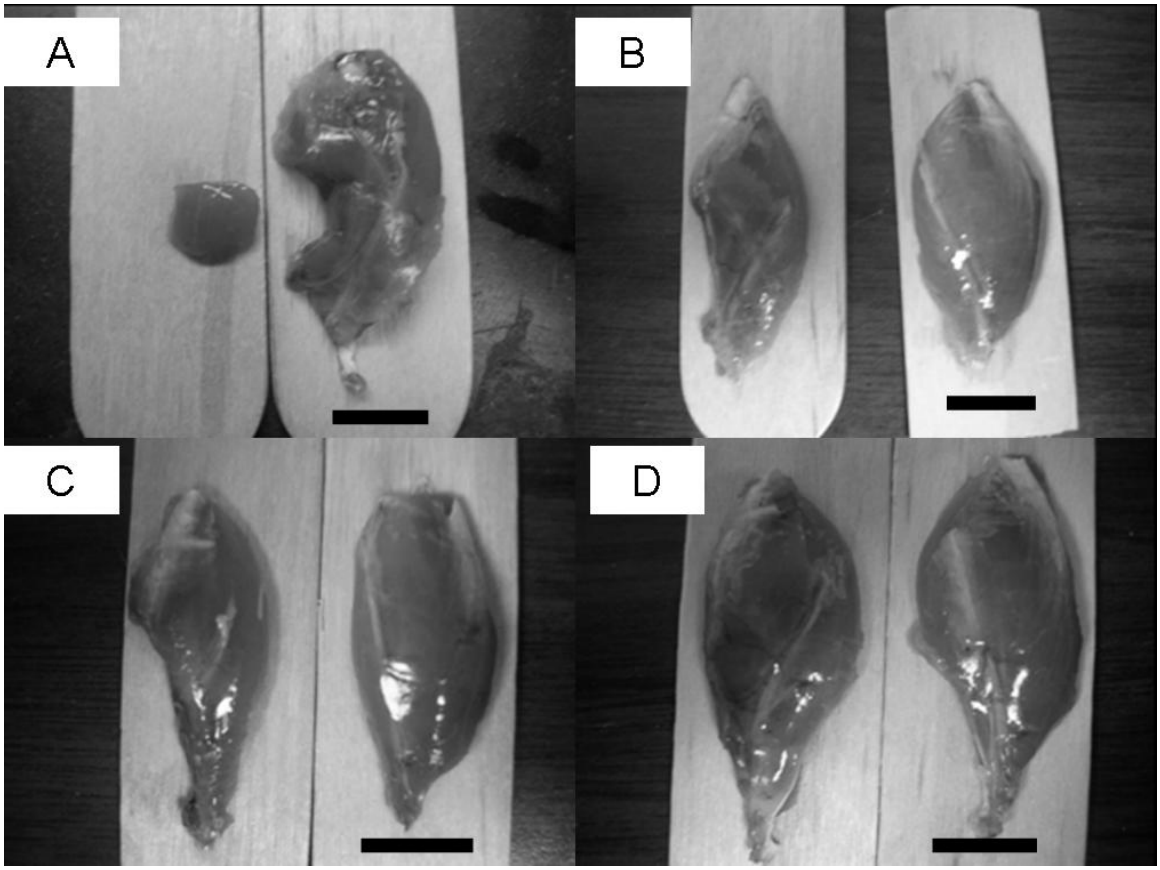

FIGURE 3.2: MORPHOLOGY - A) Defect Creation B) 28 Day Post-Defect C) 42 Day Post-Defect D) ECM Repair 42 Day Post-Defect. Scale bar = 1.0 cm

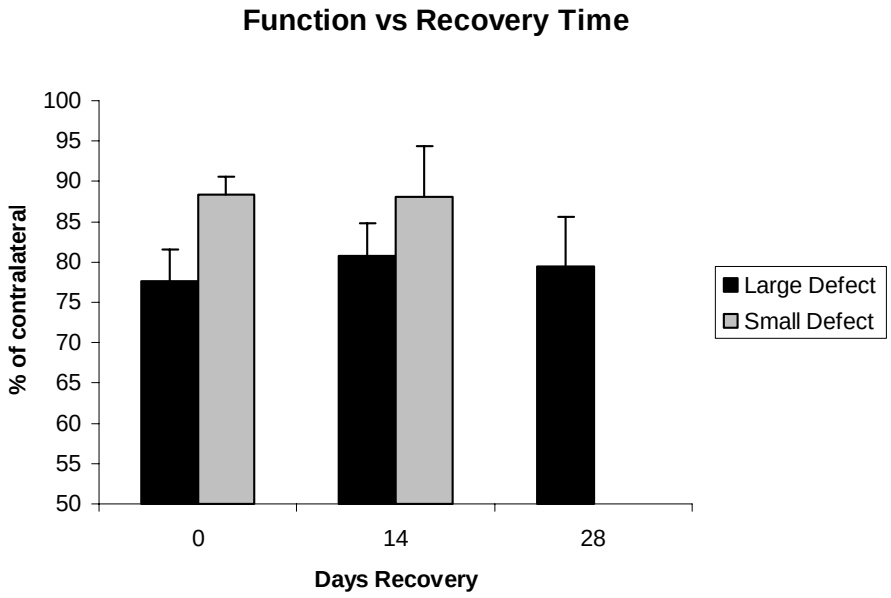

FIGURE 3.3: FUNCTION – SMALL V. LARGE DEFECT - Sprague-Dawley Rat

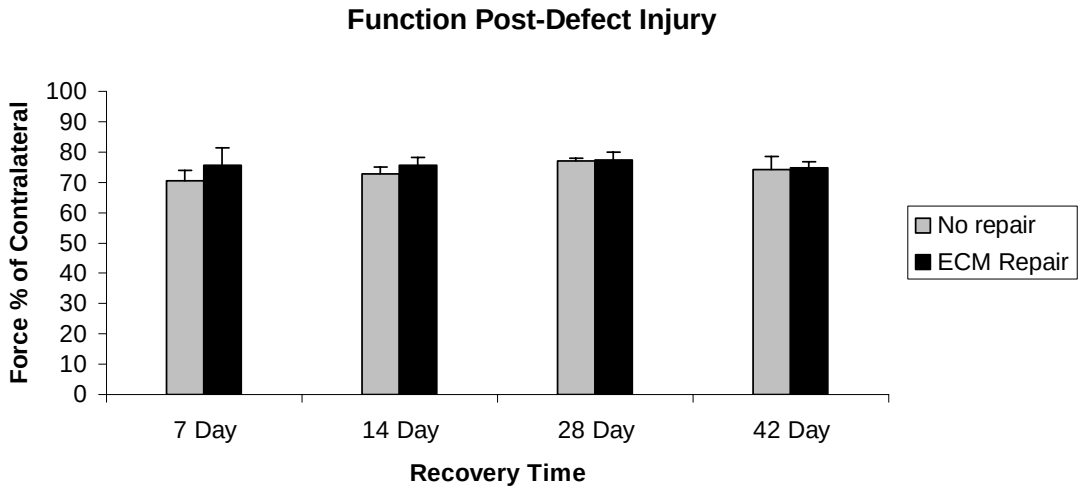

FIGURE 3.4: FUNCTION POST-DEFECT INJURY - Maximal isometric, tetanic tension of defect LGAS relative to contralateral limb 14, 28, and 42 days post injury. No significant difference exists between groups or time points.

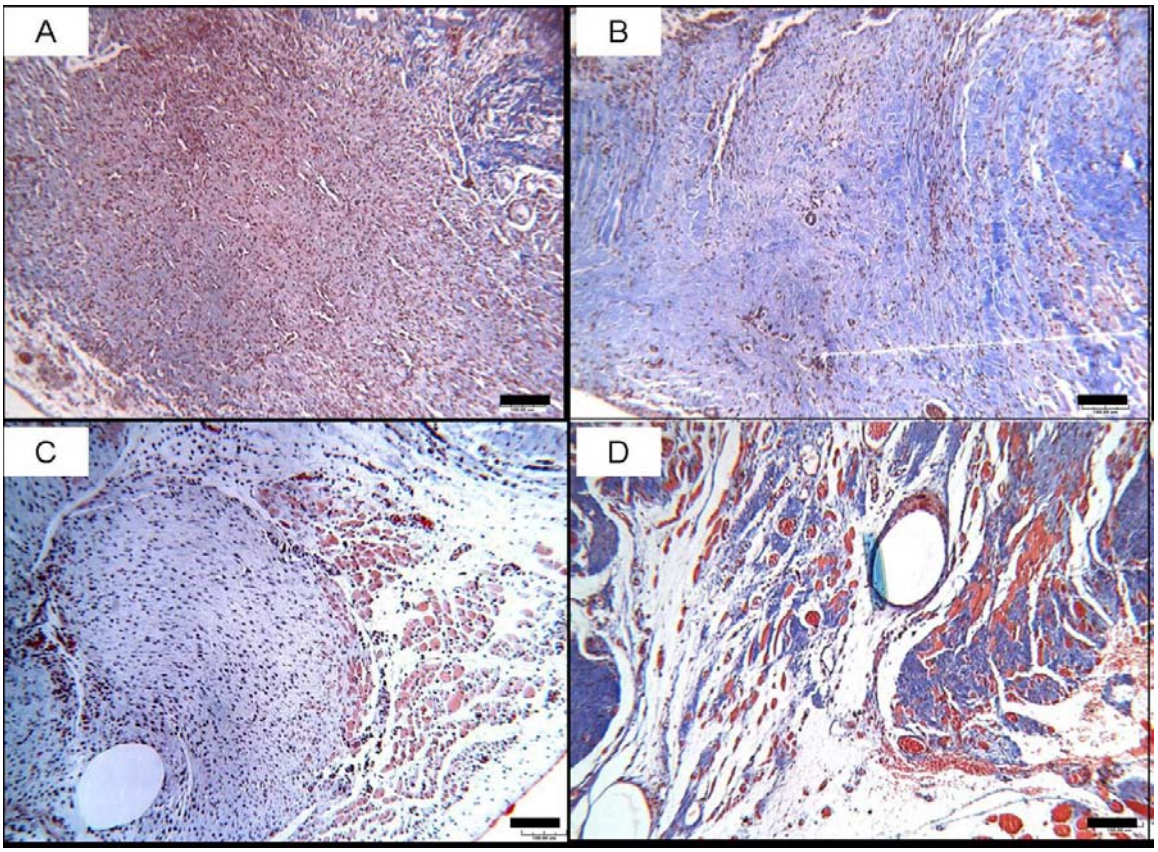

FIGURE 3.5: HISTOLOGY MASSON'S TRICHROME - defect/ECM at A) 7, B) 14, C) 28, D) 42 Days of recovery showing progressive regeneration as evidenced by increase in red staining myofibers (Confirmed with desmin immunofluorescence). Circular spaces are suture holes. Scale = 100 um

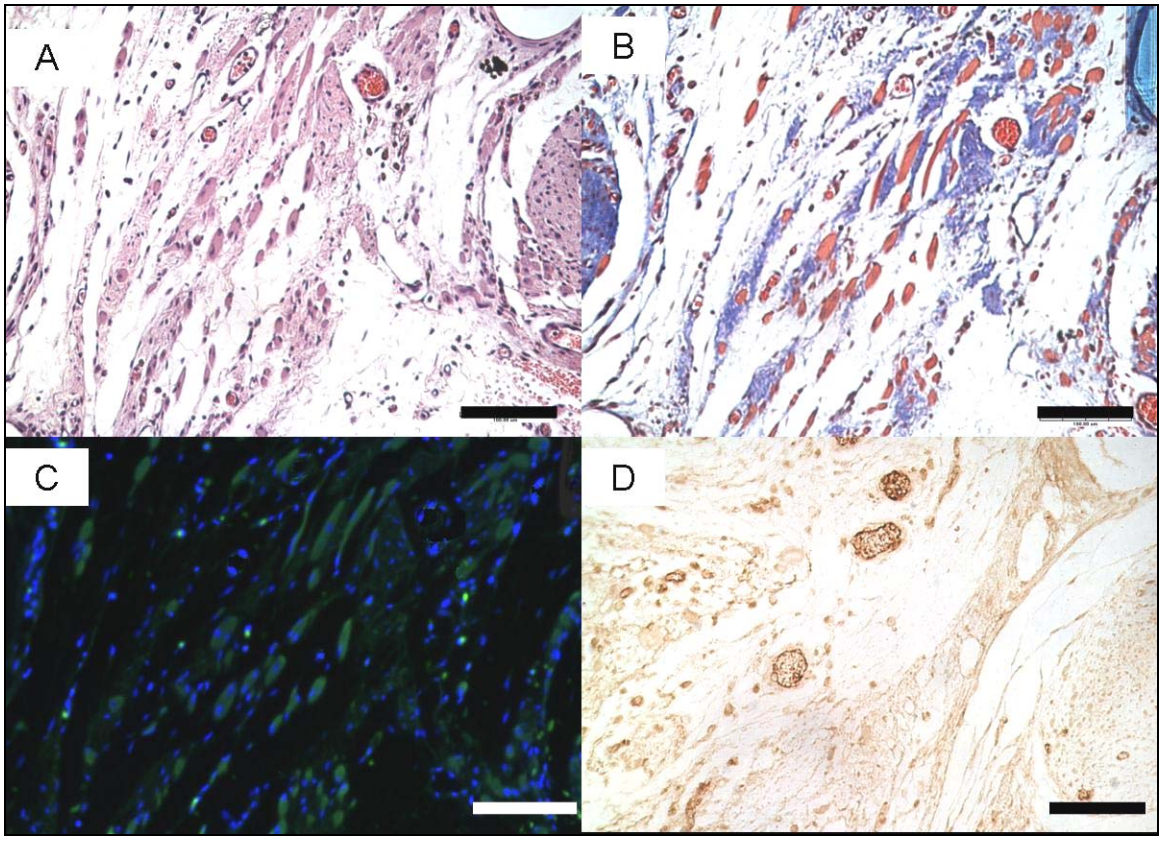

FIGURE 3.6: HISTOLOGY COMPARISON - Neighboring sections of ECM implant after 42 days recovery stained with (A) H&E, (B) Masson's Trichrome, (C) immunoflurescent desmin to identify muscle, and (D) vWF to identify blood vessels within the ECM. Scale = 100 um.

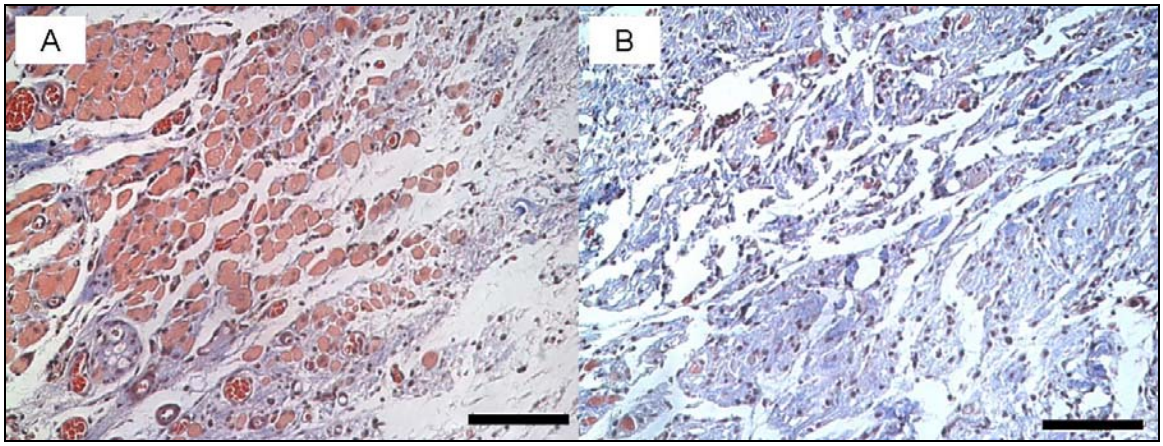

FIGURE 3.7: TRICHROME SERIAL SECTIONS - ECM implant at 28 days recovery stained with Masson's Trichrome. A) 1-2 mm from muscle/ECM border, B) 2-3 mm from muscle ECM border. Scale = 100 um.

Chapter IV: Repair of Traumatic Skeletal Muscle Injury with Bone Marrow Derived Mesenchymal Stem Cells Seeded on Extracellular Matrix

ABSTRACT

Surgical repair of a skeletal muscle injury resulting in tissue loss poses unique challenges for surgical repair. Despite the regenerative potential of skeletal muscle, if a significant amount of tissue is lost, skeletal myofibers will not grow to fill the injured area completely. Prior work in our lab has shown the potential to fill the void with an extracellular matrix scaffold (ECM) but functional recovery is limited. To improve the functional outcome of the injured muscle, a muscle-derived ECM was implanted into a 1 x 1 cm^2 defect in the lateral gastrocnemius (LGAS) of Lewis rats and seeded with bone marrow derived mesenchymal stem cells. Without the addition of cells, the ECM repaired LGAS produced 74.7 ± 2.2% of the maximal force of the contralateral LGAS after 42 days of recovery. The LGAS repaired with ECM and cells was significantly higher producing 85.4 ± 3.6% of the contralateral LGAS. The specific tension was 84% and 94% of the contralateral limb for the ECM and ECM with cells groups respectively. The implanted ECM with cells had more blood vessels and regenerating skeletal myofibers than the ECM without cells ($p < 0.05$). The data suggest that the repair of a skeletal muscle defect injury by the implantation of a muscle-derived ECM seeded with bone-marrow derived cells can improve functional recovery after 42 days. This might be due to an increase in the number of blood vessels providing better oxygen and nutrient supply to regenerating skeletal myofibers growing inside the implanted ECM.

INTRODUCTION

Traumatic injury to a skeletal muscle that involves the loss of a portion of the tissue presents a unique challenge to the normally robust regenerative capacity of skeletal muscle. Injuries such as these are often seen in military personnel wounded in action by gunshots and blasts [3, 90]. In response to damage, skeletal muscle goes through a well defined series of events including inflammation, repair, and remodeling (For Review: [17, 19]). Ultimately, repair is the result of resident muscle stem cells, known as satellite cells, which proliferate, differentiate, and fuse with existing myofibers or form new myofibers [13, 99]. The normal repair mechanisms, however, are not sufficient for the repair of injuries involving significant tissue loss [8, 100]. The remaining myofibers are incapable of bridging across gaps created by the injury and scar tissue will fill the area or the muscle will remodel such that an area is permanently devoid of tissue [39]. In the case of injuries such as these, the victim is often left with a permanent handicap.

Complete repair of a large muscle defect is dependent on the ability of an implant to fill the void in the tissue while allowing for the growth and development of functional myofibers, blood vessels, and nerves. The current standard of care for these injuries attempts to accomplish this by autologous tissue transfer (muscle flaps) using donor tissue from other areas of the victim's body. Recent reports describe functional free muscle transplantation in the forearm [4] and elbow [5], but these procedures are associated with significant donor site morbidity and are not yet applicable to large muscle defects. The implantation of a scaffold seeded with progenitor cells to repair the defect and allow for the growth of new tissue into the area could be a way around the morbidity associated with autologous tissue transfer.

The extracellular matrix (ECM) is a scaffold, comprised predominantly of collagen that naturally occurs in the body and is critical in the development and growth of skeletal muscle [51]. Skeletal muscle tissue can be decellularized such that all that remains is a three-dimensional ECM [58, 94]. Using a three-dimensional ECM derived from skeletal muscle as a scaffold is advantageous because differentiation of muscle progenitor cells is stimulated by numerous factors including their three dimensional configuration and chemical and mechanical environment [57]. The decellularized ECM serves as a platform for the growth of functional muscle, blood vessel, and nervous tissue [58, 101, 102]. The three dimensional configuration of the ECM allows it to translate linear forces throughout the construct thus applying tension through the adhesion molecules to developing cells and further simulating the developmental environment of skeletal muscle.

In myocardial damage models, defects repaired with ECM-derived implants incorporate myocardial cells and improve function [62, 63]. Implanted into skeletal muscle *in vivo*, the ECM is capable of supporting limited growth of new myofibers while maintaining the overall morphology of the area, but functional recovery does not occur [8, 9, 103]. The addition of muscle precursor cells, such as myoblasts and satellite cells, to acellular ECM implants used to repair abdominal wall defects, however, increases the amount of muscle tissue incorporated into the ECM, although the functional significance of this has yet to be determined [9, 71-73].

The full repair of a large defect in a skeletal muscle will obviously require the growth of myofibers, but it also requires blood vessel integration and nerve innervation of the myofibers. The implantation of myoblasts or other myogenically committed cells

might not be capable of regenerating vessels and nerve. A pool of cells, known as mesenchymal stem cells (MSCs), that is multipotent and easily expandable in culture is found in the red bone marrow. Cells from the bone marrow are known to participate in skeletal muscle regeneration naturally [20, 75]. Dystrophin positive myofibers are found in dystrophic skeletal muscle of mice after the addition of donor bone marrow cells [23]. Bone marrow derived cells, isolated by adherence to the plastic cell culture vials through repeated passage, are termed MSCs. These cells were originally described by Friedenstein [104] and are capable of differentiating into a number of other tissues including nerve, muscle, and vascular tissue that are necessary for viable muscular regeneration following muscle defect injury [80, 83, 85, 105]. Addition of bone marrow derived MSCs aids in the functional regeneration of skeletal muscle following both crush and laceration injury [87, 88]. The addition of MSCs to acellular ECM implants in the defected myocardium has shown the ability of MSCs to differentiate into cardiomyocytes and engraft into the ventricular wall, preserving its structure and demonstrating the potential of this technique to be beneficial for cardiac and skeletal muscle regeneration [89, 106].

Although bone marrow derived cells can aid in the repair of injured muscle and that muscle tissue can incorporate into an implanted ECM *in vivo*, the defect models studied to date, do not allow for functional analysis to determine physiological significance of large defect repair. Therefore, the purpose of this study was to determine the functional and morphological regeneration potential of an injured skeletal muscle with tissue loss and subsequent surgical replacement of the lost tissue with decellularized

ECM with or without the addition of bone marrow derived mesenchymal stem cells (MSCs).

METHODS

Subjects

Male Lewis rats from colonies maintained by the Charles River Company (Wilmington, MA) were used in experimental procedures. The rats were approximately six to nine months of age at the beginning of treatment and weighed at least 400 grams. Rats were allowed ad libitum access to food (Rodent Chow, Harlan Teklad) and water. Rats were randomly assigned to experimental groups. All experimental procedures were conducted in accordance with guidelines set by the University of Texas at Austin Institutional Animal Care and Use Committee.

For all surgical procedures, rats were under general anesthesia. Animals were anesthetized with an intraperitoneal injection of sodium pentobarbital (55 – 65 mg/kg body weight). Following experimental procedures, animals were overdosed with a bolus injection of sodium pentobarbital (80 mg/kg body weight) to the heart.

Experimental Groups

Lewis rats were randomly assigned to two groups; ECM-ONLY (n = 27) or ECM-CELL (n = 20). ECM-ONLY rats were divided into 4 recovery groups; 7-day (n = 6), 14-day (n = 6), 28-day (n = 6), and 42-day (n = 9). Rats in the ECM-CELL group were divided into 3 recovery groups; 14-day (n = 6), 28-day (n = 6), and 42-day (n = 8). Since the cells were not injected into the ECM-CELL group until 7-days post-defect/ECM

implant, no 7-day recovery group was necessary. Rats in each group underwent procedures as described below.

ECM Isolation

GAS muscles were removed from donor male Lewis rats and decellularized. Under sterile conditions, muscles were dissected free and placed in 4° C dH_2O water for one day. The muscle was placed in chloroform and continuously agitated for four to five days depending on size. The muscle was rinsed with water and submerged in 2% sodium dodecyl sulfate (SDS: Sigma-Aldrich; St. Louis, MO) and agitated continuously. The SDS solution was changed twice per week until the cellular components were washed out. The remaining ECM was rinsed in a large volume of deionized water (10:1 v/w) over several days with solution changes each day to rid the ECM of SDS. To completely insure removal of SDS, the ECMs were rinsed for 4 hours in a 0.1 M tris buffer solution of pH 9.0. The ECM was then submerged in phosphate buffered saline with 1% penicillin/streptomycin (Sigma-Aldrich; St. Louis, MO), exposed to ultraviolet light for at least twelve hours, and stored at 4°C until ready for implantation. Previously, the decellularized ECM was determined to be composed of approximately 99% collagen. No nuclei or cytoplasm were evident within the decellularized ECMs used for implant as evidenced by Masson's trichrome staining. The decellularization protocol removed all soluble proteins as determined by the Bradford Assay and Coomassie Blue staining. Preparation of the ECM for implantation also completely removed any residual SDS as determined by Arand's colorimetric assay [95].

Defect Creation & ECM Implantation

Rats were anesthetized and a two centimeter incision was made on the lateral side of the lower limb parallel to the distal portion of the tibia. The biceps femoris muscle was separated from the tibia to expose the lateral side of the LGAS muscle. The LGAS was separated from the soleus muscle along a one centimeter portion just above the Achilles tendon. A small metal plate was placed between the gastrocnemius and the soleus to prevent the soleus from being damaged during creation of the defect. To create the defect, two #9 scalpel blades separated with a spacer were inserted distal to the neuromuscular junction with the proximal most scalpel blade in line with the tibial tuberosity. The LGAS was cut such that there were two lacerations through the full thickness of the muscle. The medial edge still connected to the rest of the muscle was excised with fine surgical scissors (Figure 4.1). The portion of muscle excised was weighed and measured. A portion of ECM cut to the dimensions of the defected area was implanted in the muscle using a modified Kessler stitch (5-0 Prolene; Ethicon) with simple interrupted sutures on each of the three borders to hold the cut ends together and serve as markers for later analysis. The modified Kessler stitch was used because it has been shown to be the most effective way to suture the transected muscle segments back together [96]. The wound was closed by suturing the cut area of the biceps femoris back together with simple interrupted polypropylene sutures (5-0, Prolene, Ethicon). The skin incision was closed with simple interrupted stitches of silk suture (4-0, Ethicon) tied with the knot underneath the skin to prevent the stitches from being chewed out.

Isolation of Bone Marrow Derived Mesenchymal Stem Cells and Culturing

MSCs were isolated from Lewis rats using a procedure similar to that described by Friedenstein to isolate the adherent fraction of cells [104]. The femurs and tibias of

both legs of 2-3 month old Lewis rats were removed and trimmed of all muscle and connective tissue. The epiphyses were cut and the marrow flushed out with a Dulbecco's Modified Eagle's Medium (Invitrogen; Carlsbad, CA), 10% Fetal Bovine Serum (Invitrogen; Carlsbad, CA), 1% antibiotic/antimyctotic (Invitrogen; Carlsbad, CA) solution. The resulting cell suspension was centrifuged and the cells in the pellet plated at a density of 5 x 10^7 cells/ 100 mm^2 on a culture dish and incubated at 37° C with 5% CO_2. Media was changed every 2-3 days until cells reach 70% confluency. Cells were removed from the flask with 0.25% trypsin in 1mM EDTA at 37°C for five minutes, centrifuged at 1000g, resuspended in serum-supplemented medium, and replated at 5 x 10^5 cells/ 100 mm^2 on a culture dish. Culturing of the cells continued for 3-5 more passages at which time they were again removed from the flask and prepared for injection into the ECM at the defect site.

Flow cytometry was performed on cells from the 5^{th} passage to determine the cell population. Cells in culture were washed with PBS, trypsinized, and resuspended at 0.5 X 10^6 cells/ mL in PBS with 1% BSA. Cells were incubated for 30 min at 4º C in the following fluorochrome-conjugated antibodies; CD34-PE (Santa Cruz Biotechnologies, Santa Cruz, CA), CD45-FITC (BD Biosciences, Franklin Lakes, NJ), CD90-PerCP (BD Biosciences, Franklin Lakes, NJ), CD146-APC (R&D Systems, Minneapolis, MN). Cells were washed in PBS and fixed in 1% para-formaldehyde. Detection of fluorochrome labeling was performed on a FACS Calibur cytometer (BD Biosciences, Franklin Lakes, NJ). Analysis was conducted using CellQuest Pro software at the ICMB Flow Cytometry Core Facility of The University of Texas at Austin.

Injection of Bone Marrow Derived Mesenchymal Stem Cells into ECM

One week following the defect repair with ECM, rats in the ECM-CELL treatment groups were given an injection of 1.5 – 2 million MSCs. Cells were trypsinized and removed from the cell-culture flask, centrifuged at 1000g and resuspended in 300 µl of phosphate buffered saline. The rat was anesthetized and prepared for the injection of cells. The original skin incision was opened up to visualize the ECM in the defect of the LGAS. Using a 21 gauge needle, MSCs were injected in 4-6 locations throughout the ECM/defect area. Following injection, the skin was once again stitched closed as before.

Force Measurements

After the designated recovery time, the LGAS muscles were isolated and subjected to functional measurements. A skin incision was made down the midline of the posterior portion of the lower limb from the popliteal area to the calcaneus. The skin was reflected to expose the biceps femoris which inserts along the distal portion of the tibia in rats. The biceps femoris was cut and reflected to expose the medial and lateral GAS. With care to minimize bleeding and damage to surrounding tissues, the LGAS was isolated from the superficial skin and biceps femoris as well as the deep soleus and plantaris. In order to attach the LGAS to the muscle lever for force measurements, the Achilles tendon with an attached portion of the calcaneus was cut and tied to the lever arm of a dual-mode servomotor (model 310 B, Aurora Scientific, Aurora, ON, Canada). The muscle was stimulated to contract utilizing a stimulator (Model 2100, A-M Systems, Calsborg, WA) with leads applied to the tibial nerve 1 cm proximal to its insertion into the GAS. The muscle was kept wet in mineral oil, and the temperature maintained at 36°C with a radiant heat lamp and monitored on the muscle surface with a thermometer. The muscle length was adjusted to the length that produced the highest twitch force, and

maximal twitch tension determined. The muscle was stimulated at 150 Hz and 20V for peak tetanic tension (P_o). Each contraction was followed by two minutes of rest. The servomotor was interfaced with the computer and equipped with an A/D board (National Instruments, Austin, TX. The data were stored and analyzed using Lab View software. After the completion of contractile measurements, the muscle was dissected free and weighed.

Histology and Immunohistochemistry

The implant region of the LGAS muscles was removed and divided into thirds such that there was an equal sized top, middle, and bottom region for each muscle. The samples were placed in 10% neutral buffered Formalin (Protocol, Fisher Scientific; Waltham, MA) for 24 hours, and stored in 70% ethanol until further analysis. Samples were embedded in a Tissue Tech paraffin embedding system prior to sectioning on a Reichert-Jung microtome. Eighteen, 5 μm sections from each of the top, middle, and bottom regions of the defect area, for a total of 54 sections per muscle, were subjected to histologic or immunohistochemical staining. Three sections per region were stained per method resulting in a total of nine stained sections per technique per muscle. These sections were quantified as described below and the results were expressed as mean ± standard error for each region within each subgroup. Hematoxylin and eosin staining was performed, as was Masson's trichrome (Sigma-Aldrich; St. Louis, MO) staining to identify regions of collagen-containing ECM, as well as cells within the ECM. To visualize blood vessels, the rabbit anti-human von Willebrand Factor (vWF) polyclonal antibody (1:300: Kit, Dako; Carpinteria, CA) was used to identify endothelial cells. The signal was enhanced with biotinylated polyclonal goat-anti-rabbit IgG with streptavidin-

HRP. Color was developed after incubation with 3,3-diaminobenzidine (DAB). Muscular infiltration into the ECM was further confirmed by immunofluorescent staining for the muscle specific cytoskeleton protein, desmin. Sections were exposed to mouse monoclonal anti-desmin antibody (1:500: Sigma-Aldrich; St. Louis, MO). Sections were then incubated with $F(ab')_2$ Goat Anti-Mouse IgG Fluorescein (1:100, λ = 495nm: Thermoscientific; Waltham, MA) and counterstained with Hoescht 33258 (λ = 395 nm: AnaSpec; San Jose, CA) to identify nuclei. To identify newly regenerated myofibers, an immunofluorescent stain for the skeletal muscle transcription factor, myogenin was performed. Sections were exposed to rabbit polyclonal anti-myogenin antibody (1: 500: Santa Cruz Biotechnologies; Santa Cruz, CA). Sections were then incubated with F(ab')2 Goat Anti-Rabbit IgG Fluorescein and counterstained with Hoescht 33258 (λ = 395 nm: AnaSpec; San Jose, CA) to determine nuclear colocalization. H&E, Masson's trichrome, and vWF sections were visualized with a Nikon Diaphot microscope mounted with an Optronix Microfire digital camera interfaced with a Dell 8250 computer for storage and analysis of images. The area of each region of the ECM implant stained blue for collagen relative to red staining cytoplasm was quantified using LabView. The number of vWF positive structures within each region of the ECM implant of each rat was counted to determine the number of blood vessels/mm^2. A vessel was only counted if its lumen was greater than 20 μm in diameter. Immunofluorescent desmin and myogenin were visualized with a fluorescence microscope (Leica DM LB2) and photographed with a digital camera *(*Leica DFC340FX). The percent area of each region of the ECM implant positive for desmin was quantified using a LabView program developed by Derrell Sloan. Additionally, the number of desmin positive fibers was quantified on three

sections within each region of the ECM in at least 3 animals per group at 28 and 42 days of recovery. Fibers showing nuclear localization of myogenin were counted in randomly selected fields from three sections within each region of the ECM from at least three animals per group at 28 and 42 days of recovery. Counts were performed by investigators blinded to the treatment.

Statistical Analysis

Means of all measurements were analyzed utilizing unpaired Student's T-test and two-way ANOVA with Tukey's post hoc test where applicable. Data are represented as mean ± SEM unless otherwise stated. Significance is defined as $p < 0.05$.

RESULTS

Bone marrow MSCs were analyzed for cell surface markers by FACS analysis. Cells cultured under identical conditions and from the same passage as those injected into the ECM were consistent with described MSCs. Over 99% of cells were positive for CD90 and negative for CD45, CD34, and CD146.

The portion of the LGAS removed to create the defect was 223 ± 5 and 228 ± 6 mg wet weight for ECM-ONLY and ECM-CELL, respectively, which was nearly 20% of the mass of the LGAS. No significant differences in defect size existed between groups or within groups at any time point. Over the course of 42 days after defect creation, the overall morphology of the ECM repaired LGAS was well maintained (Figure 4.2) in both groups, and no difference existed in the LGAS mass.

The maximal isometric tetanic force produced by the LGAS of the ECM-CELL group was significantly higher after 42 days of recovery than after 14 or 28 days of

recovery, and was also significantly higher than the force of ECM-ONLY at all time points ($p < 0.05$) (Figure 4.3). No significant functional recovery of the LGAS occurred over 42 days in ECM-ONLY. Specific tension (SPo), the maximal tetanic force per unit of cross-sectional area, of the LGAS in the ECM-ONLY at 14 days of recovery was 83% ± 8 of the contralateral LGAS, and 84% ± 6 of the contralateral LGAS after 42 days of recovery, which indicated no recovery of SPo occurred. SPo increased significantly in the ECM-CELL group LGAS relative to the contralateral from 77% ± 12 at 14 days of recovery to 94% ± 9 at 42 days of recovery ($p < 0.01$).

Histological analysis of the defect area in ECM-ONLY and ECM-CELL at 14, 28, and 42 days with Masson's Trichrome stain shows increasing cellularity (Figure 4.4) and the appearance of blood vessel-like structures, which were confirmed by staining with von Willebrand Factor, within the ECM (Figure 4.5). Quantification of the Masson's trichrome staining indicated that the cytosolic, red-stained, area relative to collagen, blue-stained, area averaged across the top, middle, and bottom regions increased from recovery day 28 to recovery day 42 in both groups (Figure 4.6). Values for ECM-CELL were higher than ECM-ONLY after 42 days of recovery ($p < 0.05$). Quantification of vWF stained blood vessel walls demonstrated an increase in the number of blood vessels within the ECM implant in the ECM-CELL when compared to ECM-ONLY after 42 days of recovery ($p < 0.05$) (Figure 4.6).

The muscle specific protein desmin and the transcription factor myogenin were used to identify myofibers within the ECM implant (Figure 4.7). After 42 days of recovery, regions of the ECM nearest the transected myofibers in the ECM-CELL group were densely populated with desmin-positive myofibers (Figure 4.8). The number of

desmin positive fibers per square millimeter was significantly higher after 42 days of recovery in the ECM-CELL group compared to all other groups ($p < 0.05$) (Figure 4.9). Significantly more myogenin positive nuclei were found in the MSC-seeded ECMs at 28 and 42 days of recovery (Figure 4.9).

When the defect implant area was examined by region (top, middle, or bottom), the appearance of cellular material and blood vessels was less evident in the ECM-ONLY compared to the ECM-CELL (Figure 4.10). Values for the number of myofibers and blood vessels in the middle third, were significantly lower than the values for the respective top and bottom regions which bordered the transected myofibers, although ECM-CELL middle region values were generally higher than the corresponding ECM-ONLY values (See previously mentioned graphs).

DISCUSSION

The repair of a physical deformity after traumatic injury is important for the psychological well being of victims [107]. Therefore, developing an implant capable of filling in an area of missing tissue to prevent physical deformity is important, but the development of an implant capable of full functional repair of the muscle in addition to aesthetic restoration of the area would be ideal.

The data presented here prove that defect injuries that do not functionally regenerate at all without treatment, can be surgically repaired with an ECM seeded with MSCs such that partial functional recovery occurs and the overall aesthetic appearance is similar to non-injured muscle. This is an important step for the field of muscle regeneration. The functional restoration over 42 days when implanted ECMs were seeded

with MSCs is due to the increase in the number of blood vessels and myofibers growing within the implant, suggesting that the injected, homologous, bone marrow derived cells participate in the regeneration process.

The adherent fraction of cells derived from the bone marrow are generally considered to be a population of cells known as marrow stromal cells or mesenchymal stem cells (MSC) which are multipotent and capable of differentiating into a number of different tissues [79, 108]. To confirm that the adherent bone muscle cells used in this study were MSCs, FACS analysis was performed. The cells were CD90+, CD45-, CD34-, and CD146- which is consistent with published reports of rat MSCs [109-111] Due to the multipotent nature of MSCs, they are a good cell population to use to aid in the regeneration of a loss of a large volume of tissue such as the muscle defect model used in this study. Another reason MSCs are an attractive cell therapy candidate is because they are easily obtained and cultured from the bone marrow, and are immune privileged. In fact, they are already in use in tissue regeneration applications clinically [112].

The improved functional and histological regeneration observed after 42 days in the ECM-CELL group is likely the result of a number of different positive effects attributed to the implanted MSCs. Research from the lab of Blau et al., proved that endogenous cells from the bone marrow participate in muscle regeneration due to physiologic stress [75]. While the participation of these bone marrow cells in muscle regeneration appears to be rare (< 3.5%), they progress from the bone marrow and into the muscle where they become muscle progenitor and/or satellite cells that can be activated in response to muscle injury [20, 113]. The addition of exogenous MSCs to dystrophic skeletal muscle is able to partially restore the expression of dystrophin within

the fibers [23, 85, 114, 115]. Conflict exists as to whether or not the addition of MSCs contributes to skeletal muscle as a result of differentiation into myofibers, fusion of MSCs with existing myofibers with or without differentiation, or by the secretion of trophic substances by the MSCs. Differentiation of MSCs along a myogenic lineage and fusion to form myotubes does occur in vitro [78, 80, 85, 116] and evidence that it also occurs in vivo [86, 114]. Following irradiation and GFP+ marrow replacement, subsequent injury to skeletal muscle showed, that under these conditions, as many as 12% of myofibers may express GFP, indicating significant fusion, but these results might not translate to the direct injection of MSCs into injured areas [117]. Fusion events do appear to occur when tagged MSCs are injected directly into injured skeletal muscle, although they are relatively rare and it is difficult to determine whether or not the MSCs differentiated along a skeletal muscle lineage prior to fusion [118]. Some researchers have noted improvements in cardiac and skeletal muscle regeneration after stem cell treatment without either differentiation of the cells to a myogenic lineage or fusion with resident cells [88, 119]. MSCs release cytokines and growth factors such as vascular endothelial growth factor and improve vascularization and perfusion of damaged tissues including skeletal muscle [120]. The increase in the number of blood vessels in the ECM-CELL after 42 days is likely a result of this mechanism. Further evidence for the paracrine actions of MSCs is the improved regeneration of cardiac muscle following infarction by the injection of cell-free MSC conditioned media into the infarct site [121]. Interestingly, recent evidence proves that MSCs need not even be in the local area of injury to exert their effects. Shabbir et al. showed by injecting MSCs or MSC-conditioned media into distant skeletal muscle and saw significantly improved function in

a heart failure model [122]. Even without tracking the cells injected in this study, at least some of the beneficial effects are likely explained by the trophic factors released by the MSCs. Natsu et al. treated skeletal muscle laceration with bone marrow-derived MSCs and as was seen in this study, the muscle improved functionally without evidence of fusion or differentiation of the injected cells [88].

While this is the first time that MSCs have been seeded on a decellularized ECM, other myogenic progenitor cells have been seeded on decellularized ECMs implanted into skeletal muscle, although functional assessment of these has been limited. Similar to what others have seen with cell-seeded constructs of ECM implanted into defected skeletal muscle of the abdominal wall, the ECMs of the ECM-ONLY and ECM-CELL groups were both capable of supporting the growth of myofibers as well as blood vessels [9, 71, 72]. Gamba et al., however, did not have myofiber ingrowth into decellularized ECM constructs without addition of exogenous cells as opposed to what was observed in this study in the ECM-ONLY groups [7]. The muscle defect model used here is probably provides a more suitable environment for regeneration. The LGAS used in this model is an active, load bearing muscle that is subjected to work during normal cage activity, whereas the rabbit's abdominal muscle that was defected in the Gamba et al. study, is not subjected to the same relative functional demands. Mechanical stimulation and stretch of damaged/regenerating myofibers is known to improve regeneration [98], and it is likely that the activity levels of the LGAS aided in the regeneration of myofibers into the defect area as was observed.

Terada et al. lacerated myofibers and kept the transected ends a designated distance from each other to determine the maximal distance that they could grow to

bridge the gap [39]. A distance greater than 2-3 mm was too far for the myofibers to bridge, which was consistent with what was seen in the ECM-ONLY LGAS. Despite the fact that cells were injected throughout the top, middle, and bottom of the ECM in the ECM-CELL group, only a limited number of desmin and myogenin positive fibers were found in this region. Both groups had did have myofiber ingrowth, but most blood vessels and myofibers were located in the top and bottom thirds of the ECM implant area, less than 3mm from the border of the ECM with the LGAS. Many of the cells expressed myogenin indicating that they were newly regenerated myofibers. These myofibers were likely from the growth of injured myofibers into the ECM from the superior and inferior portions of muscle remaining after the defect injury. Since the injected MSCs were not tagged or tracked, differentiation and/or fusion of the MSCs cannot be ruled out, but the significantly higher number of fibers expressed in regions closer to the border with native muscle tissue indicate that engraftment of cells was not the main method of regeneration. Also, cells injected directly into the middle of the ECM would have been further away from a blood supply, and many of the cells could have died from lack of nutrients before the vascular supply grew to the area, although analysis of the matrix when the cells were injected 7 days post-injury, suggests that blood vessels were in the area. As an implanted ECM remodels, it releases factors that attract myogenic progenitor cells and stimulates their proliferation and differentiation [52, 54, 55]. This in combination with the trophic factors released by the bone marrow derived cells would stimulate the regeneration of myofibers transected during the creation of the defect, and this likely explains the higher population of myofibers and blood vessels in the top and bottom region of the ECM relative to the middle region.

After 42 days, the regeneration of tissue into the injured area in the ECM-CELL group is capable of contributing to significant improvements in function. This improvement of function implies that at least some of the regenerated myofibers were reinnervated, although nerve innervation was not measured. Evidence exists that despite improvements in the short term, cell-seeded ECMs implanted into muscle might not show the same improvements over the long term [71]. Regenerating myofibers that are not reinnervated will degenerate [123]. Since innervation state of the regenerating myofibers was not studied, the myofibers observed in the ECM might not be permanent and allowing longer recovery periods after the procedure might have yielded different results. Since the improvement in function was observed, it is likely that at least some of the fibers were innervated. Future research however, should focus on the neurotization of the constructs at the time of implantation as this is likely to vastly improve function [124]. Another technique that could improve the function in this model further is the use of a larger number of cells. Winkler et al. determined that the addition of 1×10^7 MSCs to a severe muscle crush injury significantly improved the functional recovery of the muscle more than 2.5×10^6 MSCs improved functional recovery [118]. Addition of only 1×10^6 MSCs did not show any significant functional improvement. In the present study, only $1.5 – 2 \times 10^6$ cells were injected into the 1 x 1 cm ECM repaired defect and significant functional improvement was observed. Had this number been higher, the possibility exists that additional functional improvement would have occurred. Further improvements in functional recovery using this model might be observed with the addition of growth factors or by the use of physical therapy regimens involving mobilization and exercise to stimulate the regenerative process.

In conclusion, the data presented demonstrate for the first time, the return of function to a large muscle defect by the addition of MSCs seeded on a decellularized ECM implant. Translation of this technique to the clinic could significantly improve the lives of wounded military personnel and other patients that have lost large portions of muscle tissue.

FIGURE 4.1: DEFECT CREATION - Removal of defect from LGAS. Repair with ECM and BMC Injection

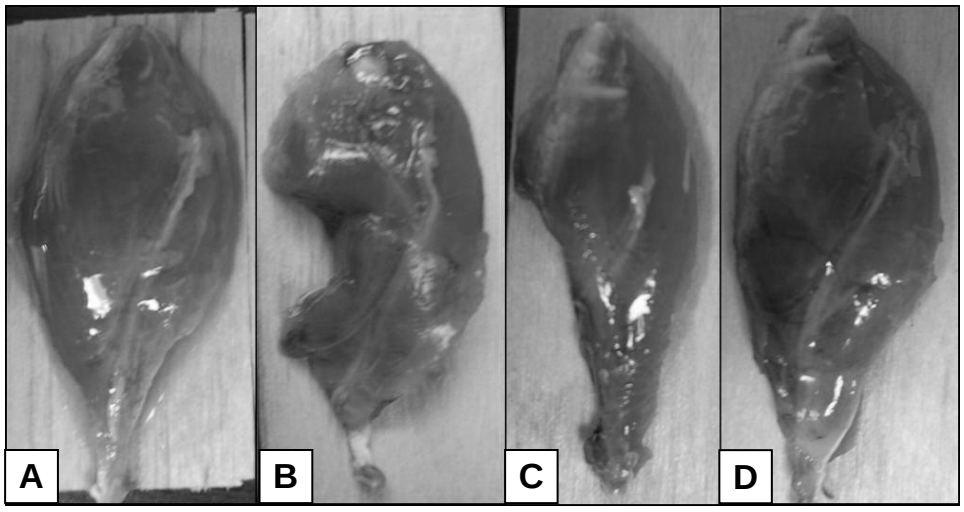

FIGURE 4.2: MORPHOLOGY - (A) Non-operated LGAS (B) Defect LGAS 0-day recovery (C) Defect LGAS 42d recovery (D) ECM LGAS 42d recovery

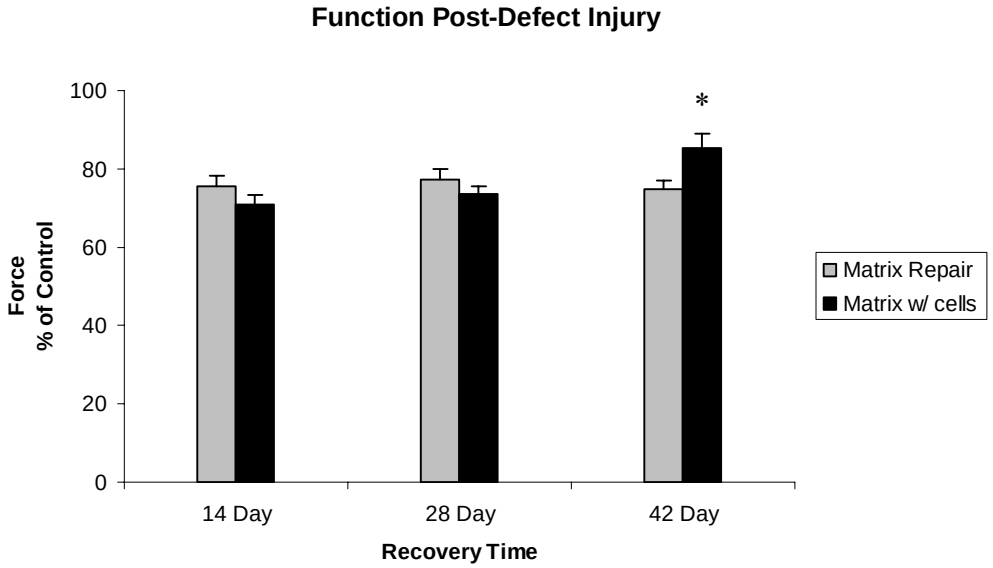

FIGURE 4.3: FUNCTION POST-DEFECT INJURY - Maximal isometric, tetanic tension of defect LGAS relative to contralateral limb 14, 28, and 42 days post injury. * Indicates statistically different from all others ($p < 0.05$).

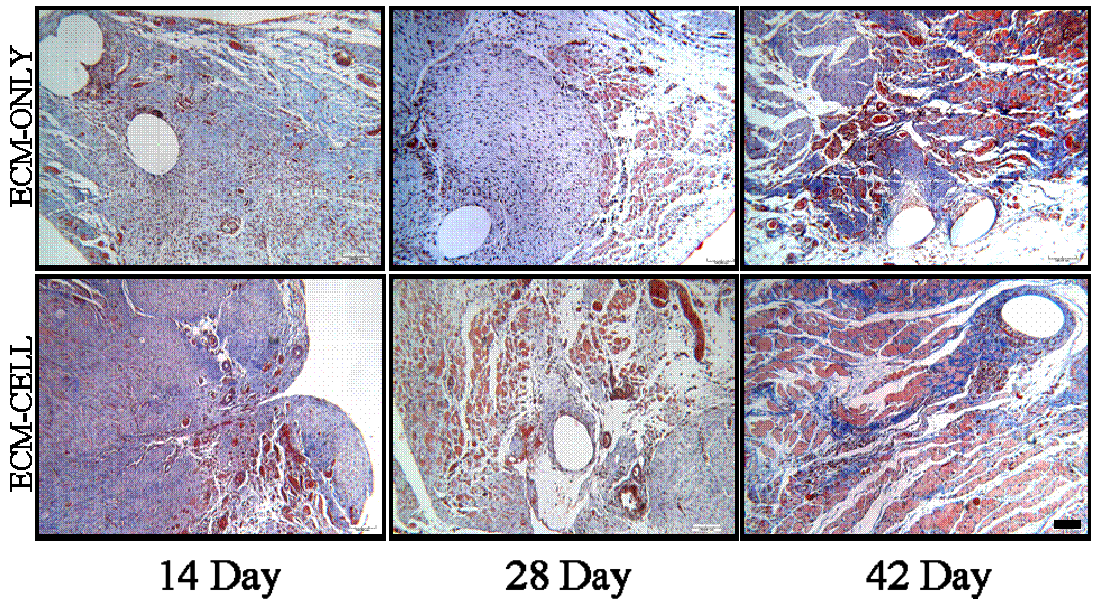

FIGURE 4.4: HISTOLOGY RECOVERY COMPARISON - Masson's Trichrome stain of sections from implanted ECM at designated recovery times. Magnification = 100x. Note: Large circular white spaces are suture holes. Scale = 100 μm.

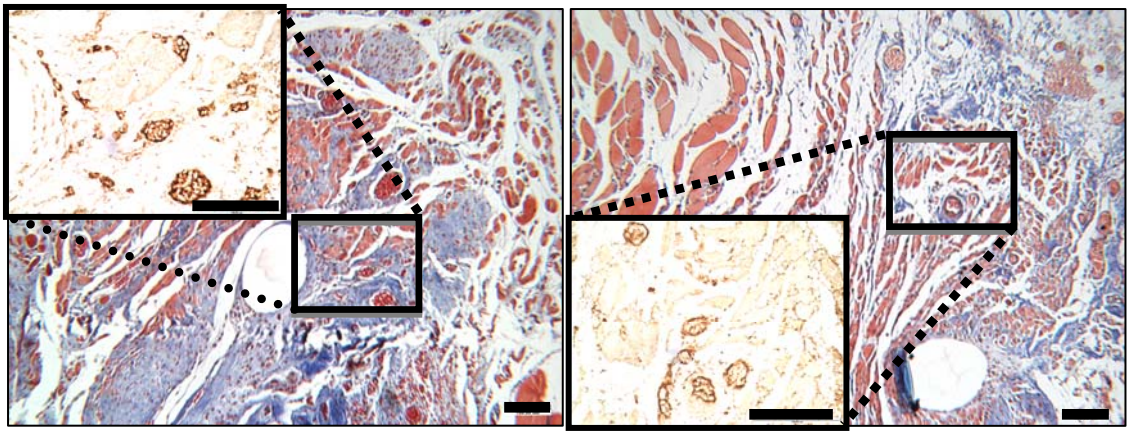

FIGURE 4.5: VON WILLEBRAND FACTOR - Masson's Trichrome stain of sections of implant from 42 Day Recovery of ECM-ONLY (left) and ECM-CELL (right) with insets demonstrating the appearance of vWF positive blood vessels. Magnification: Trichrome = 200x; inset vWF = 400x. Scale = 100 μm.

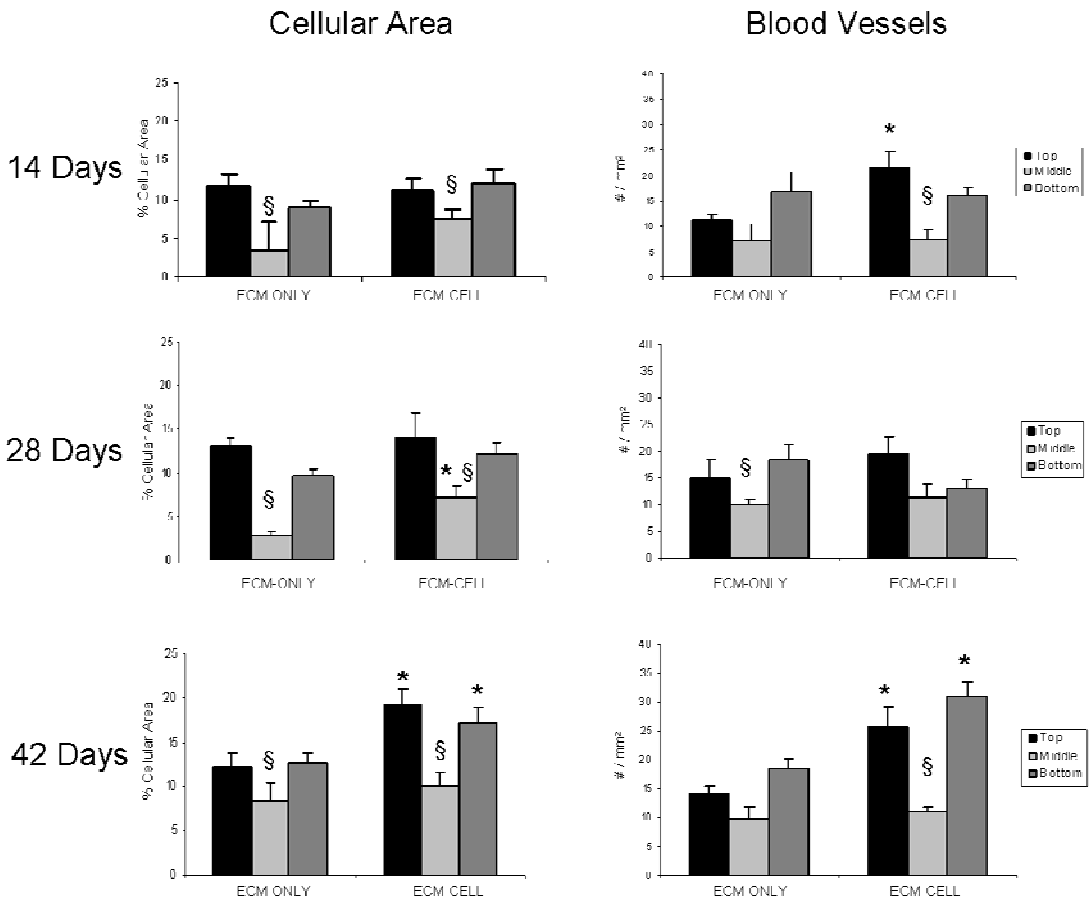

FIGURE 4.6: CELLULAR AREA & BLOOD VESSELS WITHIN DEFECT - *Significantly different from same ECM-ONLY region ($p < 0.05$). § Significantly different from Top and Bottom ($p < 0.05$).

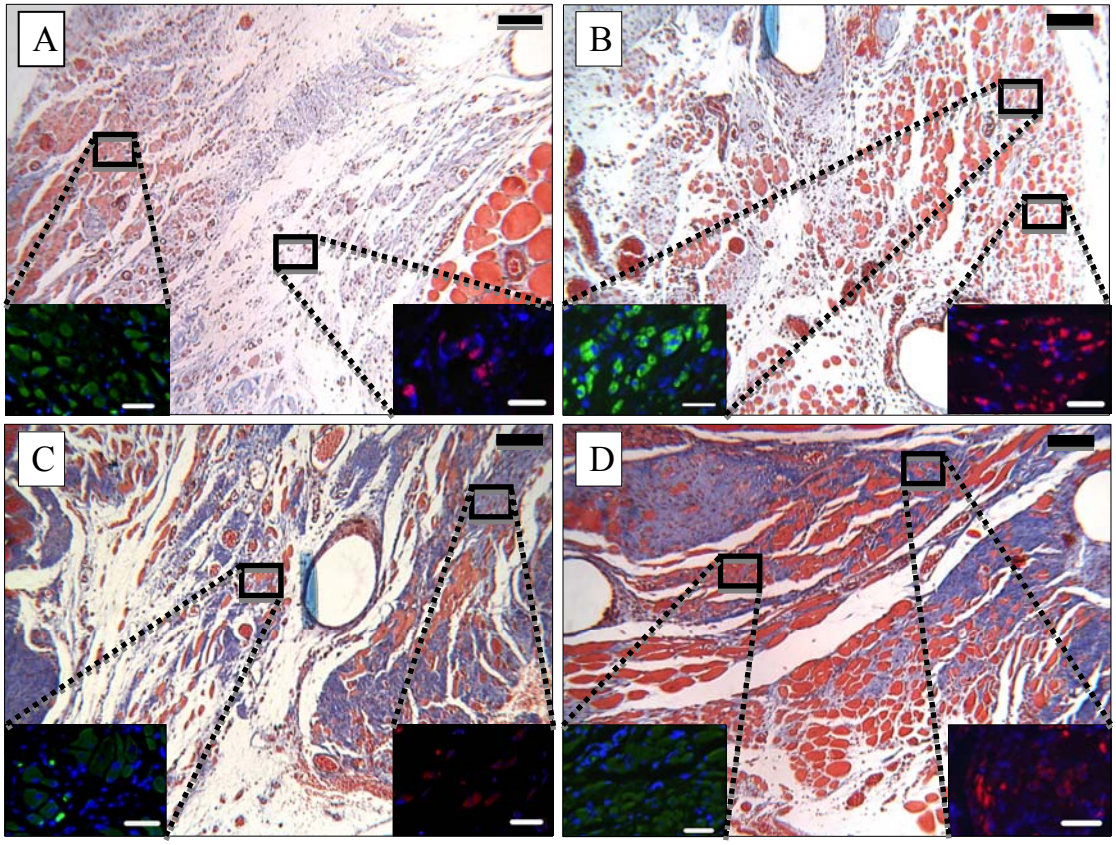

FIGURE 4.7: DESMIN & MYOGENIN IMMUNOFLUORESCENCE - (A) ECM-ONLY at 28 days, (B) ECM-CELL at 28 days, (C) ECM-ONLY at 42 days and (D) ECM-CELL at 42 days. Increased myofiber filtration, desmin and myogenin positive structures with recovery and following cell injection into the defect area. Stained with Masson's trichrome (center), desmin (lower left) and myogenin (lower right). Circular spaces are suture holes. Trichrome scale bar = 100 µm, Desmin/myogenin scale bar = 50 µm.

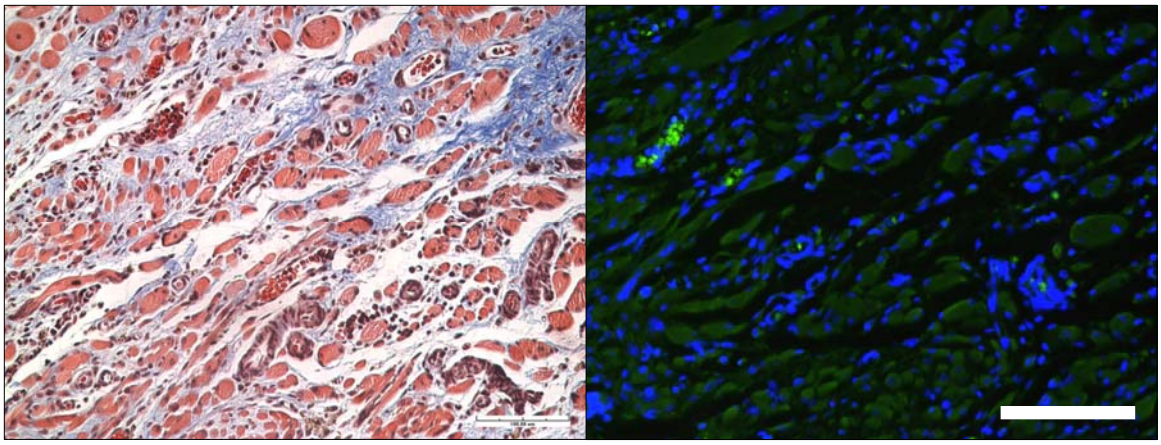

FIGURE 4.8: MASSON'S TRICHROME & DESMIN IMMUNOFLUORESCENCE – Neighboring sections of ECM-CELL 42 day recovery stained with Masson's Trichrome (left) with muscle fibers confirmed by desmin immunofluorescence (right). Scale bar = 100 μm.

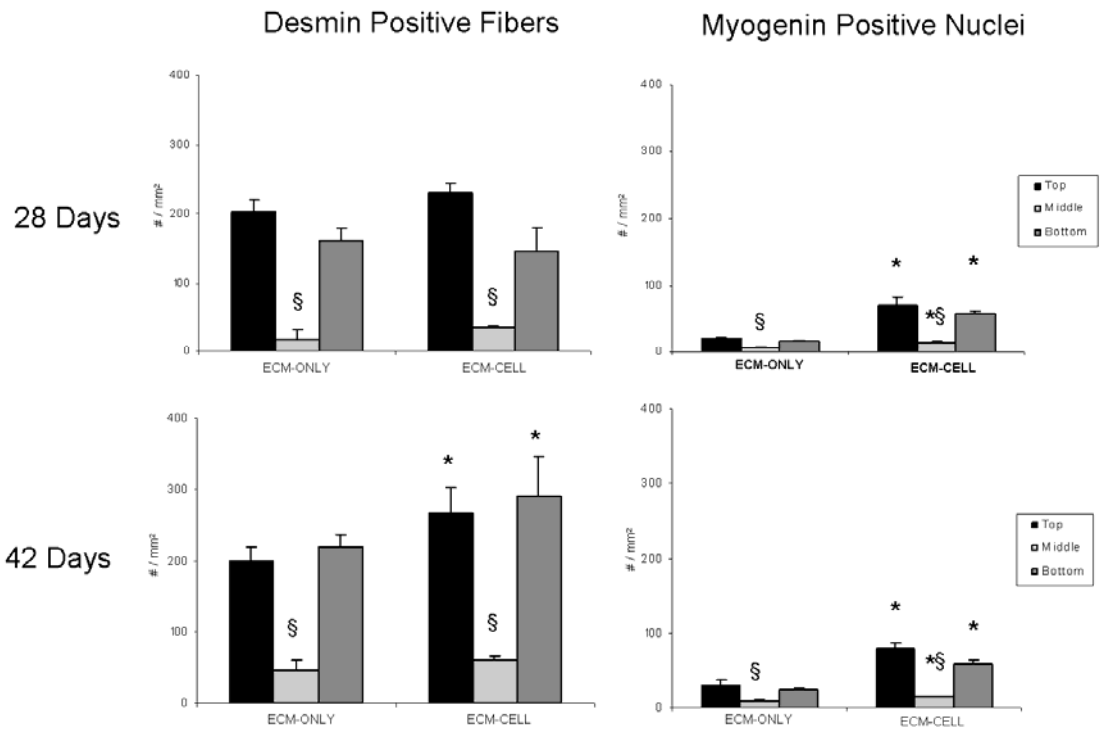

FIGURE 4.9: DESMIN POSITIVE FIBERS & MYOGENIN POSITIVE NUCLEI - *Significantly different from same ECM-ONLY region ($p < 0.05$). § Significantly different from Top and Bottom ($p < 0.05$).

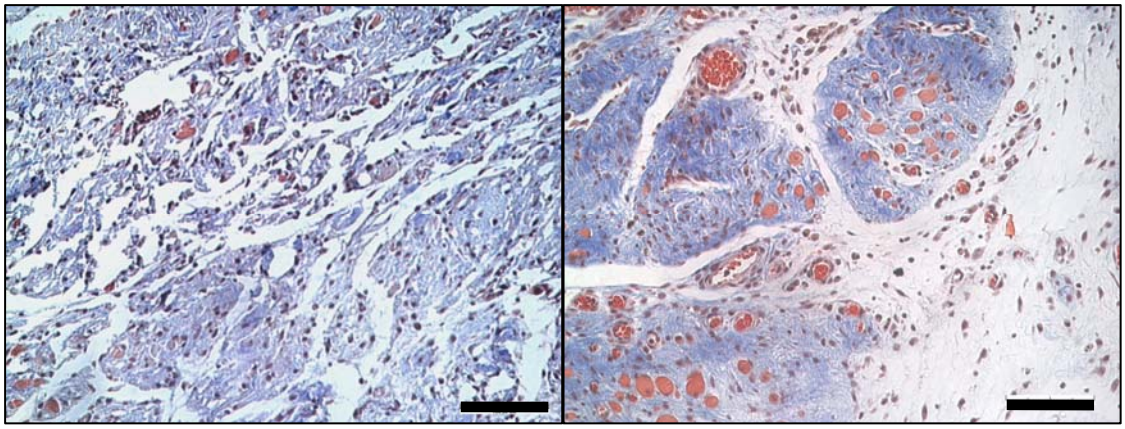

FIGURE 4.10: ECM MIDDLE - Masson's Trichrome of sections from the middle third of the implants after 28 days recovery. ECM-ONLY (left) and ECM-CELL (right). Scale bar = 100 μm.

Chapter V: General Discussion

The goal of this dissertation was to develop a skeletal muscle defect model that resulted in long-term functional deficits and to determine the effectiveness of a surgical repair technique using extracellular matrix with and without the addition of bone marrow derived cells. The results of these studies are summarized below.

SUMMARY OF RESULTS

1. Complete functional recovery of an LGAS lacerated to a depth of 1 cm through its full thickness occurs over the course of six weeks without any intervention. This demonstrates the natural regeneration potential of skeletal muscle and proves that this laceration model is not suited for the study of long-term viability of tissue engineering constructs.
2. The removal of 10% of the LGAS mass results in a functional deficit that remains constant over the course of at least 28 days. The removal of 20% of the LGAS mass results in a functional deficit that remains constant and shows no signs of regeneration over the course of at least 42 days. The lack of functional recovery over the course of six weeks and the subsequent remodeling of the muscle's size and shape indicate that functional loss is permanent.
3. Repair of the LGAS defect with decellularized skeletal muscle ECM prevents the muscle remodeling that occurs when no ECM is implanted. With ECM repair, the overall macroscopic morphology of the muscle is maintained and is relatively normal from an aesthetic perspective.

4. While an implanted ECM alone does not lead to the recovery of function, the ECM does allow for the incorporation of regenerating tissues such as blood vessels and myofibers. This is an important result, because any construct implanted to restore function must allow for the ingrowth of muscle cells and blood vessels to provide oxygen and nutrients.
5. Addition of bone marrow MSCs to the ECM implant partially restores function to the defected LGAS after 42 days of recovery.
6. Addition of bone marrow MSCs to the ECM implant in the LGAS increases the number of regenerating myofibers and blood vessels throughout the defected area. The increase in blood supply and myofibers in the implant within the defected muscle is likely the reason for the partial restoration of function observed after 42 days of recovery.

CONCLUSIONS

This study describes a reproducible skeletal muscle defect model that results in a permanent loss of function. This model can be used to better understand the regeneration process of muscle following traumatic injury involving significant tissue loss. This study also demonstrates the ability of a decellularized ECM construct to maintain morphology and incorporate regenerating tissue when implanted into a muscle defect. This incorporation of regenerating tissues can be further enhanced by the addition of exogenous bone marrow derived MSCs, which also lead to a partial restoration of function in the defected muscle.

Compared to the other defect models used in previous research, the model developed here is superior for the study of the functional aspects of muscle regeneration after tissue loss. This model was created specifically for its relative ease of the functional assessment of various types of engineered constructs designed specifically for skeletal muscle regeneration. The LGAS is a muscle that is very involved in daily activities of the rat and therefore experiences much different demands than other muscles generally used in tissue engineering research. These demands however, are very similar to the demands that must be met by engineered tissues if they are to replace large muscle defects in the clinic. The ease with which the LGAS can be perturbed by various exercise and physical therapy regimens also makes this model ideal to study muscle tissue engineering. The goal of skeletal muscle tissue engineering is to replace lost muscle with functional muscle, and this defect model more closely matches those demands than any other model currently used in research.

The lack of functional recovery in the ECM without the addition of cells is likely due to the limited number and size of myofibers incorporated within the ECM and the fact that the fibers that grow into the ECM do not penetrate more than a few millimeters. However, the addition of the MSCs partially restores the function and increases the number of myofibers and blood vessels that are found within the ECM. The exact mechanism by which the exogenous cells aid in the functional regeneration was not determined, although it is likely due to trophic factors secreted by the cells which are known to enhance regeneration [88] and/or the differentiation and fusion of the cells to form myofibers which can also occur [86, 125], although it is likely that these events are rare. While the importance of understanding the exact mechanism by which bone marrow

derived cells produce beneficial effects should not be understated, the improved functional regeneration seen in this defect model with the addition of the cells is promising and could have tremendous clinical implications.

FUTURE DIRECTIONS

Due to the strengths of this defect model, the use of a number of different tissue engineered muscle constructs is possible. The efficacy of different constructs could easily be compared by implantation of one into one leg and the other into the contralateral leg. Experimentation with muscle constructs grown *in vitro* utilizing explanted microcirculatory beds such as those proven to be effective by Chang et al. [126], could be a good way to ensure long-term viability of constructs used to repair large defects.

Several techniques specific to the ECM and cells used in this study should also be considered for future research. The neurotization of the ECM during implantation by transplantation of a nerve to the ECM is likely to vastly improve function [124]. Function could be further improved by the implantation of more cells. While partial restoration of function occurred with the addition of 1.5 – 2 million cells to the ECM, based on research of skeletal muscle crush injury performed by Winkler et al., it appears that the number of bone marrow derived cells used in this defect model was less than optimal and addition of 10 million cells might have better restored function [118]. Additionally, addition of growth factors or the use of physical therapy regimens involving mobilization and exercise to stimulate the regenerative process could further enhance the repair of the ECM-implanted skeletal muscle defect. The versatility of this model and the promise of

decellularized ECMs and bone marrow derived cells for skeletal muscle repair make this a very exciting field to research.

Appendix A: Expanded Methods

I. Skeletal Muscle Extracellular Matrix Isolation

1. Place whole skeletal muscle into a 50 ml conical tube of deionized (DI) water at 4° C for 12-24 hours.
2. Remove muscle from DI water and place in chloroform at room temperature for 2-4 days depending on the size of the muscle (Soleus 2 days; Gastrocnemius 4 days) Place on rocker to agitate solution.
3. Pour off chloroform into waste container and rinse muscle three times with DI water. Immerse muscle in 2% sodium dodecyl sulfate (w/v) and place on rocker.
4. Change SDS solution every two to three days until muscle is opaque and only ECM remains. Larger muscles might require SDS to be injected into the middle of the muscle in several places every few days.
5. Rinse muscle three times with DI water and then immerse in a 2% antibiotic/ antimyctotic (A/A) DI water solution. Store at 4° C for 24 hours.
6. Rinse muscle three times with DI water and then immerse in 2% A/A PBS and place on rocker. Change solution twice daily to rinse out SDS over 3-4 days.
7. Place muscle in a 2% A/A, PBS solution at 4° C for storage.

II. A. Isolation of Rat Bone Marrow Adherent Cells

1. Remove femurs and tibia of 2 to 4 month old rats.
2. After removing epiphyses and gaining access to marrow cavities, whole bone marrow plugs will be flushed out from tibial and femoral medullary cavities using a 10ml syringe (16 gauge needle) with DMEM supplement with 10% FBS and 1% antibiotic-antimyctotic.
3. Marrow samples will be collected and mechanically disrupted by sequential aspiration through 16, 18, 20 gauge needles attached to the same 10ml syringe.
4. The resulting cell suspension will be centrifuged for 5ml at 1000rpm with cells collected and resuspended in serum-supplemented medium.
5. A small volume of the resuspension will be mixed with 4% acetic acid to lyse red blood cells. Nucleated cells will be counted using a hemocytometer.
6. After counting, cells will be plated at $5X10^7$ cells/100mm culture dish as primary culture and incubated in 5% CO_2 at 37^oC, with fresh medium changes every 3 days.
7. When large cell colonies develop (~ 75% confluent, usually 12-14 days later), cultures are washed twice with PBS and cells are trypsinized with 0.25% trypsin in 1mM EDTA for 5 min at 37^oC.
8. After centrifugation (1000g, 5 min), cells will be resuspended with serum supplement medium, counted, and plated at a density of $5\text{-}7X10^5$ cells/100 mm dish. The resulting culture will be referred to as first passage culture.

B. Culturing of Bone Marrow Adherent Cells

Making Media:

1. Determine the total volume of media that is needed.

a. 35 ml for each flask.
b. Add an additional 10 ml for each flask that is being split.

2. Then calculate how much FBS, AA, EMEM, sodium bicarbonate, non-essential amino acids, and sodium pyruvate that is required.
    a. Volume of EMEM= 0.77*total volume of media
    b. Volume of FBS/sodium bicarbonate = 0.10*total volume of media
    c. Volume of AA/non-essential amino acids/sodium pyruvate = 0.01*total media
3. Add all the ingredients into a sterile container and then place into a water bath at 37°C for at least 15 minutes before use.

Changing Media:

1. For each flask that needs to be changed, aspirate out the old media and add in 35 ml of new media.
    a. Remember flasks that are 75% or more confluent must trypsinized and split/freeze.

Trypsinization:

1. Aspirate out all the old media.
2. Add in 10 ml of DPBS with Ca and Mg into each flask and then aspirate out.
3. Add in 6 ml of trypsin into each flask and place the flasks into incubator.
    a. After 5 minutes, take out the flasks and place under microscope to see if majority of the cells are dislodged. If not, place flasks back into incubator for additional 2-3 minutes.

b. Afterwards, again check for dislodgement. If necessary, tap the side of the flasks to promote dislodgement.

4. Add in 1 ml of FBS into each flask.
5. Transfer the trypsin+FBS solution from each flask into 15 ml conical tubes.
    a. Each flask has its own conical tubes and make sure to keep track which tubes belong to which flasks.
6. Rinse each flask with 8 ml of DPBS without Ca and Mg and then transfer the DPBS solution of each flask into the proper 15 ml conical tube.
7. Place the conical tubes into a centrifuge and spin them at about 4°C for 7 minutes at a speed of about 1250
8. Afterwards, you should get a pellet of cells on the bottom of each conical tube.

Splitting:

1. Aspirate the supernatant of each tube. Be careful not to remove any cells.
2. Add in about 10 ml of media into each tube and then evenly mix up the pellet of cells inside each tube.
3. Split each tube of cells into the desired ratio.
    a. example: 1:5 – equally divide one tube of cells into 5 new flasks.
    b. Make sure that fresh media is already inside the flasks so that the cells are being added onto the media.

Freezing:

1. Make media with 10% DMSO.

2. If necessary, place the tubes into the centrifuge again to reform the pellets.
3. Add in 1.0-1.5 ml of media with DMSO into each conical tubes.

4. Mix up the pellet of cells in each (15ml) conical tube and then transfer the solution of cells into a 1.5 ml conical tube.
5. Place the 1.5 ml conical tubes into the -80°C freezer.
    a. After 1-2 days, the conical tubes can then be placed in liquid nitrogen.

Thawing:

1. Take out the 1.5 ml conical tubes containing the frozen cells and place them into a 37°C water bath until the cells are no longer frozen.
2. Transfer the cells from the 1.5 conical tubes to 15 ml conical tubes.
3. Add 0.4-0.5 ml of FBS into each 15 ml conical tubes. (if desired)
4. Fill the 15 ml conical tubes with DPBS without Ca and Mg and then place them into centrifuge to spin the cells into pellets.
    a. spin at 4°C for 7 minutes at a speed of about 1250
5. Follow the splitting procedure to split the cells into flasks.

III. Muscle Defect Creation and Repair

Prior to beginning any surgical procedures sterilize any instruments that will come into direct or indirect contact with the subject. Rats should be anesthetized and unresponsive to tactile stimuli prior to surgery.

1. With a scalpel, cut a two centimeter incision on the lateral side of the lower limb parallel to the distal portion of the tibia.
2. Separate the biceps femoris muscle from the tibia to expose the lateral side of the lateral gastrocnemius muscle, and separate the lateral gastrocnemius from the soleus muscle along a one centimeter portion just above the Achilles tendon.
3. Place a small aluminum foil plate between the gastrocnemius and the soleus to prevent the soleus from being damaged during creation of the defect.
4. To create the defect, insert two #9 scalpel blades, separated by a spacer, distal to the neuromuscular junction with the proximal most scalpel blade in line with the tibial tuberosity. Cut the lateral gastrocnemius such that there are two lacerations through the full thickness of the muscle.
5. The medial edge still connected to the rest of the muscle should be excised with fine surgical scissors.
6. Measure and weigh the portion of muscle excised.
7. For rats in the defect/repair groups: immediately after the creation of the muscle defect in the lateral gastrocnemius, cut a piece of ECM to the exact size of the defect removed and implant it into the defect's place.
8. Suture the ECM to the remaining muscle stumps using a modified Kessler stitch (5-0 Prolene suture) with care taken to include the epimysium.

9. Mark the border of the implanted ECM with simple sutures (5-0 Prolene) and insure that the implanted ECM and the cut ends of the lateral gastrocnemius remain in contact. Place the sutures were at the medial, proximal, and distal borders of the ECM and lateral gastrocnemius.
10. Close the wound by suturing the cut area of the biceps femoris back together with simple interrupted polypropylene sutures (5-0, Prolene, Ethicon). Close the skin incision with simple interrupted stitches silk suture (4-0, Ethicon) tied with the knot underneath the skin to prevent the stitches from being chewed out.
11. Return rat to home cage for recovery.

IV. *In Situ* Force Measurements

1. Using a scalpel, make an incision in the skin down the midline of the posterior portion of the lower limb from the popliteal area to the calcaneus.
2. Reflect the skin to expose the biceps femoris which inserts along the distal portion of the tibia in rats.
3. Cut and reflect the biceps femoris to expose the medial and LGAS.
4. With care to minimize bleeding and damage to surrounding tissues, isolate the gastrocnemius from the superficial skin and biceps femoris as well as the deep soleus and plantaris.
5. Cut the Achilles tendon and a portion of the calcaneus where it inserts near the foot so that the distal end of the muscle is unattached.
6. Cut the portion of the tibial nerve supplying the medial gastrocnemius and using the calcaneus as an anchor, tie the Achilles tendon to the muscle lever arm of the dual-mode servomotor (model 310 B, Cambridge Technologies).
7. Stimulate the muscle to contract utilizing a stimulator (Model 2100, A-M Systems) with leads applied to the tibial nerve one centimeter proximal to its insertion into the LGAS.
8. Throughout the remainder of the procedure, keep the muscle wet in mineral oil, and maintain the temperature between 35 and 37.5°C with a radiant heat lamp.
9. Adjust the muscle length to optimal length with a micrometer, and determine maximal twitch tension using stimulation of 0.5 Hz.
10. Stimulate the muscle at 150 Hz for peak tetanic tension (P_o). After each contraction, allow the muscle to rest for two minutes. Save all data to the computer.

V. Muscle Removal and Preservation

In order to remove the muscles and preserve them for later analysis, the following procedure(s) should be employed:

1. Cut the skin above the knee all the way around the leg. Remove the skin from the cut end to the ankle using blunt ended scissors.
2. With rat lying on its back, extend the leg upwards (tape the foot to a clip to make it easier) and push hemostats between the hamstrings at the popliteal fossa. Separate the hemostats to split the hamstrings and expose the origin of the medial and lateral gastrocnemius heads as well as the tibial nerve.
3. Carefully run blunt ended scissors up and down medial and lateral sides of the leg between the gastrocnemius and overlying muscles to separate the tissues from the gastrocnemius.
4. Using blunt ended scissors cut away the rest of the tissue overlying the posterior midline of the gastrocnemius. Cut all the way to the calcaneus and peel the tissue off of either side of the gastrocnemius. Cut away the flaps of muscle and skin to fully expose the gastrocnemius.
5. Slide forceps or blunt scissors between the Achilles tendon and the tibia. Push them through and out the opposite side. Using force, slide the instrument down between the tibia and triceps surae muscles towards the knee (be sure to push more on the tibia than the muscles so as not to rip the soleus).
6. Cut the Achilles tendon and pull the tendon down and away from the rest of the leg. The muscles isolated are the triceps surae group - soleus, plantaris, and gastrocnemius. The soleus will be removed first. It will by lying on top of the other

two muscles as it is the deepest muscle and closest to the tibia. It is also more to the lateral side of the limb. Cut the proximal tendon of the soleus close to the knee and pull it back towards the Achilles tendon. With a little force and a small snip of the scissors at the Achilles tendon end, it will come right off. Place in saline.

7. The plantaris and the gastrocnemius both have origins on the distal end of the femur. The medial and lateral edges of the knee will need to be further isolated and some small muscles on either side of it will need to be cut. Using forceps carefully push away some of the connective tissue to expose the proximal ends of the plantaris and gastrocnemius as well as the popliteal artery. With care not to hit the popliteal artery, cut the plantaris as well as the medial and lateral heads of the gastrocnemius as close to the femur as possible.
8. The plantaris and gastrocnemius must be separated by teasing the plantaris' distal tendon away from the Achilles tendon. Once the tendons are separated, the plantaris can be pulled away from the gastrocnemius and both can be placed into saline solution. The gastrocnemius can be further separated into the medial and lateral halves if necessary. Immediately upon removal, the length and weight of all muscles must be measured.
9. The muscles should be stored according to the proper procedure for specific analysis. Usually the muscles will be pinned through the tendons onto labeled wooden sticks and immersed in 10% buffered formalin. The muscles must remain in formalin in at least a 20:1 formalin volume: muscle weight (grams) ratio for 3 hours after which the formalin should be discarded and replaced with fresh formalin. The muscles should remain in the formalin for at least 24 hours, but up to 72 hours for larger muscles that

cannot be cut to a smaller size. Following formalin, the muscles should be immersed in 70% ethanol for at least 24 hours prior to paraffin embedding.

If the muscles are to be frozen, they should first be pinned at length or placed in cassettes and immersed in isopentane (2-methylbutane) and then immediately placed in liquid nitrogen. The muscles should be stored in the -80°C freezer.

VI. Paraffin Embedding of Muscle Samples

Formalin fixed muscle tissue specimens stored in 70% ethanol are embedded in paraffin wax for sectioning on a microtome.

Solution	**Duration**
80% Ethanol	1 x 45 min
95% Ethanol	1 x 45 min
100% Ethanol	3 x 45 min
Xylenes	2 x 45 min
Paraffin (58°C)	1 x 60 min
Paraffin (58°C)	Overnight

Note:

- The dehydration step with 100% ethanol can 45 mins – 1 hour depending on time convenience.
- Clearing with xylene can be between 45 mins – 1 hour to adjust for time.

Following the overnight paraffin step above, muscles should be embedded in paraffin molds using the Tissue Tek embedding center and CryoConsole. Muscle samples should be placed in a mold (HistoPrep) of molten paraffin with care given to insure proper orientation of the muscle tissue. A labeled tissue processing cassette (Sakura) should be placed atop the mold with the muscle before the paraffin has cooled. The embedded muscle sample should be cooled to 0°C on the Tissue Tek CryoConsole. The sample can then be sectioned on the microtome or stored indefinitely at room temperature.

VII. Sectioning of Muscle Samples

1. Paraffin embedded samples should be placed wax side down on ice for at least 10 minutes prior to sectioning.
2. Turn water bath and slide warmer temperatures to 40-45°C.
3. Scrape excess paraffin off of the side of the cassette holding the muscle sample and place it into the Reichert-Jung microtome's specimen holder. Using the screws, adjust the sample so that the cutting surface lies parallel to the microtome blade.
4. Turn the coarse adjustment knob to bring the sample closer to the blade. Once the sample is near the blade, set the microtome section thickness to 10 μm. Begin turning the hand crank to begin cutting the outer paraffin layer off of the embedded muscle sample. Stop when it is apparent that the sample is being cut.
5. Set the microtome section thickness to 5 μm and continue sectioning. Sections will come off in a ribbon. Using a razor blade, isolate two of the sections from the ribbon, and carefully float them on the surface of the water in the water bath.
6. Dip a prelabeled, microscope slide just underneath the floating paraffin muscle sections and carefully pull the slide up underneath of the sections so that the section lies on the microscope slide without wrinkling or folding.
7. Lean the microscope slide and sample against the counter to drop dry for several minutes and then place them on the slide warmer for at least 45 minutes. Store slides for staining procedures.

VIII. Deparaffinization Procedure

Anytime samples have been paraffin embedded, sectioned, and placed on microscope slides, they must first be deparaffinized before staining.

Solution	**Duration**
Xylene	2 x 8 min
100% Ethanol	2 x 8 min
70% Ethanol	2 x 8 min
50% Ethanol	2 x 8 min
30% Ethanol	2 x 8 min
DI Water	3 x 5 min

Proceed to staining.

IX. Hematoxylin & Eosin Staining

If the sections are from paraffin embedded tissue, they must first be deparaffinized. For this procedure, use the tall jars with the slots in the slides. If the slides are placed back to back, 10 can be stained at once in the same jar, but it is easier to put 5 in the same jar. Hematoxylin and Eosin can both be reused, so do not pour them out. Pour them back into the bottle.

Solution	**Duration**
Harris Hematoxylin (PROTOCOL)	5 min
Gentle tap water rinse	Until water runs clear
Eosin (PROTOCOL)	2 min
Gentle tap water rinse	Until water runs clear
70% Ethanol	Rinse several seconds
100% Ethanol	Rinse several seconds
Xylene	Rinse several seconds

Allow the stained slides to dry in the hood and then coverslip with Permount (Fisher Scientific).

X. Masson's Trichrome Staining

If the sections are from paraffin embedded tissue, they must first be deparaffinized. For this procedure, use the tall jars with the slots for the slides. If the slides are placed back to back, 10 can be stained at once in the same jar, but it is easier to put 5 in the same jar.

The Working Weigert's Iron Hematoxylin is an equal volume mix of bottles A & B. The solution can be reused several times, but over time oxidizes and cannot be reused. The slide jars hold ~ 40 ml of solution, so mix 20 ml of A with 20 ml of B.

The Working Phosphotungstic/Phosphomolybdic Acid solution is a mix of the 2 acids with DI water. Mix 10 ml of phosphotungstic acid with 10 ml of phosphomolybdic acid and then add 20 ml of water. All solutions from Sigma-Aldrich.

Solution	**Duration**
Bouin's Solution	15 min at 56°C or overnight at room temp.
Tap water	Gentle rinse until clear
Working Weigert's Iron Hematoxylin	5 or 6 min
Tap water	Gentle rinse until clear
DI water	rinse
Beibrich Scarlett Acid Fuchshin	5 min
Tap water	Gentle rinse until clear
DI water	rinse
Working Phosphotungstic/phosphomolybdic acid	5 min
Aniline Blue	5 min

1% Acetic Acid	2 min
Tap water	Rinse
70% Ethanol	Rinse
100% Ethanol	Rinse
Xylenes	Rinse

Dry in hood and mount coverslip with Permount.

XI. Von Willebrand Factor Staining

Pre-treatment: Dako Target Retrieval Solution:

Solution/Step	**Duration/Notes**
Set-up: Place Coplin jar filled with Target Retrieval Solution in water bath.	Heat water bath to 95-99°C (do not boil).
Deparaffinize and rehydrate tissue sections.	See Deparaffinization Procedure.
Immerse room temperature sections into preheated Target Retrieval Solution in water bath.	20-40 min
Remove entire jar with slides from water bath. Allow to cool at room temp.	20 min
Decant Target Retrieval Solution and rinse sections 2-3x with room temperature TBST.	
Proceed with Staining.	

* During target retrieval steps set out TBST and antibody diluent to equilibrate to room temperature. Approximately 1L of TBST is needed for the entire procedure.

If more TBST is needed:

0.05 mol/L Tris-HCl	For 1L from stock solution:
0.15 mol/L NaCl	50 ml 1M Tris
0.05% v/v Tween 20	0.5 ml Tween

pH = 7.6 Bring to 1L with DI H_2O

Store @ 4°C

Antibody Diluent:

0.05 mol/L

1% BSA

Store @ 4°C

Staining Protocol:

*Note: Do not allow tissue sections to dry during the staining procedure.

Solution/Step	**Duration/Notes**
Follow Pre-treatment Dako Target Retrieval Solution Procedure before staining.	
Equilibrate all kit reagents to room temp.	Perform all incubations at room temp.
1. PEROXIDASE BLOCK:	
Tap off excess water, carefully wipe around specimen to dry. Circle tissue section with pap pen.	
Cover specimen w/ 3% H_2O_2	Incubate 5 min
DI water rinse, Place in fresh TBST bath.	

2. PRIMARY ANTIBODY AND NEGATIVE CONTROL REAGENT:	
Tap off excess TBST and dry slide as before.	
Apply enough user prepared primary antibody or negative control reagent to cover specimen.	1:300 dilution of vWF 5 ul vWF in 1.5 ml diluent for 10 slides Incubate 30 min.
Rinse gently with TBST, place in TBST bath.	
3. LINK:	
Immediately tap off excess buffer and wipe slide as before.	
Apply enough YELLOW drops of Link to cover specimen.	Incubate 15 min (or 30 for enhanced sensitivity)
Rinse slides as in Step 2.	
4. STREPTAVIDIN PEROXIDASE:	
Dry slide as before.	
Apply enough RED drops of Streptavidin to cover specimen.	Incubate 15 min(or 30)
Rinse slides as before.	

5. SUBSTRATE-CHROMOGEN SOLUTION:	
Dry slide as before.	
Cover specimen w/user prepared substrate chromagen.	Mix 1 drop of chromagen with 1 ml of substrate. Incubate 5 min
Rinse in TBS (no tween), then PBS, and allow to dry completely	
Permount	

XII. Immunofluorescence

Primary (1°) Antibodies:

- α-Desmin: identifies the wide desmin band, an intermediate filament found near the Z-disk in sarcomeres (MW = 50-55 kDa); found predominantly in skeletal, cardiac or smooth tissue
    - Sigma, D1033. Stored at 2-8ºC up to one month, -20ºC if stored in working aliquots
- Hoechst 33258: labels nucleic acid (DNA); used to identify nuclei
    - AnaSpec, 83219. Stored at 4ºC, free from light
- Myogenin (M-255): muscle-specific transcription factor that can induce myogenesis; expressed in differentiating muscle cells
    - Santa Cruz Biotechnologies, sc-576. Store at 4ºC up to one year

Secondary (2°) Antibodies

- $F(ab')_2$ Goat Anti-Mouse IgG Fluorescein-Conjugated
    - Thermo Scientific, 31565. Stored at 4ºC, -20ºC if glycerol is added, protect from light
- $F(ab')_2$ Goat Anti-Rabbit IgG Fluorescein-Conjugated
    - Fischer Scientific, 31579. Stored at 4ºC, -20ºC if glycerol is added, protect from light
- Antibody Label: fluorescein- or rhodamine-conjugated 2° antibodies are appropriate; may contain a fluorochrome (ex. FITC)

- Two-step biotin/avidin system may be used to increase amplification; avidin will bind to multiple sites on biotinylated 2° antibody; high affinity, essentially irreversible reaction
- Excitation Wavelengths
  - Fluorescein: 495 nm; broad spectrum; easily photobleached
  - Rhodamine: 570 nm
  - Hoechst: 395 nm

Blocking Agents:

- Bovine Serum Albumin (BSA): can stabilize enzymes and enzymatic reactions; also prevents adhesion of enzymes to equipment surfaces
  - Fischer Scientific, BP1605-100
  - Stored at 4ºC
- Normal Rat Serum: used to inhibit non-specific binding of antibodies during immunofluorescent staining procedures
  - MP Biomedicals, 64294
  - Stored at 2-8ºC (both freeze-dried and reconstituted)

Desmin/Hoechst Staining Protocol

Solutions:

- α-Laminin/α-Desmin
- $F(ab')_2$ Goat Anti-Goat IgG Fluorescein
- Hoechst 33258
- Xylenes
- Ethanol
- Tris-buffered saline (TBS)
- TBST
- Tween 20
- Phosphate-buffered saline (PBS)
- Bovine serum albumin (BSA)
- Normal rat serum
- Mounting medium

Deparaffinization & Hydration:

- Place slides in slide holders and immerse slides in each solution, contained in Columbia staining dishes:
    - Xylenes: 2 x 8 minutes
        - Xylenes must be handled under the hood; be careful to not spill and always used glove when handling xylenes
    - 100% Ethanol: 2 x 8 minutes
    - 70% Ethanol: 2 x 8 minutes
    - 50% Ethanol: 2 x 8 minutes

- 30% Ethanol: 2 x 8 minutes
- DI H_2O: 3 x 5 minutes
  - Avoid drying (may cause background resulting from non-specific binding); if dry, rehydrate with DI H_2O for 15-30 min

Antigen Exposure & Retrieval:

- Immerse slides in 2 N HCl for 30 – 60 minutes @ 21ºC
- Immerse slides in 1x TBST (0.1% Tween 20) for 4 hours – overnight @ 21ºC
  - PBS may be used but may precipitate; TBST is preferred
  - Tween 20 is used to decrease surface tension, allowing for increased antigen exposure
- Immerse slides in 10% normal rat serum in 1x TBS (1.0% BSA): 2 hours @ 21ºC
  - Rat serum is preferred but goat serum may be substituted
  - Solution can be reused once within one week if stored at 4ºC

Primary Antibody Incubation:

- Dry slides for 5 minutes and place in humid boxes
  - Humid boxes will prevent drying during incubation; they are covered and consist of TBS-soaked tissue paper and glass rods suspending the slides over TBS
- Apply several drops (until section is covered) of the primary antibody:
  - α-Desmin: 1:500 in 1x PBS (1.0% BSA)
- Incubate for 12 hours – overnight @ 4ºC

Secondary Antibody Incubation:

- Wash slides with 1x TBST (0.1% Tween 20): 3 x 5 minutes
- Dry slides for 5 minutes and place in humid boxes

- Repeat the above incubation procedure with the secondary antibody
    - $F(ab')_2$ Goat Anti-Mouse IgG Fluorescein: 1:100 in PBS
- Incubate for 60 – 90 minutes @ 4ºC; must be protected from light

Counterstain Incubation:

- Wash slides with 1x TBST (0.1% Tween 20): 3 x 5 minutes
- Dry slides for 5 minutes and place in humid boxes
- Repeat the above incubation procedure with desired counterstain
    - Hoechst 33258 (pentahydrate bis-benzimide): 1 µL/mL H_2O
- Incubate for 45-60 min @ 4ºC; must be protected from light
    - Hoechst used in place of DAPI because it will not precipitate, while DAPI may in the presence of TBS

Mounting:

- Wash slides with 1x TBS: 3 x 5 minutes
    - Last wash is not TBST because Tween 20 causes coverslips to come off easily
- View slides before mounting as they may need an additional PBS wash to remove background; PBS has a lower pH and is easier on the slides
- Dry slides for 20 – 30 minutes
- Mount slides by pipetting several drops of mounting medium onto slides and cover with coverslips
    - May also used antifade mounting reagent (Prolong Gold, Invitrogen) to protect fluorescence and better maintain slides
    - Slides can be viewed for 1-2 weeks using regular mounting medium

Myogenin/Hoechst Staining Protocol

Solutions:

- MyoD/Myogenin
- $F(ab')_2$ Goat Anti-Rabbit IgG Fluorescein
- Hoechst 33258
- Xylenes
- Ethanol
- Tris-buffered saline (TBS)
- TBST
- Tween 20
- Phosphate-buffered saline (PBS)
- Bovine serum albumin (BSA)
- Normal rat serum
- Mounting medium

Deparaffinization & Hydration:

- Place slides in slide holders and immerse slides in each solution, contained in Columbia staining dishes:
    - Xylenes: 2 x 8 minutes
        - Xylenes must be handled under the hood; be careful to not spill and always used glove when handling xylenes
    - 100% Ethanol: 2 x 8 minutes
    - 70% Ethanol: 2 x 8 minutes
    - 50% Ethanol: 2 x 8 minutes

- 30% Ethanol: 2 x 8 minutes
- DI H_2O: 3 x 5 minutes
  - Avoid drying (may cause background resulting from non-specific binding); if dry, rehydrate with DI H_2O for 15-30 min

Antigen Exposure & Retrieval:

- Immerse slides in 2 N HCl for 30 – 60 minutes @ 21ºC
- Immerse slides in 1x TBST (0.1% Tween 20) for 4 hours – overnight @ 21ºC
  - PBS may be used but may precipitate; TBST is preferred
  - Tween 20 is used to decrease surface tension, allowing for increased antigen exposure
- Immerse slides in 10% normal rat serum in 1x TBS (1.0% BSA): 2 hours @ 21ºC
  - Rat serum is preferred but goat serum may be substituted
  - Solution can be reused once within one week if stored at 4ºC

Primary Antibody Incubation:

- Dry slides for 5 minutes and place in humid boxes
  - Humid boxes will prevent drying during incubation; they are covered and consist of TBS-soaked tissue paper and glass rods suspending the slides over TBS
  - Myogenin (M-225)
- Incubate for 12 hours – overnight @ 4ºC

Secondary Antibody Incubation:

- Wash slides with 1x TBST (0.1% Tween 20): 3 x 5 minutes
- Dry slides for 5 minutes and place in humid boxes
- Repeat the above incubation procedure with the secondary antibody

- $F(ab')_2$ Goat Anti-Rabbit IgG Fluorescein

- Incubate for 60 – 90 minutes @ 4ºC; must be protected from light

Counterstain Incubation:

- Wash slides with 1x TBST (0.1% Tween 20): 3 x 5 minutes
- Dry slides for 5 minutes and place in humid boxes
- Repeat the above incubation procedure with desired counterstain
  - Hoechst 33258 (pentahydrate bis-benzimide): 1 µL/mL H_2O
- Incubate for 45-60 min @ 4ºC; must be protected from light
  - Hoechst used in place of DAPI because it will not precipitate, while DAPI may in the presence of TBS

Mounting:

- Wash slides with 1x TBS: 3 x 5 minutes
  - Last wash is not TBST because Tween 20 causes coverslips to come off easily
- View slides before mounting as they may need an additional PBS wash to remove background; PBS has a lower pH and is easier on the slides
- Dry slides for 20 – 30 minutes
- Mount slides by pipetting several drops of mounting medium onto slides and cover with coverslips
  - May also use antifade mounting reagent (Prolong Gold, Invitrogen) to protect fluorescence and better maintain slides
  - Slides can be viewed for 1-2 weeks using regular mounting medium

XIII. Measurement of Muscle Fiber Length and Angle

1. Pin the muscle at resting length and fix overnight in 10% Formalin.
2. Immerse the muscle in 20% nitric acid for 12 - 24 hours to dissolve connective tissue.
3. Replace nitric acid solution with a 50% glycerol solution.
4. Measure the resting length of the whole muscle and measure the angle of pinnation, then separate the muscle into several bundles.
5. Tease single fibers out from the bundles from proximal, middle, and distal portions and measure their length under 10x magnification. Measure at least 12 fibers from each muscle to get the mean fiber length.

Appendix B: Raw Data

I: Laceration Data

	Pre Lac Body Wt (g)	Post Lac Body Wt (g)	LAC *in situ* Force (N)	CON *in situ* Force (N)	LAC Twitch (N)	CON Twitch (N)	LAC Gas Mass (mg)	Lac Plan Mass (mg)	Lac Sol Mass (mg)	Con Gas Mass (mg)	Con Plan Mass (mg)	Con Sol Mass (mg)
L4201	480	495	25	21.5	3.1	4.4	2651	596	232	2676	554	212
L4202	485	502	40	32.5	5.5	7	2965	715	239	3061	664	260
L4203	513	513	39.5	36	8		2715	597	214	2804	555	240
L4204	527	531	42	48	6	7	2891	719	229	3012	675	226
L4205	475	521	47	42	8.7	9.4	3142	702	260	3119	680	214
L4206	560	580	46	46	7	7.6	3202	790	294	3406	750	295
L4207	465	475	29	38	6.3	7.9	2616	526	193	2574	535	185

II: Small Defect Data –Sprague Dawley Rats

0 Day Recovery

SD	Body Wt (g)	Defect Size (mg)	Defect Force (N) (in situ)	Defect Twitch (N)	Con Force (N) (in situ)	Con Twitch (N)	Def Medial Gas Wt (mg)	Def Lateral Gas Wt (mg)	Con Medial Gas Wt (mg)	Con Lateral Gas Wt (mg)
D001	552	172	41	8	49	9.3	1356	1631	1457	1784
D002	518	124	45	8.1	51	8.8	1335	1491	1345	1614
D002-2		140	44		51					
D003	517	134	42	9.2	48	9	1349	1578	1376	1712
D004	560	103	45	7.6	47	8.5	1293	1723	1275	1814

14 Day Recovery

SD	Pre Def Body Wt (g)	Def Wt (mg)	Post Def Wt (g)	Defect Force (N) (in situ)	Defect Twitch (N)	Con Force (N) (in situ)	Con Twitch (N)	Def Medial Gas Wt (mg)	Def Lateral Gas Wt (mg)	Con Medial Gas Wt (mg)	Con Lateral Gas Wt (mg)
D1401	575	227	566	42.5	42	6.7	6.6	1412	1422	1387	1746
D1402	576	123	560	32	47	7.5	8.1	1364	1643	1423	1808
D1403	560	202	555	40.5	47	7.1	7.5	1351	1487	1369	1806
D1404	479	154	487	22.5	25	5.2	5.1	1432	1364	1279	1723
D1405	494	154	508					1374	1389	1268	1707
D1406	530	155	534	44		6.8	7	1276	1540	1498	1939
D1407	537	140	549	38	40	7	7.7	1492	1583	1901	1920

III. Large Defect Data

0 Day Recovery

SD	Body Wt (g)	Defect Size (mg)	Defect Force (N) (in situ)	Defect Twitch (N)	Con Force (N) (in situ)	Con Twitch (N)	Def Medial Gas Wt (mg)	Def Lateral Gas Wt (mg)	Con Lateral Gas Wt (mg)	Con Medial Gas Wt (mg)
D005	520	301	44.5	8.2	52	9.8	1241	1335	1699	1291
D006	598	289	41	8	52	10	1290	1613	1634	1299
D007	551	315	42	6.5	46	10.5	1284	1385	1714	1287
D008	549	263	43	8.2	53	8.3	1244	1517	1785	1415
D009	551	333.3	35	9.5	53	10.5	1341	1627	1847	1432
D010	485	275	33	6.1	44	10.2	1295	1320	1632	1382
D011	560	355	38	7	53	10				
D012	516	347	34	9.8			1263	1513	1804	1724

14 Day Recovery

SD	Body Wt (g)	Defect Size (mg)	Post Def Body Wt (g)	Defect Force (N) (in situ)	Con Force (N) (in situ)	Defect Twitch (N)	Con Twitch (N)	Def Medial Gas Wt (mg)	Def Lateral Gas Wt (mg)	Con Lateral Gas Wt (mg)	Con Medial Gas Wt (mg)
D1408	516	330	517	37	42	6.1	11	1181	1246	1132	1573
D1409	498	239	480	34.25	44.75	7.2	9.6	1265	1278	1157	1551
D1410	615	354	615	38	52			1536	1705	1404	1937
D1411	580	308	578	46	54	8.4		1470	1579	1380	1854

28 Day Recovery

SD	Body Wt (g)	Defect Size (mg)	Post Def Body Wt (g)	Defect Force (N) (in situ)	Con Force (N) (in situ)	Defect Twitch (N)	Con Twitch (N)	Def Medial Gas Wt (mg)	Def Lateral Gas Wt (mg)	Con Lateral Gas Wt (mg)	Con Medial Gas Wt (mg)
D2801	434	325	450	39	48.2	8.6	10.6	1233	1073	1178	1492
D2802	475	242	494	43.5	52	9.8	11.6	1381	1350	1316	1633
D2803	488	386	506	41	50.5	9	12.3	1287	1661	1301	1997
D2804	470	216	495	37.5	47.5	10.2	11.6	1296	1316	1272	1547
D2805	400	281	420	37	42			1161	1112	1062	1395
D2806	437	271	464	26	46	7.8	11.7	1201	1245	1155	1394
D2807	437	327	448	42.5	49	8.1	10.1	1223	1238	1212	1605
D2808	470	353	485	38		8.4		1263	1238	1224	1547

IV: Lewis Rat Defect Data

A. Defect Only

Defect 0 Day Recovery

	Pre Def Wt (g)	Def Wt (mg)	Post Def Wt (g)	DEF in situ (N)	CON in situ (N)	DEF twitch (N)	CON twitch (N)	Def Sol Wt (mg)	Def Plan Wt (mg)	Def MGAS Wt (mg)	Def LGAS Wt (mg)	Con Sol Wt (mg)	Con Plan Wt (mg)	Con MGAS Wt (mg)	Con LGAS Wt (mg)	Def L Gas Length	Con L Gas Length
D013	502	270	502	15.7	23.5	4.8	11.9	254.8	482.2	1178	1168.6	231.9	491.7	1262.2	1294.9	33	32.5
D014	535	226	535	17.2	20.33	4.1	4.8	221.7	560.7	1319.5	1219.1	233.3	540.3	1442	1444.7		
D015	510	250	510	11.2	22.4	2.7	3.3	195	458	1028	1034	179	438	1066	1255		

Defect 7 Day Recovery

	Pre Def Body Wt (g)	Def Wt (mg)	Post Def Body Wt (g)	DEF in situ (N)	CON in situ (N)	DEF twitch (N)	CON twitch (N)	Def Sol Wt (mg)	Def Plan Wt (mg)	Def MGAS Wt (mg)	Def LGAS Wt (mg)	Con Sol Wt (mg)	Con Plan Wt (mg)	Con MGAS Wt (mg)	Con LGAS Wt (mg)	Def L Gas Length	Con L Gas Length
D0701	463	264	468	13.4	23.5	3.6	10.6	231.3	490.8	1162.5	1116.7	232	477.1	1141.6	1355.7	32	32
D0702	502	299	499	14.8	22	4.3		239	532.7	1203	1081.6	211.2	473.4	1155.2	1255	31	30
D0703	516	202	521	14.2	21.3	2.9		265	528	1193	1072	206	470	1188	1211	33	33
D0704	506	212	493	16.9	23	1.75	4.3	280	509	1219	946	237	440	1048	1265		
D0705	540	238	523	17.6	22.4	4.1	5.5	244	525	1210	1069	231	476.2	1147.1	1288.9	32	31
D0706	496	233	490	16.4	20.7	3.88	5.4	231	506.3	1183	1040	218	449.8	1120.1	1252	31.5	31

Defect 14 Day Recovery

	Pre Def Body Wt (g)	Def Wt (mg)	Post Def Body Wt (g)	DEF in situ (N)	CON in situ (N)	DEF twitch (N)	CON twitch (N)	Def Sol Wt (mg)	Def Plan Wt (mg)	Def MGAS Wt (mg)	Def LGAS Wt (mg)	Con Sol Wt (mg)	Con Plan Wt (mg)	Con MGAS Wt (mg)	Con LGAS Wt (mg)	Def L Gas Length	Con L Gas Length
D1413	461	280	468	15.1	23.2	7.2	8.7	253.6	556.5	1160.7	1083	229	486.7	1121.2	1249.6	31	30
D1414	463	202	496	18.5	23.9	5.3	8.2	227.1	494.5	1146.1	1157.9	209.3	462.2	1148.9	1255.5	30	30
D1415	454	250	476	15.1	21.4	5.7	7.8	237.2	511.5	1212.6	1044.8	213.3	500.6	1137.5	1220.2	30	29
D1416	476	202	502	17.5	21.6	3.8		230	430	1248	1134	202	494	1172	1250	31.5	31
D1417	501	210	524	15.2	20.8	2.5	4.4	200	584	1265	977	226	496	1150	1365	31	30
D1418	463	242	455	15.1	21.5	2.54	5.3	269	524	1155	1000	219	466	1016	1246	33.5	33

Defect 28 Day Recovery

	Pre Def Body Wt (g)	Def Wt (mg)	Post Def Body Wt (g)	DEF in situ (N)	CON in situ (N)	DEF twitch (N)	CON twitch (N)	Def Sol Wt (mg)	Def Plan Wt (mg)	Def MGAS Wt (mg)	Def LGAS Wt (mg)	Con Sol Wt (mg)	Con Plan Wt (mg)	Con MGAS Wt (mg)	Con LGAS Wt (mg)	Def L Gas Length	Con L Gas Length
D2810	465	235	505	17.9	23.1	3.3	4.0	249.0	511	1194	1148	221	517	1090	1263	31	30.5
D2811	479	265	505	16.6	22.2	3.6		229.0	530	1168	1088	201	466	1019	1278	32	31
D2812	515	215	545	17.7	23.8	3.1	4.7	250.0	519	1329	1178	222	498	1219	1250	31.5	31
D2813	509	237	552	17.7	22.4	3.8	3.8	242.0	522	1256	1113	232	479	1213	1418	34	33
D2814	517	212	540	18.1	23.1	4.2	4.4	255.0	553	1215	1226	219	513	1185	1400	33	32
D2815	467	245	494	15.4	19.8	3.7	4.1	236.0	532	1255	940	201	451	1092	1208	32	32

Defect 42 Day Recovery

	Pre Def Body Wt (g)	Def Wt (mg)	Post Def Body Wt (g)	DEF in situ (N)	CON in situ (N)	DEF twitch (N)	CON twitch (N)	Def Sol Wt (mg)	Def Plan Wt (mg)	Def MGAS Wt (mg)	Def LGAS Wt (mg)	Con Sol Wt (mg)	Con Plan Wt (mg)	Con MGAS Wt (mg)	Con LGAS Wt (mg)	Def L Gas Length	Con L Gas Length
D4201	465	292	465	23.5	25.2	3.3	4.1	266	683	1350	1382	245	583	1261	1590	32	31
D4202	475	209	525	14.7	20.2	2.1		230	491	1240	1120	211	478	1121	1311	33	32
D4203	443	212	479	13.3	20.5	2	3.1	220	466	1109	979	222	454	1056	1219	32	32
D4204	468	266	517	18.1	22.9	3.4	4.5	270	533	1195	1030	219	461	1129	1264	32	31.5
D4205	450	263	476	14.6	21	3.6	4.7	245	490	1162	955	205	427	1047	1167	31	30
D4206	415	238	454	13.9	21.3	2.9	4.84	260	468	1043	862	202	397	966	1152	32	31

B. ECM-ONLY

ECM-ONLY 7 Day Recovery

	Pre Def BodyWt (g)	Def Body Wt (mg)	Post Def Body Wt (g)	DEF in situ (N)	CON in situ (N)	DEF twitch (N)	CON twitch (N)	Def Sol Wt (mg)	Def Plan Wt (mg)	Def MGAS Wt (mg)	Def LGAS Wt (mg)	Con Sol Wt (mg)	Con Plan Wt (mg)	Con MGAS Wt (mg)	Con LGAS Wt (mg)	Def LGas Length	Con LGas Length
M0701	417	315	417	12.9	20.2	3.8	4.5	204	435	1080	1737	192	414	970	1135		
M0703	496	211	486	20.2	22.4	3.6	4.2	221	529	1236	1304	204	460	1117	1250	32	31.5
M0704	498	236		19.1	21.5	4.06	5.2	191	478	1189	1515	185	439	1049	1262	34	34
M0705	493	211	490	15.4	23.9	3.7	5.2	221	487	1178	1382	221	490	1126	1260	33	33
M0706	420	197	421	14.8	20.8	3.1	4.7	176	441	1521	955	164	431	1049	915	30	30

ECM-ONLY 14 Day Recovery

	Pre Def BodyWt (g)	Def Body Wt (mg)	Post Def Body Wt (g)	DEF in situ (N)	CON in situ (N)	DEF twitch (N)	CON twitch (N)	Def Sol Wt (mg)	Def Plan Wt (mg)	Def MGAS Wt (mg)	Def LGAS Wt (mg)	Con Sol Wt (mg)	Con Plan Wt (mg)	Con MGAS Wt (mg)	Con LGAS Wt (mg)	Def LGas Length	Con LGas Length
M1406	480	240	504	16.3	22.3	2.9	3.6	224	483	1109	1081	204	427	1107	1161	32.5	32
M1407	485	218	490	16.1	21.3	3.2	3.8	220	484	1160	1214	225	473	1090	1285	35	36
M1408	478	217	487	14.6	22	2.85	4.5	243	513	1270	1095	214	467	1110	1251	32	32
M1409	470	235	498	16.1	21.4	3.4	4	212	523	1211	1295	207	436	1130	1276	32	31
M1410	519	208	526	15.1	19.6	2.4	2.4	266	540	1286	1034	226	509	1167	1237	31	32
M1411	479	212	488	16.2	18.8	3.2	4.2	212	473	1192	1033	181	432	1067	1244	33	33

ECM-ONLY 28 Day Recovery

	Pre Def BodyWt (g)	Def Body Wt (mg)	Post Def Body Wt (g)	DEF in situ (N)	CON in situ (N)	DEF twitch (N)	CON twitch (N)	Def Sol Wt (mg)	Def Plan Wt (mg)	Def MGAS Wt (mg)	Def LGAS Wt (mg)	Con Sol Wt (mg)	Con Plan Wt (mg)	Con MGAS Wt (mg)	Con LGAS Wt (mg)	Def L Gas Length	Con L Gas Length
M2811	507	205	508	16.6	20.6	3.4	4.3	234	527	1161	1105	205	440	1041	1313	32	32
M2812	492	210	503	16.2	19.1	3.5	3.8	230	532	1168	1095	205	437	1072	1238	32.5	33
M2813	461	211	493	16.6	21	3.2	3.5	240	537	1202	1025	185	453	1094	1249	32	32
M2814	495	224	510	15.4	19.7	3.1	4.4	240	497	1265	1085	205	439	1050	1335	30.5	31
M2815	512	246	521	13.9	21.3	2.9	4.1	240	513	1197	1029	200	469	1020	1232	31	32
M2816	546	287	552	15.6	20.6	3.3	4.2	255	529	1240	1101	207	454	1079	1309	31.5	31.5

ECM-ONLY 42 Day Recovery

	Pre Def BodyWt (g)	Def Body Wt (mg)	Post Def Body Wt (g)	DEF in situ (N)	CON in situ (N)	DEF twitch (N)	CON twitch (N)	Def Sol Wt (mg)	Def Plan Wt (mg)	Def MGAS Wt (mg)	Def LGAS Wt (mg)	Con Sol Wt (mg)	Con Plan Wt (mg)	Con MGAS Wt (mg)	Con LGAS Wt (mg)	Def L Gas Length	Con L Gas Length
M4201	455	303	525	16.5	22.55	2.5	4.5	286	572	1376	1231	219	497	1174	1233	30.5	30.5
M4202	427	279	505	14.9	23.1	3.9	6.1	245	575	1240	1285	258	524	1209	1431	32	30
M4203	487	216	515	18.1	23.7	2.9	4.3	228	508	1240	1100	205	498	1142	1301	32	32
M4204	503	205	525	18.95	24.5	4.1	4.7	234	511	1285	1189	214	464	1139	1323	32	32.5
M4205	463	228	500	19.3	22.4	3.3	4.9	243	542	1199	1073	193	480	1096	1243	33	33
M4206	476	189	516	19	23.5	4.4	7.2	218	515	1166	1208	202	473	1096	1200	31.5	31.5
M4207	513	226	531	16	23.7	3.1	4.9	235	529	1244	1108	211	470	1144	1334	33	33.5
M4208	452	207	475	14.7	19.3	3.1	2.6	206	474	1072	959	185	401	1030	1111	31	31
M4209	546	287	550	15.3	21.8	3	3.8	269	510	1172	1077	223	453	1071	1318	31.5	32

C. ECM-CELL

ECM-CELL 14 Day Recovery

	Pre Def BodyWt (g)	Def Body Wt (mg)	Post Def Body Wt (g)	DEF in situ (N)	CON in situ (N)	DEF twitch (N)	CON twitch (N)	Def Sol Wt (mg)	Def Plan Wt (mg)	Def MGAS Wt (mg)	Def LGAS Wt (mg)	Con Sol Wt (mg)	Con Plan Wt (mg)	Con MGAS Wt (mg)	Con LGAS Wt (mg)	Def L Gas Length	Con L Gas Length
C1401	521	228	502	12.5	20.4	2.2	4.5	234	522	1145	1207	210	469	1087	1227	33	32
C1402	479	268		12.9	19.6	2.9	4.1	206	474	1091	949	192	401	971	1140	32	31
C1403	414	209	417	14.8	20.8	2.4	4.9	195	457	1029	845		421	988	1028	31	31
C1404	490	226	475	15.9	20.7	2.5	4.2	193	436	957	1182		409	957	1080	32	32
C1405	423	211	415	15.1	19.8	3.2	4.5	193	448	901	905		353	808	922	32.5	32
C1406	473	221	461	15.4	20.8	2.9	4.6	212	456	1031	953	156	396	869	1038	32	32

ECM-CELL 28 Day Recovery

	Pre Def BodyWt (g)	Def Body Wt (mg)	Post Def Body Wt (g)	DEF in situ (N)	CON in situ (N)	DEF twitch (N)	CON twitch (N)	Def Sol Wt (mg)	Def Plan Wt (mg)	Def MGAS Wt (mg)	Def LGAS Wt (mg)	Con Sol Wt (mg)	Con Plan Wt (mg)	Con MGAS Wt (mg)	Con LGAS Wt (mg)	Def L Gas Length	Con L Gas Length
C2801	509	195	511	14.5	21.8	3.5	4.5	223	505	1230	1081	208	467	1052	1289	31.5	31.5
C2802	522	266	536	16.7	20.9	3.8	4.5	266	521	1240	1376	271	514	1200	1448	32.5	32.5
C2803	547	285	540	15.1	21.7	2.2	3.9	154	498	1248	999	213	441	1042	1267	32	33
C2804	456	255	420					197	410	913	1140	208	459	1057	774		
C2805	416	203	469	15	20.5	3.6	5.8	153	495	1000	949		423	1177	973	31	31
C2806	427	219	445	15.1	19.8	2.6	4.4	192	424	1002	983		366	900	1036	31.5	30.5
C2807	443		465	15.4	20.2	3.3	4.3	249	505	1006	1066	174	504	1062	1156	30	30

ECM-CELL 42 Day Recovery

	Pre Def BodyWt (g)	Def Body Wt (mg)	Post Def Body Wt (g)	DEF in situ (N)	CON in situ (N)	DEF twitch (N)	CON twitch (N)	Def Sol Wt (mg)	Def Plan Wt (mg)	Def MGAS Wt (mg)	Def LGAS Wt (mg)	Con Sol Wt (mg)	Con Plan Wt (mg)	Con MGAS Wt (mg)	Con LGAS Wt (mg)	Def L Gas Length	Con L Gas Length
C4201	479	239	513	16.4	17.5	3.1	3.2	226	528	1139	1141	235	483	1209	1325	31	31.5
C4202	503	211	512	15.8	20.4	3.6	3.2	214	468	1095	1055	201	448	1009	1166	30	30
C4203	520	222	525					241	481	1182	1030	191		1104	1262		31
C4204	520	243	507	18.9	21.5			238	531	1187	1035	175	475	1070	1110	31.5	31.5
C4205	500	227	497	18.8	22.5	3.5	4.4	240	469	1152	1126	220	455	1101	1186	33.5	33
C4206	519	206	521	16.9	21	3.5	4.5	233	489	1129	1023	198	435	1079	1225	30	30
C4207	496	211	515	16.5	22.8	2.7	4.4	232	478	1179	1073	219	1050	1205	1205	30	30
C4208	535	226	550	20.7	20.2	3.1	2.9	218	510	1214	1274	201	1184	1327	1327	32	31.5

V: Stained Muscle Sections

A: Control

Sample	# of Sections	H&E	Masson's	Desmin	vWF	Myogenin
D0703	3	1	1			
D0704	2+	M1				
D0705		10um	1			
D1413	8		1	1	1	1
M0701	6	2	1	1		1
M0704	18	1	1	1	1	1
M1403	6	ll	1		1	
M1408	4+	T1		M1		B1
M2802	6	ll	T2			
M2807		T1				T3
M2814	1+			1		
M2815	6	1	2	4	5	6
M4201	6	M2		T2		
M4207	6	I			M1	
M4209	9	T2, M3	T1			
C1401	6	1	1	1	1	1
C1402	6	I	1	1	1	1
C1403	6	1	1	1	1	1
C4204	6	1		3	6	2
C4207	6	I	1		1	
C4208	7	I	1	7	6	5

B: Defect Top

Sample	# of Sections	H&E	Masson's	Desmin	vWF	Myogenin
D016	6	T1	M3			
D0701	18	T2,M3,B1	T5,M1	B6	M6	T1
D0702	18	M2,B5	T2	B4	M5	M3
D0703	18	T1-T3, M1-M5, B1, B2, B4, B5	T3,B4	B3	M6	T4
D0704	6	1	1	1	1	1
D0705	6	3	4	1	6	2
D0706	6	5	1	3	2	4
D1412	4	1	1	1		
D1413	6	2	5	1	6	4
D1414	6	T3	M2,M3	M1	T2	
D1415	9	M1	T2	M3	M2	B1
D1416	6	M3	M2	T2	M1	
D1417	6	M1	M2	T1	T2	M3
D1418	6	T2	T1	M1	M2	T3
D2810	6	5	4	1	6	3
D2811	9	T1, M1, B1	M4,B2	M2	B3	M3
D2812	6	2	3	5		
D2813	6		4	1	3	6
D2814	6	6	4	2	1	3
D2815	6	6	3	1	4	5
D4201	5	T4	M2	M1	T1	
D4202	6	4	6	2	1	3
D4203	6	2	6	4	T3	
D4204	6	2	6	4	1	3
D4205	9	5	1	7	9	2
D4206	6	4	2	6	5	3

C: Defect Bottom

Sample	# of Sections	H&E	Masson's	Desmin	vWF	Myogenin
D016	6	M3	T1			
D0701	6	4	6	2	5	3
D0702	6		3		4	1
D0703	6	5	6	2	1	3
D0704	6	3	2	4		1,5
D0705	6	1	2	3		
D0706	6	4	2	1	3	5
D1412	6	3	4	1	6	
D1413	18	B5	T3	M1	T6	
D1414	6	2	6	4	5	
D1415	6	T2	M3	M1		T3
D1416	18	T1,M1	M4,B3	T6	M2	B5
D1417	6	2	6	1	3	5
D1418	6	4	5	3	1	6
D2810	6					
D2811	6	3	4,5	2	1,6	
D2812	6	2	6	4	5	3
D2813	6	M2	T3	M1	M3	T2
D2814	6	6	T1	M2	T2	M3
D2815	6	T1	M2	M1	5	M3
D4201	7	M2,B3	B1	M1		B2
D4202	6	M3	T3	M1	M2	
D4203	18	T4	M3	M2	T1,M4	
D4204	6	T1	T3,M3	M1		
D4205	9	M2	T2	M3	T1	M1
D4206	6	M1	T1	M2	T2	M3

D: ECM-ONLY Top

Sample	# of Sections	H&E	Masson's	Desmin	vWF	Myogenin
M0701	4+	1,2				
M0703	19	T1, M4, B1	T2,M3,B2	T5, M2 B7	M5	B4
M0704	8	T1,T6,T2		T5, B2		T4, M6, B4
M0705	17	T1, M1, B1	T2,T5,M2	M3	M4,B2	T3,M6,B4
M0706	20	M4, B21, B32	M3,B4	T3,M1	T2,T5	M6,B6
M1406	18	T3, M5,B3	T1, M1,B6	T6, M2, B2	B5	T4, M6, B4
M1407	19	T1, M4,M5, B4	T2,M6,B7	T6, M2, B3		M3
M1408	19	T2,M3,M5, B1	T1,B6	T6, M2, B3	T4	T3,M6,B4
M1409	20	T1,T4,M2,M5,B1,B5	T7,M7	T6, M3, B2		T3,M4,B4
M1410	18		T2,M4,B6	T7,M2,B3	M2,B1	T3,M6,B4
M1411	18		T1,B3	T6,M1,B4	T2,M3,B2	T3,M4,B5
M2811	22	T1, M1, B1	M3,M4,B22	T5, M2, B2	B31	T3, M7, B4
M2812	20	T1,M2, B6	T3,M3,B1,B4	M1, B3	T6,M5	T4, M6, B5
M2813	18	T1, M4,B4	T3,B3,B5	T2,M2		T4, M6
M2814	18	T3,M4,M5,B6	T1,M2,M3	T6,M1,B2,B3	T2	T4,M6,B4
M2815	21	T4,T6,M3,B1	T3,T7,M1,M2,B3	T5,M4,B2	T1,B5	T2,B4
M2816	18		T1,M1,B4	T6,M2,B3	M4,B1	T4,M6,B5
M4201	18	T1, M2, B2	T5,M4,B4	T6,M3,M5,B3,B6	T3,B1	M6, B5
M4202	22	T1, M3,	T2,T5,M4	T6, B1	M4,B3	T3, M6, B4
M4203	16	T1, M1, B2	M5	T3, M2, B3	M4	
M4204	18	T4,M6,B8	T5,M5,B2	T3,M2,M5,B3,B6	T1,M3	T6, M2, B4
M4205	18	T4, M4,B3	T1,T5,M1	T6, M2, B2		
M4206	20	T6, M2, B2	T2,M5,B1	T5		
M4207	18	T4,M3,M4,B4	M1,M6,B5	T2,T6,B3,M2	B1	T1,T3,M5
M4208	18	T1,M7,B1	M5,B5	T4, M3, B3	T2,B2	T3,M6,B4
M4209	20	T4,M1,B4	T5,M4,B	B3		B2

E: ECM-ONLY Middle

Sample	# of Sections	H&E	Masson's	Desmin	vWF	Myogenin
M0701	18	M1,B3	T2,M1,B5	T2,B2	M6,B4	M3,B1
M0703	18	T2,M6	T3,M1,B1	T6,M3	B2	M4,B6
M0704	18	T3,M3,B1	T1,M1,B3	M2,B4	M6,B6	B2
M0705	18	T1,M1,B6	T3,M2,B3		T4,M4,B5	
M0706	21	M6	T2,M1,B4	M2,B5	T1,B6	T3,M5
M1406	18	T3,B4	M6,B6	T4,B5	M1,M6	M5,B1
M1407	18	T6,M6,B3	T1,B2	T3,M2	M5,B1	M1
M1408	18	M2,B1	T6,B3	B4	M1,T1	M5,B6
M1409	18	T5,M2,B1,B6	T4,M6,B3	T6,M2,B2	M5,B4	M4
M1410	18	T6, M1	T1,B2	M4,B6	B5	T3,M5
M1411	18	B3	M1,B6	T3,M4	T2,B5	T1,T6
M2811	18	T2,M5,B5	T4,B6,M1	T3	T6,B4	T5,M2
M2812	18	T2,M3,B3	T3,M5,B4		T4,M2	T6,B1
M2813	18	T1,B6	M2,B4	T3,M3,B3	T6,M1,B1	M5,B5
M2814	18	T3,M1	M6,B2	T1,B6	B5	M6,B3
M2815	18	T3,M3,B1	T1,M1,B3	M2,B5	M6,B6	B2
M2816	18	T6,B2	B3	T4,B4	T5,M6	B6
M4201	18	T3,M5	M3,B1	T6,B5	M4	M2
M4202	18	T1,M1,B1	T3,M3,B5		T2,M4	
M4203	16	T2,M6	T3,M1	T6,M3	B1,B2	M4,B6
M4204	18	M2,B3	T4,M3	B3	T1,B5	T3,B1
M4206	18	M3, B2	T1,T2,M1	T6,M2,B3		T4,M6,B4
M4207	18	M6,B1	M4	T3,B2	T1,B6	T2,B4
M4208	19	T1,M1,B1	T3,M3,B3	M5,B6	T2,M2	T5,T6

F: ECM-ONLY Bottom

Sample	# of Sections	H&E	Masson's	Desmin	vWF	Myogenin
M0701	6	1,3,5	2,4,6			
M0703	18	T1,M2,B4	T6,M1,B1	T5,M3,B3	M4,B2	T3,M5,M6,B5
M0704	18	T3,M4,B6	T1,M5,B1	T6,M2,M3,B3	T2,M6,B5	T5,M1,B2
M0705	19	T1,B6	T2,B2,B5	M1,M5,B1	M3,B5	T3,M6,B4
M0706	18	T4,M4,B6	T3,M5,B4	T1,M6,B6	M2,B1	T2,M1
M1406	18	T4,M3,B5	T1,M1	T5,M2,B1	T2,M4	M3,B3
M1407	18	T3,M2,B6	T2,M1	T1,M5,B5	T6,M6,B1	M4,B3
M1408	18	T2,B1	M1,M6,B7	T6,M2,B3	T1,M3	M5
M1409	18	T1,M1,B5	T3,M5,B1	T5,M3,B2,B3	T2,B6	T6, M4, B6
M1410	18	T6, M3, B3	T2,M1,B1	T5, M2, B2		T3,M6,B4
M1411	18	T1,T4,M4,M6,B1,B6	T2,B2,B5	T5, M2, B3	T6	
M2811	18	T1,T5,M5,B1	T3,M1,M3	T6, M5, B3	M4,B5,B6	T4,M6,B4
M2812	18		T3,B1,M1	T5,M3,B3	T6,M4,B2	M6,B4
M2813	18	T2,M2,B6	T1,B5	T6	T2,M3	T3,M6,B2
M2814	10	T2,M1,B3	B5	T5, M3, B3	M6,B4	T3,M5,B1
M2815	20	T4, M4, B3	T3,M1,B1	T5,T6,M2,B2		T2,M6,B4
M2816	18	T2,M1,B3	T1,M1,B4	T6,M2,B3	M4,B1	T4,M6,B5
M4201	18	T2,T3,M3,M4,B2	T1,B1	T6, B3, M2		T4, M6, B4
M4202	18		T2	T6, M2, B2	T5,B3	T4,M6,B4
M4203	18	T1,M1,B1		T5, M3, B2	M4,B2	T3,M5,M6,B5
M4204	20	T3, M3, B10	T2,M4,B4	T6, M2, B3	B2	T3,M5,B5
M4205	18	T2,M4,B3	M5,T4,B1	T6, M2, B2	T5	T4,M6,B4
M4206	18	T2,M4,B4	M2,M6	T6, M3, B2	T1,M1	T3,M5,B3
M4207	18	T3,M1,B1	T1,M3,B5	T5, M2, B3	T2,B6	T4,M6,B4
M4208	18	T2,M4,B6		T6, M2, B2	T3,B1	T4,M6,B4
M4209	18	T3,M2,B2	T1,M4,B5	M3, B3	M1,B6	T4, M6, B4

G: ECM-CELL Top

Sample	# of Sections	H&E	Masson's	Desmin	vWF	Myogenin
C1401	18	T3,M3,B1	T2,T4,B5	M2,B3	T7,B6	T5,M4,B4
C1402	21	T1,T5,M1,M3	T2,T4,T7,M5	T6, M2, B3		T3, M4, B4
C1403	18	T2,M3,B3	T3,M5,B4	M1,B6	T4,M2	T1,M6
C1404	18	T5, M2, B1	T4,M6,B3	T6,M2,B2	B4	M5
C1405	18	T3,M4,B3	T4,M5,B5	T1,M2	M2,B2	T6,B6
C1406	19	T4,M3,B5	T1,M1	T5,M2,B1	T2,M4	B3
C2801	18	T1,M5,B2,B6	T2,T3,M1,M4,B3	T5,M3	T6,B1	T4,M6,B4
C2802	18	T1,T2,M2,B?	M3,B2	T6,M5	M4,B1	T3,B5
C2803	18	T1,T4,M6,B3,B5	T3,T5,M5,B1,B2,B6	T6,M2,B3,B4	T2	M1,M6
C2804	18	T1,M6,B4	T3,M2,B6	T5,M5,B3	T2,M4	T6,M3
C2805	18	T4,M2,B1	T5,M4,B3		T4,T6	
C2806	13		T6,M2,B6	T3,M1,B3	T2,B4	T5,M3
C4201	19	T2,T3,M2	T1,M6,B3	T6,M3,B2	M4,B1	T4, M5, B4
C4201-2	18	T5, M2, B1	T4,M6,B3	T6,M2,M6,B2	M5,B4	
C4202	18	M3,B2	B4	T6, M1,B1	B6	M4
C4203	18	T4,M1,B4	T2, M5, B5	T6	T3	M2,B3
C4204	18	T2,M2,B4	T4,M6,B6	T6,M2,M4,B3	T1,M3	M5, B3
C4207	18	T1,T6,M1,M4,B5	T4,M3,B4	T5, M2, B3	T1,B1,B6	T3,M5,B2
C4208	21	T2,M2,M5,B1,B4	T1,M4,M6,	M3, T6		T3, M1, B2

H: ECM-CELL Middle

Sample	# of Sections	H&E	Masson's	Desmin	vWF	Myogenin
C1401	18	T5,M4,B3	T1,M5,B4	M1,B1	M6,B6	T6,B5
C1402	18	M3	T4,M1	T3,B2	M1,B5	T2,M6
C1403	18	T2,M3	T3,M5,B4	M1,B6	T4,M2	T1,M6
C1404	21	M6,B2	T1,M3,B7	T2,M5	T6	T3,M4
C1405	18	T4	T2,M2,B5	T3,B1	T1,M6	M5,B3
C1406	18	T4,M3,B5	T1,M1	T5,M2,B1	M4	T2,B3
C2801	18	T1,M3,B3	T3,M1,B5	T6,M2,B3	T4,M6	T5,M5
C2802	18	T3,M3,B2	T5,M5,B4	T1,M2	T6,B6	T2,B3
C2803	18	T3,M5,B5	T2,M2,B2	T5,M1,B1	T1,M6,M2	T6,B3
C2805	18	M2,B1	T5,M4,B3	T4,M3	T4,T6	B2,B4
C2806	18	T3	M2	T2	B4	B1
C4201	18	T1,M5,B5	T3,M3,B3	T6,M2,B3	T4,B6	T5,M4
C4202	18	T1,M3,B5	T3,M2,B3	T6,M1,B6	T2,M4	T5,B1
C4203	18	T2,M2,B5	T5,M1,B6	M3,B4	T6,B2	T1,M2
C4204	16	T2,M2,B4	T4,M6,B6	6,M2, M4, B	T1,M3	M5, B3
C4207	18	T4,M6,B4	T2,M4,B2	T1,M2	M5,B5	M3
C4208	18	T3,M3,B3	T1,M5,B5	T6,M2,B4	T2,B4	T1,M2,B1

I: ECM-CELL Bottom

Sample	# of Sections	H&E	Masson's	Desmin	vWF	Myogenin
C1401	18	T1, M3, B4	T5,M4,B1,B6	T6, M2, B3		T3,M6, B2
C1402	18	T5,M3,B5,B6	T1,M5,	T3, M1, B1	T2,M4	T4,M6,B3
C1403	18	T2,M3,B3	T3,M5,B4	M1,B6	T4,M2	T1,M6
C1404	18	T6,M2,B5	T3,M4,B1	T4,M1,B2	T1,M5	T3,M6, B2
C1405	18	T1,M4,B1	T5,M3,B6	T3,M5,B3	B2	T6,M2
C1406	18	T6,M2,B6	T3	T2,B4	T5,M3	T1,B3
C2801	20	T4,T5,M2,M4,B2	T3,M5,B1	T6,B3	T1,M3	M6
C2802	18	T5,T6,M5,B5	T3,M3,	T1,M6	M4,B6	T2,M4
C2803	18	T3,M3,B3	T5,B3,B6	T4,M6,B4	T1,M4	B1,B5
C2804	18	T1,M3,B5	T2,M4,B2	T3,M5	T6,M2	M1,B4
C2805	18	T4,M2,B1	T5,M4,B3	T1,B2	T4,T6	M6,B4
C2806	18	T3,M2,B5	T1,M5	M1,B4	M4,B1	T6,M3
C4201	18	T4,M6,B6	T1,M4,M5,B2	T6,M3,B5	M6,B5	T2,M6,B4
C4201-2	18	T3,M3,B3	T1,M5,B2			
C4202	18	T1,M3,B3	T5,M1,B1	T6,M4,B4	T4,M4	T3,M5,M6,B5
C4203	20	T6,M5,B2,B7	T5,M2,B1	T7	T2,B5	T3, M6, B3
C4204	18	T5,M1,B1	T1,T3,M5,B5	T6,M3,B3	T2,B2	T2, M6, B4
C4207	18	T1,T2,M3,B3	T5,B1,B3,B6	T6, M2, B2	M4,M5	T3, M6, B4
C4208	20	T7, M3, B2	T1,T2,M1	T6, M2, B3	M1	T4, M6, B4

VI: Masson's Trichrome Sections: Red Stained Area

A. ECM-ONLY 14 Day Recovery

Slide	% red
M1406 Top M1 10x Trichrome	5.3
M1406 Top T1 10x Trichrome	11.0
M1406 Top T1 10x Trichrome.2	11.5
M1407 Top T2 10x Trichrome	5.2
M1407 Top M6 10x Trichrome	7.6
M1408 Top T1 10x Trichrome	12.5
M1408 Top B6 10x Trichrome	11.1
M1409 Top M7 10x trichrome	21.4
M1409 Top M7 10x trichrome.2	16.3
M1409 Top T7 10x trichrome	10.2
M1409 Top T7 10x trichrome.2	19.6
M1410 Top B6 10x Trichrome	19.9
M1410 Top M4 10x Trichrome	13.2
M1410 Top T2 10x Trichrome	13.8
M1411 Top T1 10x Trichrome	8.2
M1411 Top B3 10x Trichrome	10.6
M1406 Mid M6 10x Trichrome	4.7
M1406 Mid B6 10x Trichrome	2.8
M1407 Mid T1 10x Trichrome	1.8
M1407 Mid B2 10x Trichrome	2.5
M1408 Mid T6 10x Trichrome	2.9
M1408 Mid B3 10x Trichrome	1.2
M1409 mid T4 10x Trichrome	2.7
M1409 Mid M6 10x Trichrome	0.9
M1409 Mid B3 10x Trichrome	1.8
M1410 Mid T1 10x Trichrome	2.8
M1410 Mid B2 10x Trichrome	5.1
M1411 Mid M1 10x Trichrome	6.4
M1411 Mid B6 10x Trichrome	8.5
M1406 Bot M1 10x Trichrome	6.1
M1406 Bot T1 10x Trichrome	6.8
M1407 Bot M1 10x Trichrome	8.5
M1407 Bot M6 10x Trichrome	2.3
M1408 Bot B7 10x trichrome	12.0
M1408 Bot B7 10x trichrome.2	8.9
M1408 Bot M1 10x trichrome	13.9
M1408 Bot M1 10x trichrome.2	10.2
M1408 Bot M6 10x Trichrome	9.5
M1409 Bot B1 10x Trichrome	10.1
M1409 Bot M5 10x trichrome	9.2
M1409 Bot T3 10x trichrome	4.2
M1410 Bot B1 10x Trichrome	11.1
M1410 Bot B2 10x trichrome	9.0
M1410 Bot M1 10x trichrome	9.8
M1411 Bot B2 10x Trichrome	16.9
M1411 Bot B5 10x trichrome	13.0
M1411 Bot T2 10x trichrome	7.2

B. ECM-ONLY 28 Day Recovery

Slide	% red
M2811 Top M4 10x Trichrome	10.3
M2811 Top M3 10x Trichrome	10.3
M2811 Top B22 10x Trichrome	11.5
M2812 Top B1 10x Trichrome	8.8
M2812 Top B4 10x Trichrome	22.7
M2812 Top T3 10x Trichrome	11.4
M2812 Top B1 10x Trichrome	25.6
M2813 Top B3 10x Trichrome	11.5
M2813 Top B5 10x Trichrome	6.8
M2813 Top M5 10x Trichrome	16.0
M2814 Top M2 10x Trichrome	12.7
M2814 Top M3 10x Trichrome	10.6
M2814 Top T1 10x Trichrome	14.0
M2815 Top M2 10x Trichrome	18.7
M2815 Top T3 10x Trichrome	11.8
M2815 Top T7 Trichrome 10x	12.3
M2816 Top T1 10x Trichrome	10.6
M2816 Top B4 10x Trichrome	13.0
M2811 Mid B6 10x Trichrome	2.7
M2811 Mid M1 10x trichrome	1.1
M2811 Mid T4 10x trichrome	0.7
M2812 Mid T3 10x Trichrome	2.2
M2812 Mid M5 10x Trichrome	3.3
M2813 Mid M2 10x Trichrome	4.6
M2813 Mid B4 10x Trichrome	2.1
M2814 Mid M6 10x Tricrhome	3.4
M2814 Mid B2 10x Trichrome	1.2
M2815 mid B5 10x trichrome	3.1
M2815 mid T5 10x trichrome	2.0
M2816 Mid B3 10x Trichrome	4.6
M2811 Bot M1 10x trichrome	8.8
M2811 Bot M3 10x Trichrome	12.0
M2811 Bot T3 10x Trichrome	4.5
M2812 Bot B1 10x Trichrome	10.6
M2812 Bot T3 10x Trichrome	14.0
M2812 Bot M1 10x Trichrome	12.4
M2813 Bot B5 10x Trichrome	13.9
M2813 Bot T1 10x Trichrome	7.7
M2814 Bot B5 10x Trichrome	6.6
M2815 Bot B1 Trichrome 10x	11.6
M2815 Bot M1 10x Trichrome	13.2
M2815 Bot T3 Trichrome 10x	6.7
M2816 Bot M1 10x Trichrome	11.0
M2816 Bot B3 10x Trichrome	6.6

C. ECM-ONLY 42 Day Recovery

Slide	% red
M4201 Top B4 10x trichrome	9.3
M4201 Top B4 10x trichrome.2	20.6
M4201 Top M4 10x trichrome	11.2
M4201 Top M4 10x trichrome.2	20.2
M4201 Top T5 10x trichrome	19.6
M4201 Top T5 10x trichrome.2	25.3
M4202 Top B2 10x trichrome B2	9.5
M4202 Top M4 10 x Trichrome	5.7
M4202 Top T2 10x Trichrome	11.7
M4203 Top M5 10x trichrome	3.9
M4204 Top B2 10x trichrome	6.1
M4204 Top B5 10x trichrome	12.2
M4204 Top M4 10x trichrome	16.0
M4204 Top T5 10x trichrome	14.1
M4205 Top T1 10x trichrome	16.0
M4205 Top T5 10x Trichrome	15.4
M4205 Top M1 10x trichrome	10.2
M4206 Top M5 10x Trichrome	19.7
M4207 Top M6 10x trichrome	13.2
M4207 Top B5 10x Trichrome	10.5
M4208 Top M5 10x Trichrome	8.6
M4208 Top B5 10x Trichrome	9.0
M4209 Top M4 10x Trichrome	8.4

M4201 Mid T3 10x Trichrome	8.1
M4201 Mid M5 10x Trichrome	7.4
M4202 Mid B5 10x Trichrome	19.5
M4202 Mid B5 10x Trichrome	17.4
M4202 Mid M3 10x Trichrome	19.8
M4203 Mid T3 10x Trichrome	5.6
M4203 Mid M1 10x Trichrome	5.3
M4204 Mid T4 10x Trichrome	6.2
M4204 Mid M3 10x Trichrome	7.1
M4206 Mid T1 10x Trichrome	12.8
M4206 Mid M1 10x Trichrome	11.7
M4207 Mid M4 10x trichrome	3.9
M4208 Mid B3 10x trichrome	3.3
M4208 Mid B3 10x trichrome.2	3.2
M4208 Mid M3 10x trichrome	4.3
M4208 Mid T3 10x trichrome	2.1

M4201 Bot B1 10x trichrome	19.5
M4201 Bot T1 10x Trichrome	17.2
M4202 Bot T2 10x Trichrome	13.3
M4204 Bot B4 10x trichrome	4.9
M4204 Bot M4 10x trichrome	10.9
M4204 Bot T2 10x trichrome	10.8
M4205 Bot B1 10x Trichrome	13.5
M4205 Bot M5 10x trichrome	12.1
M4205 Bot T4 10x trichrome	11.3
M4206 Bot M2 10x trichrome	14.3
M4207 Bot B5 10x trichrome	11.2
M4207 Bot M3 10x Trichrome	13.2
M4207 Bot T1 10x Trichrome	5.0
M4209 Bot B5 10x trichrome	11.6
M4209 Bot M4 10x trichrome	19.4
M4209 Bot M4 10x trichrome.2	6.8
M4209 Bot T1 10x trichrome	5.6
M4209 Bot T1 10x trichrome.2	11.7

D. ECM-CELL 14 Day Recovery

Slide	% red
C1401 Top B5 10x trichrome	15.7
C1401 Top T2 10x trichrome	10.5
C1401 Top T4 10x trichrome	11.0
C1402 Top T2 10x trichrome	5.7
C1402 Top T4 10x trichrome	3.3
C1402 Top T7 10x trichrome	4.4
C1403 Top B4 10x Trichrome	10.9
C1403 Top M5 10x Trichrome	9.6
C1403 Top T3 10x Trichrome	7.0
C1404 Top T4 10x Trichrome	10.4
C1404 Top M6 10x Trichrome	14.7
C1404 Top B3 10x Trichrome	18.2
C1405 Top B5 10x Trichrome	17.7
C1405 Top M5 10x trichrome	13.3
C1405 Top T4 10x trichrome	15.4
C1406 Top T1 10x Trichrome	9.4
C1406 Top M1 10x Trichrome	11.8
C1401 Mid 10x B4 trichrome	22.5
C1401 Mid 10x B4 trichrome.2	7.9
C1401 Mid T1 10x Trichrome	3.7
C1401 Mid M4 10x Trichrome	10.3
C1402 Mid T4 10x Trichrome	5.2
C1402 Mid M1 10x Trichrome	3.3
C1403 Mid T3 10x Trichrome	4.6
C1403 Mid B4 10x Trichrome	4.2
C1404 Mid M3 10x Trichrome	13.9
C1404 Mid T1 10x Trichrome	11.0
C1404 Mid B7 10x Trichrome	4.1
C1405 Mid T2 10x Trichrome	8.7
C1405 Mid M2 10x Trichrome	10.5
C1405 Mid B5 10x Trichrome	8.0
C1406 Mid T1 10x Trichrome	5.1
C1406 Mid M1 10x Trichrome	10.5
C1406 Mid M1 10x Trichrome.2	1.8
C1401 Bot B6 Trichrome 10x	17.1
C1401 Bot M4 Trichrome 10x	9.1
C1401 Bot T5 Trichrome 10x	20.3
C1402 Bot M5 10x Trichrome	6.7
C1402 Bot M5 10x.2 Trichrome	5.1
C1402 Bot T1 Trichrome 10x	14.4
C1403 Bot T3 10x Trichome	10.5
C1403 Bot M5 10x Trichome	7.1
C1403 Bot B4 10x Trichome	11.4
C1404 Bot T3 10x Trichrome	16.9
C1404 Bot M4 10x Trichrome	21.3
C1404 Bot B1 10x Trichrome	18.3
C1405 Bot T5 10x Trichrome	11.7
C1405 Bot M3 10x Trichrome	14.0
C1405 Bot B6 10x Trichrome	12.7
C1406 Bot T3 10x Trichrome	6.5

E. ECM-CELL 28 Day Recovery

Slide	% red
C2802 Top B2 10x trichrome	11.4
C2802 Top M3 10x trichrome	23.6
C2803 Top B1 10x trichrome	36.7
C2803 Top B2 10x trichrome	15.0
C2803 Top B6 10x trichrome	20.3
C2803 Top B6 10x trichrome.2	17.6
C2803 Top M5 10x trichrome	12.2
C2803 Top M5 10x trichrome.3	22.6
C2803 Top M6 10x trichrome	28.8
C2803 Top T3 10x trichrome	25.8
C2803 Top T5 10x trichrome	19.9
C2804 Top T3 10x Trichrome	10.3
C2804 Top M2 10x trichrome	13.2
C2804 Top B6 10x trichrome	21.2
C2805 Top B3 10x trichrome	8.4
C2805 Top B3 10x trichrome.2	12.3
C2805 Top B3 10x trichrome.3	8.3
C2805 Top T5 10x Trichrome	10.1
C2806 Top M2 10x trichrome	6.7
C2806 Top T6 10x trichrome	3.4
C2801 Mid B5 10x trichrome	4.5
C2801 Mid M1 10x trichrome	4.2
C2801 Mid M1 10x trichrome 2	8.8
C2801 Mid T3 10x Trichrome	4.1
C2802 Mid M5 10x Trichrome	4.7
C2802 Mid B4 10x Trichrome	6.2
C2802 Mid T5 10x trichrome	5.2
C2803 mid B2 10x trichrome	19.2
C2803 Mid M2 10x Trichrome	13.4
C2803 Mid T2 10x Trichrome	2.7
C2805 Mid T5 10x Trichrome	7.9
C2805 Mid M4 10x Trichrome	2.3
C2805 Mid B3 10x Trichrome	3.0
C2806 Mid M2 10x Trichrome	8.6
C2801 Bot M5 10x Trichrome	12.9
C2801 Bot T3 10x trichrome	7.0
C2802 Bot T3 10x trichrome	12.7
C2802 Bot M3 10x trichrome	17.2
C2803 Bot T5 10x trichrome	11.0
C2803 Bot B3 10x trichrome	11.8
C2803 Bot B6 10x trichrome	17.2
C2804 Bot T2 10x trichrome	6.0
C2804 Bot M4 10x trichrome	7.5
C2804 Bot B2 10x Trichrome	6.9
C2805 Bot T5 10x Trichrome	11.1
C2805 Bot M4 10x Trichrome	12.6
C2805 Bot B3 10x Trichrome	11.1
C2806 Bot T1 10x Trichrome	14.7
C2806 Bot M5 10x Trichrome	17.1

F. ECM-CELL 42 Day Recovery

Slide	% red
C4201 Top B3 10x Trichrome	17.1
C4201 Top T1 trichrome 10x	14.1
C4201 Top T1 trichrome 10x.2	27.0
C4201 Top M6 10x trichrome	21.5
C4202 Top B4 10x Trichrome	19.3
C4203 Top B5 10x trichrome	28.3
C4203 Top M5 10x trichrome	25.6
C4203 Top T2 10x trichrome	20.0
C4203 Top T2 trichrome 10x	9.6
C4204 Top B6 10x trichrome	11.1
C4204 Top M6 10x trichrome	13.6
C4204 Top T4 10x trichrome	15.1
C4207 Top B4 10x trichrome.2	50.0
C4207 Top M3 10x Trichrome	10.7
C4207 Top M3 10x Trichrome.2	34.3
C4207 Top T4 10x Trichrome	6.6
C4208 Top M4 10x Trichrome	20.3
C4208 Top M6 10x Trichrome	15.4
C4208 Top T1 10x Trichrome	14.6
C4201 Mid B3 10x Trichrome	11.6
C4201 Mid B3 10x Trichrome.2	15.2
C4201 Mid M3 10x Trichrome	19.8
C4201 Mid T3 10x Trichrome	15.8
C4202 Mid B3 10x trichrome	5.9
C4202 Mid M2 10x trichrome.2	4.0
C4202 Mid M2 10x trichrome.4	8.5
C4202 Mid T3 10x trichrome	23.9
C4203 Mid B6 10x trichrome	8.4
C4203 Mid B6 10x trichrome.2	16.3
C4203 Mid T5 10x trichrome	13.8
C4204 Mid T4 10x trichrome	11.0
C4204 Mid B6 10x trichrome	5.8
C4207 Mid B2 10x Trichrome	5.2
C4207 Mid M4 10x Trichrome	4.1
C4207 Mid M4 10x Trichrome	4.7
C4207 Mid T2 10x trichrome	7.0
C4208 Mid T1 10x trichrome	13.3
C4208 Mid B5 10x trichrome	3.5
C4208 Mid M5 10x Trichrome	4.3
C4201 Bot M4 10x Trichrome	25.1
C4201 Bot M5 10x Trichrome	24.3
C4201 Bot B2 10x trichrome	21.4
C4201 Bot M5 10x trichrome	14.2
C4201 Bot T1 10x trichrome	17.8
C4202 Bot B1 10x trichrome	11.3
C4202 Bot M1 10x trichrome	16.3
C4202 Bot T5 10x trichrome	11.8
C4203 Bot B1 10x trichrome	8.9
C4203 Bot M2 10x trichrome	20.8
C4203 Bot T5 10x trichrome	7.0
C4204 Bot B5 10x Trichrome	3.9
C4204 Bot M5 10x Trichrome	15.7
C4204 Bot T1 10x trichrome	16.4
C4204 Bot T3 10x Trichrome	16.3
C4204 Bot T3 10x Trichrome.2	18.7
C4207 Bot B1 10x Trichrome	22.2
C4207 Bot B6 10x Trichrome	26.0
C4207 Bot T5 10x Trichrome	16.6
C4208 Bot M1 10x Trichrome	17.9
C4208 Bot T1 10x Trichrome	21.3
C4208 Bot T2 10x Trichrome	25.7

VII. Von Willebrand Factor Stained Sections: Blood Vessels

A. ECM-ONLY 14 Day Recovery

Slide	Area of interest (mm^2)	# of Blood Vessels	BV/mm^2
M1406 Top B5 10x vWF	1.001	14	13.99
M1408 Top T4 10x vWF	1.088	12	11.03
M1410 Top M2 10x vWF	0.959	9	9.39
M1410 Top B1 10x vWF	1.003	15	14.96
M1411 Top T2 10x vWF	0.899	5	5.56
M1411 Top M3 10x vWF	0.949	9	9.48
M1411 Top B2 10x vWF	0.910	9	9.89
M1406 Mid M1 10x vWF	1.005	13	12.94
M1406 Mid M6 10x vWF	1.036	9	8.69
M1407 Mid M5 10x vWF	1.115	9	8.07
M1407 Mid B1 10x vWF	1.099	12	10.92
M1408 Mid T1 10x vWF	0.984	3	3.05
M1409 Mid M5 10x vWF	0.977	7	7.16
M1409 Mid B4 10x vWF	0.934	9	9.63
M1410 Mid B5 10x vWF	1.082	4	3.70
M1411 Mid T2 10x vWF	1.022	8	7.83
M1411 Mid B5 10x vWF	1.001	9	8.99
M1406 Bot M4 10x vWF	1.113	38	34.14
M1406 Bot T2 10x vWF	0.897	27	30.10
M1407 Bot T6 10x vWF	1.136	14	12.32
M1407 Bot M6 10x vWF	1.129	10	8.85
M1408 Bot T1 10x vWF	0.803	12	14.94
M1408 Bot T1 10x vWF	0.769	6	7.80
M1409 Bot B6 10x vWF	0.928	17	18.31
M1409 Bot B6 10x vWF	0.938	25	26.64
M1409 Bot T2 10x vWF	1.083	4	3.69
M1409 Bot T2 10x vWF	1.117	3	2.69
M1411 Bot T6 10x vWF	0.685	12	17.51

B. ECM-ONLY 28 Day Recovery

Slide	Area of interest (mm^2)	# of Blood Vessels	BV/mm^2
M2811 Top B3 10x vWF	0.748	3	4.01
M2812 Top T6 10x vWF	1.082	17	15.72
M2812 Top M5 10x vWF	0.961	10	10.41
M2812 Top M5 10x vWF	1.024	26	25.39
M2812 Top T6 10x vWF	1.070	19	17.76
M2812 Top T6 10x vWF	1.096	12	10.95
M2813 Top M5 10x vWF	0.796	22	27.63
M2814 Top T2 10x vWF	1.056	10	9.47
M2815 Top B5 10x vWF	1.116	13	11.65
M2815 Top T1 10x vWF	1.104	22	19.93
M2815 Top B5 10x vWF	1.104	20	18.11
M2816 Top M4 10x vWF	1.108	19	17.14
M2816 Top B1 10x vWF	1.098	18	16.40
M2811 Mid B4 10x vWF	1.076	7	6.50
M2811 Mid B4 10x vWF	1.104	22	19.94
M2811 Mid T6 10x vWF	1.011	7	6.92
M2812 Mid T4 10x vWF	1.061	9	8.48
M2812 Mid T4 10x vWF	1.035	1	0.97
M2812 Mid M2 10x vWF	1.045	27	25.84
M2813 Mid T6 10x vWF	1.009	7	6.94
M2813 Mid M1 10x vWF	1.117	16	14.33
M2813 Mid B1 10x vWF	1.003	19	18.94
M2814 Mid B5 10x vWF	1.018	10	9.82
M2815 mid B4 10x vWF	1.049	0	0.00
M2815 mid B4 10x vWF	1.083	10	9.24
M2815 Mid M2 10x vWF	0.984	1	1.02
M2815 mid M2 10x vWF	1.081	11	10.18
M2815 mid T4 10x vWF	1.064	1	0.94
M2815 Mid T4 10x vWF	1.068	14	13.11
M2816 Mid T5 10x vWF	1.060	5	4.72
M2816 Mid M6 10x vWF	1.090	12	11.01
M2811 Bot M4 10x vWF	0.905	19	20.98
M2811 Bot B5 10x vWF	0.938	31	33.03
M2811 Bot B6 10x vWF	1.035	25	24.15
M2812 Bot B2 10x vWF	1.064	6	5.64
M2812 Bot B2 10x vWF	1.068	12	11.23
M2812 Bot B2 10x vWF	1.078	5	4.64
M2812 Bot M4 10x vWF	1.063	9	8.46
M2812 Bot M4 10x vWF	1.107	4	3.61
M2812 Bot T6 10x vWF	1.095	18	16.44
M2812 Bot T6 10x vWF	1.096	12	10.95
M2813 Bot T2 10x vWF	1.091	24	21.99
M2814 Bot B4 10x vWF	1.020	21	20.59
M2814 Bot M6 10x vWF	1.073	20	18.63
M2814 Bot M6 10x vWF	1.079	15	13.90
M2815 Bot T5 10x vWF	1.096	20	18.25
M2816 Bot M4 10x vWF	1.059	20	18.88
M2816 Bot B1 10x vWF	1.029	16	15.55

C. ECM-ONLY 42 Day Recovery

Slide	Area of interest (mm^2)	# of Blood Vessels	BV/mm^2
M4201 Top B1 10x vWF	0.949	7	7.38
M4201 Top T3 10x vWF	0.739	6	8.11
M4202 Top M4 10x vWF	0.991	11	11.10
M4202 Top B3 10x vWF	0.884	9	10.19
M4203 Top M4 10x vWF	1.025	16	15.61
M4204 Top T1 10x vWF	0.952	20	21.01
M4204 Top M3 10x vWF	1.005	19	18.90
M4205 Top T3 10x vWF	1.103	14	12.69
M4205 Top B1 10x vWF	1.088	21	19.30
M4207 Top B1 10x vWF	1.092	17	15.56
M4208 Top T2 10x vWF	1.079	20	18.54
M4208 Top B2 10x vWF	0.955	13	13.61
M4208 Top T2 10x vWF	0.649	5	7.70
M4208 Top T2 10x vWF	1.056	11	10.41
M4201 Mid M4 10x vWF	0.831	3	3.61
M4202 Mid M4 10x vWF	0.967	4	4.14
M4202 Mid M4 10x vWF	0.989	11	11.12
M4202 Mid T2 10x vWF	0.908	5	5.51
M4203 Mid B1 10x vWF	1.000	16	15.99
M4203 Mid M2 10x vWF	1.020	12	11.77
M4204 Mid T1 10x vWF	1.066	15	14.07
M4204 Mid B5 10x vWF	1.071	14	13.07
M4207 Mid T1 10x vWF	1.099	11	10.01
M4207 Mid B6 10x vWF	1.044	13	12.45
M4208 Mid M2 10x vWF	0.938	4	4.27
M4208 Mid T2 10x vWF	0.923	13	14.08
M4202 Bot B3 10x vWF	0.9429	6	6.36
M4202 Bot T5 10x vWF	1.0138	1	0.99
M4203 Bot B2 10x vWF	1.0812	32	29.60
M4203 Bot B2 10x vWF	1.1155	41	36.76
M4203 Bot M4 10x vWF	1.0999	24	21.82
M4203 Bot M4 10x vWF	1.1041	22	19.93
M4203 Bot M4 10x vWF	1.1361	29	25.53
M4204 Bot B2 10x vWF	1.0940	32	29.25
M4205 Bot T5 10x vWF	1.0802	9	8.33
M4206 Bot M1 10x vWF	0.8577	17	19.82
M4206 Bot T1 10x vWF	0.4435	5	11.27
M4207 Bot B6 10x vWF	1.1186	23	20.56
M4207 Bot B6 10x vWF	1.1361	35	30.81
M4207 Bot T2 10x vWF	1.0550	29	27.49
M4207 Bot T2 10x vWF	1.0543	32	30.35
M4207 Bot T2 10x vWF	1.0702	24	22.43
M4208 Bot B1 10x vWF	1.0727	3	2.80
M4208 Bot T3 10x vWF	0.9689	19	19.61
M4208 Bot T3 10x vWF	0.9793	27	27.57
M4209 Bot M1 10x vWF	1.1257	17	15.10
M4209 Bot M1 10x vWF	1.0120	31	30.63
M4209 Bot B6 10x vWF	1.1186	15	13.41

D. ECM-CELL 14 Day Recovery

Slide	Area of interest (mm^2)	# of Blood Vessels	BV/mm^2
C1401 Top B6 10x vWF	1.100	10	9.09
C1401 Top B6 10x vWF	1.078	13	12.06
C1401 Top T7 10x vWF	1.084	27	24.91
C1401 Top T7 10x vWF	1.071	34	31.76
C1403 Top M2 10x vWF	1.077	27	25.08
C1403 Top M2 10x vWF	1.057	16	15.14
C1403 Top T4 10x vWF	1.075	31	28.83
C1403 Top T4 10x vWF	1.071	32	29.89
C1403 Top T4 10x vWF	1.080	34	31.49
C1404 Top B4 10x vWF	1.063	19	17.88
C1405 Top B2 10x vWF	1.102	40	36.30
C1405 Top B2 10x vWF	1.094	30	27.43
C1405 Top B2 10x vWF	1.108	28	25.28
C1405 Top M2 10x vWF	1.088	43	39.52
C1405 Top M2 10x vWF	1.081	31	28.69
C1406 Top T2 10x vWF	1.050	14	13.34
C1406 Top M4 10x vWF	1.047	13	12.41
C1401 Mid B6 10x vWF	1.039	11	10.58
C1401 Mid M6 10x vWF	1.125	4	3.56
C1401 Mid M6 10x vWF	1.091	6	5.50
C1402 Mid M1 10x vWF	0.982	6	6.11
C1402 Mid B5 10x vWF	0.895	3	3.35
C1403 Mid M2 10x vWF	1.047	13	12.42
C1403 Mid T4 10x vWF	1.076	18	16.73
C1404 Mid T6 10x vWF	1.032	4	3.88
C1405 Mid M6 10x vWF	1.083	12	11.08
C1405 Mid T1 10x vWF	1.083	14	12.92
C1406 Mid M4 10x vWF	1.078	3	2.78
C1402 Bot M4 10x vWF	1.018	22	21.60
C1402 Bot M4 10x vWF	1.021	17	16.66
C1402 Bot T2 10x vWF	0.974	7	7.19
C1402 Bot T2 10x vWF	1.023	16	15.63
C1403 Bot M2 10x vWF	0.995	26	26.13
C1403 Bot T4 10x vWF	1.028	16	15.56
C1404 Bot T1 10x vWF	0.948	10	10.55
C1404 Bot M5 10x vWF	0.988	11	11.13
C1405 Bot B2 10x vWF	1.004	15	14.94
C1406 Bot T5 10x vWF	1.036	14	13.52
C1406 Bot M3 10x vWF	1.029	19	18.47

E. ECM-CELL 28 Day Recovery

Slide	Area of interest (mm^2)	# of Blood Vessels	BV/mm^2
C2801 Top B1 10x vWF	1.012	25	24.69
C2801 Top T6 10x vWF	1.043	30	28.76
C2802 Top M4 10x vWF	0.998	25	25.04
C2802 Top B1 10x vWF	0.998	23	23.04
C2803 Top T2 10x vWF	1.006	13	12.93
C2804 Top M4 10x vWF	1.100	11	10.00
C2804 Top T2 10x vWF	1.114	13	11.67
C2805 Top T4 10x vWF	1.115	48	43.04
C2805 Top T4 10x vWf	1.037	31	29.91
C2805 Top T6 10x vWF	1.136	13	11.44
C2806 Top B4 10x vWF	1.131	4	3.54
C2806 Top M4 10x vWF	0.906	23	25.38
C2806 Top M4 10x vWF	0.967	15	15.51
C2801 Mid M6 10x vWF	0.929	23	24.75
C2801 Mid M6 10x vWF	0.926	18	19.45
C2801 Mid M6 10x vWF	0.964	20	20.75
C2801 Mid T4 10x vWF	0.949	17	17.92
C2802 Mid B6 10x vWF	0.925	19	20.54
C2802 Mid B6 10x vWF	1.038	19	18.30
C2802 Mid B6 10x vWF	1.030	18	17.48
C2802 Mid T6 10x vWF	1.136	7	6.16
C2803 Mid M2 10x vWF	1.120	9	8.03
C2803 Mid M6 10x vWF	1.025	7	6.83
C2803 Mid T1 10x vWF	1.001	4	4.00
C2805 Mid T4 10x vWF	0.998	8	8.01
C2805 Mid T6 10x vWF	1.004	6	5.98
C2806 Mid B4 10x vWF	0.925	7	7.56
C2801 Bot T1 10x vWF	1.000	13	12.99
C2801 Bot M3 10x vWF	0.993	11	11.08
C2802 Bot M4 10x vWF	0.995	14	14.08
C2802 Bot B6 10x vWF	1.049	25	23.83
C2802 Bot B6 10x vWF	1.136	20	17.60
C2802 Bot M4 10x vWF	1.121	7	6.25
C2803 Bot T1 10x vWF	1.046	11	10.51
C2803 Bot M4 10x vWF	1.061	13	12.25
C2804 Bot M2 10x vWF	0.979	19	19.41
C2805 Bot T4 10x vWF	0.973	7	7.19
C2805 Bot T6 10x vWF	0.990	12	12.12
C2806 Bot M4 10x vWF	1.087	18	16.55
C2806 Bot B1 10x vWF	1.003	6	5.98

F. ECM-CELL 42 Day Recovery

Slide	Area of interest (mm^2)	# of Blood Vessels	BV/mm^2
C4201 Top M4 10x vWF	0.961	29	30.16
C4201 Top B1 10x vWF	0.980	31	31.63
C4202 Top B6 10x vWF	0.951	15	15.77
C4203 Top T3 10x vWF	1.001	36	35.95
C4204 Top T1 10x vWF	0.880	16	18.17
C4204 Top M3 10x vWF	0.929	14	15.07
C4204 Top M3 10x vWF	0.949	15	15.81
C4204 Top T1 10x vWF	0.731	10	13.69
C4207 Top B6 10x vWF	1.091	37	33.90
C4207 Top T1 10x vWF	1.070	29	27.10
C4207 Top B1 10x vWF	1.084	38	35.07
C4208 Top M5 10x vWF	1.036	24	23.16
C4201 Mid T4 10x vWF	0.991	16	16.14
C4201 Mid B6 10x vWF	1.006	11	10.93
C4202 Mid T2 10x vWF	1.040	10	9.61
C4202 Mid M4 10x vWF	1.033	9	8.71
C4203 Mid B2 10x vWF	1.066	10	9.38
C4204 Mid M4 10x vWF	0.871	8	9.18
C4207 mid B5 10x vWF	1.107	20	18.07
C4207 Mid M5 10x vWF	1.063	16	15.06
C4207 Mid M5 10x vWF	1.072	19	17.72
C4208 Mid B4 10x vWF	1.065	11	10.33
C4208 Mid B2 10x vWF	1.014	15	14.79
C4201Bot M6 10x vWF	0.881	29	32.92
C4201 Bot B5 10x vWF	0.901	33	36.64
C4202 Bot M4 10x vWF	0.754	36	47.73
C4202 Bot M4 10x vWF	1.059	30	28.34
C4202 Bot T4 10x vWF	1.088	24	22.06
C4203 Bot T2 10x vWF	1.050	26	24.76
C4203 Bot B2 10x vWF	1.074	45	41.89
C4204 Bot B2 10x vWF	1.080	33	30.55
C4204 Bot T2 10x vWF	1.016	21	20.68
C4207 Bot M4 10x vWF	1.004	24	23.91
C4207 Bot M5 10x vWF	1.001	20	19.99
C4208 Bot M1 10x vWF	1.010	38	37.64

VIII: Desmin Stained Sections: Desmin Positive Area

A. ECM-ONLY 14 Day Recovery

Slide	% Area Desmin Positive
M1406 TOP M2 01	5.2
M1406 TOP B2 01	10.0
M1407 TOP T6 01	3.3
M1407 TOP B3 01	6.5
M1408 TOP M2 01	3.1
M1408 TOP T6 01	7.1
M1409 TOP M3 01	8.3
M1409 TOP T6 01	9.3
M1410 TOP T5 02	23.9
M1410 TOP M2 02	23.0
M1410 TOP B3 01	10.0
M1410 TOP B3 02	3.0
M1411 TOP T6 01	4.7
M1411 TOP B4 01	10.0
M1406 MID T4 01	2.2
M1406 MID B5 01	1.2
M1406 MID B5 02	3.4
M1407 MID T3 01	4.2
M1407 MID M2 01	1.2
M1408 MID B4 01	0.4
M1409 MID T6 01	1.0
M1409 MID M2 01	1.0
M1409 MID B2 01	1.6
M1410 MID M4 01	3.7
M1410 MID B6 01	4.3
M1411 MID T3 01	6.3
M1411 MID M4 01	5.5
M1406 BOT B1 02	18.0
M1406 BOT T5 01	7.9
M1407 BOT T3 01	2.6
M1407 BOT M2 01	5.3
M1408 BOT B4 01	6.7
M1408 BOT B4 02	1.4
M1409 BOT B3 02	15.5
M1409 BOT M3 02	5.4
M1409 BOT T5 02	14.0
M1410 BOT M4 01	12.8
M1410 BOT B6 01	6.8
M1411 BOT T3 01	7.5

B. ECM-ONLY 28 Day Recovery

Slide	% Area Desmin Positive
M2811 TOP T5 01	7.8
M2811 TOP M2 01	11.0
M2812 TOP M1 01	20.9
M2812 TOP M1 02	15.9
M2812 TOP M1 03	12.3
M2813 TOP T2 01	10.4
M2814 TOP B2 02	22.2
M2814 TOP B3 01	12.9
M2814 TOP M1 01	6.7
M2814 TOP T6 01	6.4
M2815 TOP B2 01	8.0
M2815 TOP B2 01	8.4
M2815 TOP M4 01	7.0
M2815 TOP M4 02	9.3
M2815 TOP T5 01	5.3
M2816 TOP T6 01	9.8
M2816 TOP M2 01	11.9
M2811 MID T3 01	3.8
M2811 MID T3 02	1.2
M2813 MID T3 01	2.3
M2813 MID M3 01	6.3
M2813 MID B3 01	5.4
M2814 MID T1 01	0.7
M2814 MID B6 01	1.6
M2815 MID M2 01	1.9
M2815 MID B5 01	4.4
M2816 MID T4 01	1.1
M2816 MID B4 01	2.1
M2811 BOT M5 01	7.8
M2811 BOT M5 02	7.1
M2811 BOT T6 01	15.4
M2811 BOT T6 01	24.7
M2812 BOT B3 02	15.4
M2812 BOT M3 02	15.8
M2812 BOT M3 03	7.5
M2812 BOT T5 01	6.6
M2812 BOT T5 02	11.4
M2813 BOT B3 01	11.0
M2813 BOT T6 01	9.5
M2814 BOT B3 01	20.2
M2814 BOT B3 02	14.9
M2814 BOT M3 01	7.8
M2814 BOT M3 02	8.3
M2814 BOT T5 01	6.1
M2815 BOT M2 01	9.4
M2815 BOT T6 01	10.3
M2816 BOT T6 01	3.6
M2816 BOT M2 01	6.4

C. ECM-ONLY 42 Day Recovery

Slide	% Area Desmin Positive
M4201 TOP B3 01	23.2
M4201 TOP B6 03	10.8
M4201 TOP M5 01	6.5
M4201 TOP M5 02	17.9
M4201 TOP T6 02	21.1
M4202 TOP T6 01	11.1
M4203 TOP T3 01	6.8
M4203 TOP M2 01	7.7
M4203 TOP B3 01	7.1
M4204 TOP M2 01	8.8
M4204 TOP T6 01	10.9
M4205 TOP T6 01	12.4
M4205 TOP M2 01	16.6
M4205 TOP B5 01	18.1
M4206 TOP T5 01	13.5
M4206 TOP T5 02	11.7
M4207 TOP T2 01	7.7
M4207 TOP M2 01	7.6
M4208 TOP M4 01	9.6
M4208 TOP B3 01	7.4
M4201 MID T6 01	3.8
M4201 MID B5 01	5.5
M4203 MID T6 01	1.3
M4203 MID M3 01	3.5
M4204 MID B4 01	6.1
M4206 MID T6 01	6.2
M4206 MID M2 01	8.1
M4206 MID B3 01	7.5
M4207 MID B2 01	0.9
M4208 MID M5 01	5.7
M4208 MID B6 01	2.5
M4201 BOT B3 01	10.5
M4201 BOT M2 01	18.6
M4201 BOT M2 02	9.1
M4201 BOT T6 01	9.4
M4202 BOT B2 01	13.3
M4202 BOT M2 01	6.4
M4203 BOT M3 01	4.2
M4203 BOT T5 01	6.3
M4204 BOT B3 01	8.5
M4205 BOT M2 01	7.5
M4205 BOT B3 01	9.6
M4206 BOT M3 01	10.1
M4206 BOT B2 01	11.0
M4207 BOT B3 01	18.4
M4207 BOT M2 03	8.8
M4208 BOT B2 01	2.4
M4208 BOT B2 03	7.9

D. ECM-CELL 14 Day Recovery

Slide	% Area Desmin Positive
C1401 TOP M2 01	7.5
C1401 TOP B3 01	9.3
C1402 TOP T6 01	2.4
C1402 TOP M2 01	5.0
C1403 TOP M1 01	6.2
C1403 TOP B6 01	5.5
C1404 TOP T6 01	19.9
C1404 TOP T6 02	5.1
C1404 TOP M2 01	8.6
C1404 TOP B2 01	10.0
C1405 TOP T1 01	4.0
C1405 TOP M2 01	5.4
C1406 TOP T5 01	3.5
C1406 TOP M2 01	5.5
C1406 TOP B1 01	9.4
C1401 MID M1 01	2.3
C1402 MID T3 01	1.1
C1402 MID B2 01	5.5
C1403 MID M1 01	2.1
C1404 MID T2 01	8.8
C1404 MID M5 01	8.1
C1405 MID T3 01	3.4
C1405 MID B1 01	2.3
C1406 MID T5 01	10.2
C1406 MID B1 01	4.7
C1406 MID B1 02	5.5
C1401 BOT M2 01	18.0
C1402 BOT B1 02	11.8
C1402 BOT M1 01	6.6
C1402 BOT T3 01	5.5
C1403 BOT M1 01	7.4
C1404 BOT M1 01	7.5
C1404 BOT B2 01	19.5
C1404 BOT B2 02	6.3
C1405 BOT M5 01	9.3
C1405 BOT B3 01	5.2
C1406 BOT T2 01	4.5
C1406 BOT B4 01	2.4

E. ECM-CELL 28 Day Recovery

Slide	% Area Desmin Positive
C2801 TOP M3 01	9.2
C2801 TOP M3 02	15.3
C2801 TOP M3 03	20.5
C2802 TOP T6 01	13.0
C2802 TOP M5 01	12.1
C2803 TOP B4 01	16.6
C2803 TOP M2 01	11.4
C2803 TOP M3 01	8.1
C2803 TOP T6 01	8.6
C2804 TOP T5 01	10.5
C2804 TOP M5 01	16.3
C2804 TOP M5 02	8.5
C2806 TOP B3 01	4.5
C2806 TOP M1 01	16.1
C2806 TOP M1 02	14.5
C2806 TOP M1 03	17.0
C2806 TOP T3 03	19.6
C2801 MID T6 01	7.8
C2801 MID T6 02	2.8
C2801 MID M2 01	6.1
C2801 MID B3 01	3.8
C2802 MID T1 01	2.4
C2802 MID M2 01	6.9
C2803 MID M1 01	6.2
C2803 MID B1 01	13.3
C2805 MID T4 01	3.5
C2805 MID M3 01	11.9
C2805 MID M3 02	1.5
C2806 MID T2 01	6.6
C2801 BOT B3 01	0.6
C2801 BOT M3 02	2.3
C2801 BOT T6 03	11.9
C2801 BOT T6 01	1.7
C2802 BOT T1 01	10.7
C2802 BOT M6 01	12.2
C2803 BOT T4 01	8.6
C2803 BOT M6 01	13.0
C2803 BOT B4 01	18.6
C2804 BOT T3 01	4.0
C2804 BOT M5 01	3.7
C2804 BOT M5 02	11.9
C2805 BOT T1 01	10.6
C2806 BOT M1 01	10.6
C2806 BOT B4 01	12.4

F. ECM-CELL 42 Day Recovery

Slide	% Area Desmin Positive
C4201 TOP B2 01	20.9
C4201 TOP M3 01	9.7
C4201 TOP M3 02	12.2
C4201 TOP T6 01	20.1
C4201 TOP T6 02	20.3
C4202 TOP B1 02	16.0
C4202 TOP B2 03	11.3
C4202 TOP M2 01	28.4
C4202 TOP M2 02	18.1
C4202 TOP M2 03	49.9
C4202 TOP T6 01	40.2
C4202 TOP T6 02	8.9
C4203 TOP M1 01	10.7
C4203 TOP T6 01	6.3
C4203 TOP T6 02	21.5
C4204 TOP B3 01	20.5
C4204 TOP B3 02	24.6
C4207 TOP M2 01	4.4
C4207 TOP T6 02	10.1
C4207 TOP M2 01	10.3
C4207 TOP T6 03	17.5
C4208 TOP M3 01	17.0
C4201 MID T6 01	11.6
C4201 MID M2 01	8.4
C4201 MID B3 02	7.2
C4202 MID T6 01	8.6
C4202 MID T6 02	11.7
C4202 MID B6 01	10.6
C4203 MID M3 01	6.9
C4203 MID B4 01	11.6
C4204 MID M2 01	3.4
C4204 MID M4 01	6.1
C4204 MID M4 02	4.4
C4207 MID T1 01	7.7
C4207 MID M2 01	5.2
C4208 MID B4 01	8.6
C4201 Bot T6 01	17.2
C4201 Bot B5 01	14.9
C4202 Bot T6 01	13.5
C4202 Bot M4 02	10.7
C4203 BOT T7 01	9.2
C4204 BOT T6 01	11.4
C4204 BOT M4 01	14.2
C4207 BOT B2 01	4.9
C4207 BOT M2 01	4.8
C4208 BOT M2 01	0.6
C4208 BOT M2 02	6.5
C4208 TOP B3 01	13.0

IX. Desmin Stained Sections: Desmin Positive Fibers

A. ECM-ONLY 28 Day Recovery

Slide	Area (mm^2)	Desmin-Positive Myofibers	Fibers/mm^2
M2811 TOP M2 01	0.0680	12	177
M2811 TOP T5 01	0.0850	9	106
M2814 Top B3 01	0.0658	18	273
M2814 Top T6 01	0.0672	14	208
M2814 TOP B3 01	0.1448	41	283
M2815 TOP B2 01	0.1343	30	223
M2816 TOP T6 01	0.0680	12	176
M2816 TOP M2 01	0.1001	19	190
M2811 MID T3 01	0.2701	5	19
M2811 MID T3 02	0.1698	4	24
M2813 MID M3 01	0.1419	3	21
M2813 MID B3 01	0.1931	5	26
M2814 MID B6 01	0.2872	4	14
M2816 MID T4 01	0.1969	3	15
M2816 MID B4 01	0.3379	7	21
M2811 BOT M5 01	0.1624	25	154
M2811 Bot M5 01	0.1048	20	191
M2811 BOT T6 02	0.1622	21	129
M2811 Bot T6 01	0.1064	8	75
M2812 BOT B3 02	0.1334	23	172
M2812 Bot B3 02	0.0775	14	181
M2812 BOT M3 03	0.1870	16	86
M2812 Bot M3 02	0.1102	20	181
M2812 Bot T5 02	0.0999	9	90
M2812 BOT T5 02	0.1874	13	69
M2813 BOT T6 01	0.1942	47	242
M2814 BOT B3 01	0.1283	35	273
M2814 BOT M3 01	0.1698	17	100
M2815 BOT M2 02	0.1692	30	177
M2815 BOT T6 02	0.2678	10	37

B. ECM-ONLY 42 Day Recovery

Slide	Area (mm^2)	Desmin-Positive Myofibers	Fibers/mm^2
M4201 Top B3 02	0.0643	22	342
M4201 Top T6 02	0.0537	9	168
M4201 TOP T6 02	0.1779	27	152
M4204 TOP M2 01	0.1460	22	151
M4204 Top T6 01	0.1062	23	217
M4204 TOP T6 01	0.1666	46	276
M4205 Top T6 01	0.1108	28	253
M4205 Top M5 01	0.0588	22	374
M4203 MID T6 01	0.1697	5	29
M4203 MID M3 01	0.2689	8	30
M4206 MID M2 01	0.1585	13	82
M4206 MID B3 01	0.1503	10	67
M4208 MID M5 01	0.3366	13	39
M4208 MID B6 01	0.2165	7	32
M4201 BOT B3 01	0.1322	39	295
M4201 BOT M2 01	0.1635	43	263
M4203 BOT M3 01	0.1449	39	269
M4204 Bot B3 02	0.0467	14	300
M4204 BOT B3 01	0.1622	10	62
M4204 BOT B3 02	0.1426	32	224
M4204 BOT M2 01	0.1369	29	212
M4205 BOT B2 01	0.1411	25	177
M4205 Bot B2 01	0.1016	20	197
M4205 BOT B3 04	0.1676	31	185
M4205 BOT M2 01	0.1706	46	270
M4205 BOT T6 01	0.1928	22	114
M4207 BOT B3 01	0.1176	34	289
M4207 BOT M2 03	0.0963	15	156
M4207 Bot M2 03	0.1297	15	116
M4208 BOT B2 01	0.1571	35	223
M4208 BOT B2 03	0.1739	23	132
M4208 BOT M2 01	0.1823	37	203
M4208 BOT T6 01	0.1230	26	211

C. ECM-CELL 28 Day Recovery

Slide	Area (mm^2)	Desmin-Positive Myofibers	Fibers/mm^2
C2801 TOP M3 03	0.0815	37	454
C2801 Top M3 02	0.0895	5	56
C2803 TOP T6 01	0.0840	34	405
C2803 Top B4 01	0.0543	12	221
C2803 Top M5 03	2.8141	167	59
C2803 Top T6 01	0.0745	12	161
C2806 TOP T3 03	0.1239	32	258
C2806 Top B3 01	0.0502	13	259
C2806 Top T3 03	0.1531	24	157
C2801 MID T6 02	0.1764	9	51
C2801 MID M2 01	0.2692	5	19
C2801 MID B3 01	0.3250	11	34
C2802 MID T1 01	0.1524	5	33
C2802 MID M2 01	0.1706	8	47
C2805 MID T4 01	0.2365	6	25
C2805 MID M3 01	0.2924	12	41
C2805 MID M3 02	0.3384	8	24
C2801 Bot B3 01	0.3800	20	53
C2801 Bot T6 01	0.0837	9	108
C2803 BOT M6 01	0.0592	12	203
C2803 BOT B4 01	0.1586	31	195
C2804 BOT M5 01	0.0998	11	110
C2804 BOT M5 02	0.0580	13	224
C2804 BOT T3 01	0.1589	21	132

D. ECM-CELL 42 Day Recovery

Slide	Area (mm^2)	Desmin-Positive Myofibers	Fibers/mm^2
C4201 TOP B2 01	0.1240	45	363
C4201 Top B2 01	0.0575	18	313
C4201 TOP M3 01	0.1343	57	424
C4201 Top M3 01	0.0662	16	242
C4201 TOP T6 01	0.1371	54	394
C4201 Top T6 01	0.1055	17	161
C4202 TOP B1 01	0.1757	33	188
C4202 TOP B1 02	0.1359	17	125
C4202 TOP B1 03?	0.1665	59	354
C4202 Top B2 03	0.0859	26	303
C4202 TOP M1 01	0.1510	22	146
C4202 TOP M1 03	0.1811	15	83
C4203 TOP M1 01	0.0890	34	382
C4204 TOP B3 01	0.1961	36	184
C4204 TOP B3 02	0.1614	32	198
C4207 TOP M2 02	0.1431	67	468
C4207 Top M2 02	0.0996	32	321
C4207 TOP T6 02	0.2016	11	55
C4207 TOP T6 03	0.1860	24	129
C4202 MID T6 01	0.2189	21	96
C4202 MID T6 02	0.1850	13	70
C4202 MID B6 01	0.3367	17	50
C4204 MID M2 01	0.1555	9	58
C4204 MID M4 01	0.3751	13	35
C4204 MID M4 02	0.1702	8	47
C4207 MID T1 01	0.2585	20	77
C4207 MID M2 01	0.3737	15	40
C4201 BOT T6 01	0.1071	39	364
C4201 BOT B5 01	0.1208	49	406
C4202 BOT T6 01	0.1256	46	366
C4207 Bot B2 01	0.0721	19	263
C4207 BOT M2 01	0.1882	26	138
C4207 BOT M2 02	0.1967	26	132
C4207 Bot M2 02	0.0980	24	245
C4208 BOT M2 01	0.1707	38	223
C4208 BOT M2 02	0.1824	38	208

X. Myogenin Stained Sections: Myogenin Positive Nuclei

A. ECM-ONLY 28 Day Recovery

Slide	Area (mm^2)	Myogenin Positive Nuclei	Density (#/mm^2)
M2812 Top M6 02	0.1151	3	26
M2812 Top T4 02	0.1141	2	18
M2814 Top B4 03	0.1105	2	18
M2814 Top M6 04	0.1076	3	28
M2815 Top B4 02	0.1014	2	20
M2815 Top M6 02	0.1167	1	9
M2815 Top T2 02	0.0857	3	35
M2811 Mid T5 01	0.1300	0	0
M2811 Mid M2 01	0.1165	1	9
M2812 Mid T6 02	0.1521	1	7
M2812 Mid B1 01	0.1490	2	13
M2814 Mid M6 01	0.1259	0	0
M2814 Mid B3 01	0.1708	2	12
M2815 Mid B2 01	0.1401	1	7
M2811 Bot B4 03	0.1096	3	27
M2811 Bot M6 01	0.1308	2	15
M2812 Bot B4 01	0.1428	2	14
M2812 Bot M6 04	0.1596	3	19
M2813 Bot B2 03	0.1178	1	8
M2813 Bot M6 02	0.1570	2	13
M2813 Bot T3 02	0.1329	2	15
M2814 Bot B1 02	0.2023	3	15
M2815 Bot M6 02	0.1023	2	20
M2815 Bot T2 01	0.0924	2	22

B. ECM-ONLY 42 Day Recovery

Slide	Area (mm^2)	Myogenin Positive Nuclei	Density (#/mm^2)
M4201 Top B5 02	0.0959	4	42
M4201 Top M6 03	0.1277	6	47
M4202 Top M6 03	0.0890	2	22
M4207 Top B2 01	0.1296	2	15
M4208 Top T3 01	0.1063	4	38
M4201 Mid M2 01	0.1356	1	7
M4201 Mid M2 02	0.1163	3	26
M4203 Mid M4 01	0.1289	0	0
M4203 Mid B3 01	0.1709	1	6
M4206 Mid T4 01	0.1360	2	15
M4206 Mid M6 01	0.1335	1	7
M4206 Mid B4 01	0.1449	0	0
M4207 Mid T2 01	0.1352	1	7
M4207 Mid B4 01	0.1604	2	12
M4201 Bot M6 01	0.1547	5	32
M4203 Bot B3 02	0.1465	4	27
M4203 Bot M6 03	0.1190	3	25
M4203 Bot T3 02	0.1490	4	27
M4204 Bot B5 02	0.1250	4	32
M4204 Bot M5 02	0.1889	3	16
M4206 Bot B3 02	0.1551	4	26
M4207 Bot M6 02	0.1783	2	11
M4207 Bot T4 03	0.1414	1	7
M4208 Bot M6 03	0.1853	2	11
M4208 Bot T4 03	0.1683	4	24
M4209 Bot B4 02	0.0799	4	50
M4209 Bot M6 02	0.2010	3	15

C. ECM-CELL 28 Day Recovery

Slide	Area (mm^2)	Myogenin Positive Nuclei	Density (#/mm^2)
C2801 Top M6 03	0.1408	12	85
C2803 Top M6 03	0.1515	9	59
C2806 Top B3 02	0.1506	10	66
C2806 Top M3 03	0.1492	7	47
C2806 Top T5 02	0.1666	14	84
C2802 Mid T2 01	0.1831	1	5
C2802 Mid B3 01	0.1362	3	22
C2803 Mid T6 02	0.1523	2	13
C2805 Mid B4 01	0.1307	0	0
C2805 Mid B2 01	0.1406	2	14
C2806 Mid B1 02	0.1156	1	9
C2801 Bot B4 01	0.1207	7	58
C2801 Bot M6 02	0.1871	12	64
C2801 Bot T2 01	0.0951	7	74
C2802 Bot B3 02	0.1589	6	38
C2802 Bot T4 02	0.1537	9	59
C2804 Bot T6 01	0.1155	6	52
C2804 Bot M3 01	0.1487	9	61

D. ECM-CELL 42 Day Recovery

Slide	Area (mm^2)	Myogenin Positive Nuclei	Density (#/mm^2)
C4201 Top M5 01	0.1107	7	63
C4201 Top T4 01	0.1251	5	40
C4202 Top M4 02	0.1529	11	72
C4202 Top M4 03	0.1217	12	99
C4204 Top B3 03	0.1173	15	128
C4204 Top M5 01	0.1823	19	104
C4204 Top T3 03	0.1949	12	62
C4201 Mid T5 01	0.1400	2	14
C4201 Mid M4 01	0.1496	1	7
C4203 Mid T1 01	0.1287	2	16
C4203 Mid M2 01	0.1722	4	23
C4208 Mid B1 01	0.1660	3	18
C4208 Mid M2 01	0.1469	1	7
C4201 Bot B4 02	0.1345	9	67
C4201 Bot M6 02	0.1122	7	62
C4201 Bot T3 02	0.1398	8	57
C4202 Bot B5 02	0.1278	6	47
C4202 Bot M5 01	0.1284	7	55
C4203 Bot B3 02	0.1356	9	66
C4203 Bot T3 02	0.1727	14	81
C4204 Bot T2 03	0.1376	8	58
C4208 Bot T4 02	0.1622	8	49

Works Cited

1. Owens, B.D., et al., *Characterization of extremity wounds in Operation Iraqi Freedom and Operation Enduring Freedom.* J Orthop Trauma, 2007. 21(4): p. 254-7.
2. Mabry, R.L., et al., *United States Army Rangers in Somalia: an analysis of combat casualties on an urban battlefield.* J Trauma, 2000. 49(3): p. 515-28; discussion 528-9.
3. Zouris, J.M., et al., *Wounding patterns for U.S. Marines and sailors during Operation Iraqi Freedom, major combat phase.* Mil Med, 2006. 171(3): p. 246-52.
4. Fan, C., et al., *Functional reconstruction of traumatic loss of flexors in forearm with gastrocnemius myocutaneous flap transfer.* Microsurgery, 2008. 28(1): p. 71-5.
5. Vekris, M.D., et al., *Restoration of elbow function in severe brachial plexus paralysis via muscle transfers.* Injury, 2008. 39 Suppl 3: p. S15-22.
6. Beier, J.P., et al., *Y chromosome detection of three-dimensional tissue-engineered skeletal muscle constructs in a syngeneic rat animal model.* Cell Transplant, 2004. 13(1): p. 45-53.
7. Gamba, P.G., et al., *Experimental abdominal wall defect repaired with acellular matrix.* Pediatr Surg Int, 2002. 18(5-6): p. 327-31.
8. Kin, S., et al., *Regeneration of skeletal muscle using in situ tissue engineering on an acellular collagen sponge scaffold in a rabbit model.* Asaio J, 2007. 53(4): p. 506-13.
9. Vindigni, V., et al., *Reconstruction of ablated rat rectus abdominis by muscle regeneration.* Plast Reconstr Surg, 2004. 114(6): p. 1509-15; discussion 1516-8.
10. Carlson, B.M. and E. Gutmann, *Development of contractile properties of minced muscle regenerates in the rat.* Exp Neurol, 1972. 36(2): p. 239-49.
11. Hurme, T., et al., *Healing of skeletal muscle injury: an ultrastructural and immunohistochemical study.* Med Sci Sports Exerc, 1991. 23(7): p. 801-10.
12. Orimo, S., et al., *Analysis of inflammatory cells and complement C3 in bupivacaine-induced myonecrosis.* Muscle Nerve, 1991. 14(6): p. 515-20.
13. Mauro, A., *Satellite cell of skeletal muscle fibers.* J Biophys Biochem Cytol, 1961. 9: p. 493-5.
14. Best, T.M., et al., *Analysis of changes in mRNA levels of myoblast- and fibroblast-derived gene products in healing skeletal muscle using quantitative reverse transcription-polymerase chain reaction.* J Orthop Res, 2001. 19(4): p. 565-72.
15. Hurme, T. and H. Kalimo, *Activation of myogenic precursor cells after muscle injury.* Med Sci Sports Exerc, 1992. 24(2): p. 197-205.
16. Chazaud, B., et al., *Satellite cells attract monocytes and use macrophages as a support to escape apoptosis and enhance muscle growth.* J Cell Biol, 2003. 163(5): p. 1133-43.

17. Jarvinen, T.A., et al., *Muscle injuries: biology and treatment.* Am J Sports Med, 2005. 33(5): p. 745-64.
18. Bischoff, R., *Chemotaxis of skeletal muscle satellite cells.* Dev Dyn, 1997. 208(4): p. 505-15.
19. Charge, S.B. and M.A. Rudnicki, *Cellular and molecular regulation of muscle regeneration.* Physiol Rev, 2004. 84(1): p. 209-38.
20. LaBarge, M.A. and H.M. Blau, *Biological progression from adult bone marrow to mononucleate muscle stem cell to multinucleate muscle fiber in response to injury.* Cell, 2002. 111(4): p. 589-601.
21. Qu-Petersen, Z., et al., *Identification of a novel population of muscle stem cells in mice: potential for muscle regeneration.* J Cell Biol, 2002. 157(5): p. 851-64.
22. Menetrey, J., et al., *Growth factors improve muscle healing in vivo.* J Bone Joint Surg Br, 2000. 82(1): p. 131-7.
23. Fukada, S., et al., *Muscle regeneration by reconstitution with bone marrow or fetal liver cells from green fluorescent protein-gene transgenic mice.* J Cell Sci, 2002. 115(Pt 6): p. 1285-93.
24. Lehto, M., V.C. Duance, and D. Restall, *Collagen and fibronectin in a healing skeletal muscle injury. An immunohistological study of the effects of physical activity on the repair of injured gastrocnemius muscle in the rat.* J Bone Joint Surg Br, 1985. 67(5): p. 820-8.
25. Li, Y., et al., *Transforming growth factor-beta1 induces the differentiation of myogenic cells into fibrotic cells in injured skeletal muscle: a key event in muscle fibrogenesis.* Am J Pathol, 2004. 164(3): p. 1007-19.
26. Jarvinen, M., *Healing of a crush injury in rat striated muscle. 4. Effect of early mobilization and immobilization on the tensile properties of gastrocnemius muscle.* Acta Chir Scand, 1976. 142(1): p. 47-56.
27. Jarvinen, M., *Healing of a crush injury in rat striated muscle. 2. a histological study of the effect of early mobilization and immobilization on the repair processes.* Acta Pathol Microbiol Scand [A], 1975. 83(3): p. 269-82.
28. Kaariainen, M., et al., *Integrin and dystrophin associated adhesion protein complexes during regeneration of shearing-type muscle injury.* Neuromuscul Disord, 2000. 10(2): p. 121-32.
29. Vaittinen, S., et al., *Transected myofibres may remain permanently divided in two parts.* Neuromuscul Disord, 2002. 12(6): p. 584-7.
30. Jarvinen, M., *Healing of a crush injury in rat striated muscle. 3. A micro-angiographical study of the effect of early mobilization and immobilization on capillary ingrowth.* Acta Pathol Microbiol Scand [A], 1976. 84(1): p. 85-94.
31. Borisov, A.B. and B.M. Carlson, *Cell death in denervated skeletal muscle is distinct from classical apoptosis.* Anat Rec, 2000. 258(3): p. 305-18.
32. Rantanen, J., et al., *Denervated segments of injured skeletal muscle fibers are reinnervated by newly formed neuromuscular junctions.* J Neuropathol Exp Neurol, 1995. 54(2): p. 188-94.
33. Thompson, W., *Reinnervation of partially denervated rat soleus muscle.* Acta Physiol Scand, 1978. 103(1): p. 81-91.

34. Kaariainen, M., et al., *Correlation between biomechanical and structural changes during the regeneration of skeletal muscle after laceration injury.* J Orthop Res, 1998. 16(2): p. 197-206.
35. Aarimaa, V., et al., *Restoration of myofiber continuity after transection injury in the rat soleus.* Neuromuscul Disord, 2004. 14(7): p. 421-8.
36. Shen, W., et al., *NS-398, a cyclooxygenase-2-specific inhibitor, delays skeletal muscle healing by decreasing regeneration and promoting fibrosis.* Am J Pathol, 2005. 167(4): p. 1105-17.
37. Kragh, J.F., Jr. and C.J. Basamania, *Surgical repair of acute traumatic closed transection of the biceps brachii.* J Bone Joint Surg Am, 2002. 84-A(6): p. 992-8.
38. Garrett, W.E., Jr., et al., *Recovery of skeletal muscle after laceration and repair.* J Hand Surg [Am], 1984. 9(5): p. 683-92.
39. Terada, N., et al., *Muscle repair after a transsection injury with development of a gap: an experimental study in rats.* Scand J Plast Reconstr Surg Hand Surg, 2001. 35(3): p. 233-8.
40. Almekinders, L.C., *Results of surgical repair versus splinting of experimentally transected muscle.* J Orthop Trauma, 1991. 5(2): p. 173-6.
41. Menetrey, J., et al., *Suturing versus immobilization of a muscle laceration. A morphological and functional study in a mouse model.* Am J Sports Med, 1999. 27(2): p. 222-9.
42. Foster, W., et al., *Gamma interferon as an antifibrosis agent in skeletal muscle.* J Orthop Res, 2003. 21(5): p. 798-804.
43. Fukushima, K., et al., *The use of an antifibrosis agent to improve muscle recovery after laceration.* Am J Sports Med, 2001. 29(4): p. 394-402.
44. Chan, Y.S., et al., *Antifibrotic effects of suramin in injured skeletal muscle after laceration.* J Appl Physiol, 2003. 95(2): p. 771-80.
45. Negishi, S., et al., *The effect of relaxin treatment on skeletal muscle injuries.* Am J Sports Med, 2005. 33(12): p. 1816-24.
46. Kasemkijwattana, C., et al., *Use of growth factors to improve muscle healing after strain injury.* Clin Orthop Relat Res, 2000(370): p. 272-85.
47. Sato, K., et al., *Improvement of muscle healing through enhancement of muscle regeneration and prevention of fibrosis.* Muscle Nerve, 2003. 28(3): p. 365-72.
48. Engert, J.C., E.B. Berglund, and N. Rosenthal, *Proliferation precedes differentiation in IGF-I-stimulated myogenesis.* J Cell Biol, 1996. 135(2): p. 431-40.
49. Vandenburgh, H.H., et al., *Insulin and IGF-I induce pronounced hypertrophy of skeletal myofibers in tissue culture.* Am J Physiol, 1991. 260(3 Pt 1): p. C475-84.
50. Jenkins, S.D., et al., *A comparison of prosthetic materials used to repair abdominal wall defects.* Surgery, 1983. 94(2): p. 392-8.
51. Osses, N. and E. Brandan, *ECM is required for skeletal muscle differentiation independently of muscle regulatory factor expression.* Am J Physiol Cell Physiol, 2002. 282(2): p. C383-94.
52. Stern, M.M., et al., *The influence of extracellular matrix derived from skeletal muscle tissue on the proliferation and differentiation of myogenic progenitor cells ex vivo.* Biomaterials, 2009.

53. Cronin, E.M., et al., *Protein-coated poly(L-lactic acid) fibers provide a substrate for differentiation of human skeletal muscle cells.* J Biomed Mater Res A, 2004. 69(3): p. 373-81.
54. Reing, J.E., et al., *Degradation Products of Extracellular Matrix Affect Cell Migration and Proliferation.* Tissue Eng Part A, 2008.
55. Beattie, A.J., et al., *Chemoattraction of Progenitor Cells by Remodeling Extracellular Matrix Scaffolds.* Tissue Eng Part A, 2008.
56. Sarikaya, A., et al., *Antimicrobial activity associated with extracellular matrices.* Tissue Eng, 2002. 8(1): p. 63-71.
57. Engler, A.J., et al., *Myotubes differentiate optimally on substrates with tissue-like stiffness: pathological implications for soft or stiff microenvironments.* J Cell Biol, 2004. 166(6): p. 877-87.
58. Borschel, G.H., R.G. Dennis, and W.M. Kuzon, Jr., *Contractile skeletal muscle tissue-engineered on an acellular scaffold.* Plast Reconstr Surg, 2004. 113(2): p. 595-602; discussion 603-4.
59. Thorrez, L., et al., *Growth, differentiation, transplantation and survival of human skeletal myofibers on biodegradable scaffolds.* Biomaterials, 2008. 29(1): p. 75-84.
60. Adams, J.E., et al., *Rotator cuff repair using an acellular dermal matrix graft: an in vivo study in a canine model.* Arthroscopy, 2006. 22(7): p. 700-9.
61. Zantop, T., et al., *Extracellular matrix scaffolds are repopulated by bone marrow-derived cells in a mouse model of achilles tendon reconstruction.* J Orthop Res, 2006. 24(6): p. 1299-309.
62. Robinson, K.A., et al., *Extracellular matrix scaffold for cardiac repair.* Circulation, 2005. 112(9 Suppl): p. I135-43.
63. Kochupura, P.V., et al., *Tissue-engineered myocardial patch derived from extracellular matrix provides regional mechanical function.* Circulation, 2005. 112(9 Suppl): p. I144-9.
64. Partridge, T.A., et al., *Conversion of mdx myofibres from dystrophin-negative to -positive by injection of normal myoblasts.* Nature, 1989. 337(6203): p. 176-9.
65. Huard, J., et al., *Myoblast transplantation produced dystrophin-positive muscle fibres in a 16-year-old patient with Duchenne muscular dystrophy.* Clin Sci (Lond), 1991. 81(2): p. 287-8.
66. Arcila, M.E., et al., *Mass and functional capacity of regenerating muscle is enhanced by myoblast transfer.* J Neurobiol, 1997. 33(2): p. 185-98.
67. DeRosimo, J.F., et al., *Enhancement of adult muscle regeneration by primary myoblast transplantation.* Cell Transplant, 2000. 9(3): p. 369-77.
68. Torrente, Y., et al., *Intraarterial injection of muscle-derived CD34(+)Sca-1(+) stem cells restores dystrophin in mdx mice.* J Cell Biol, 2001. 152(2): p. 335-48.
69. Peault, B., et al., *Stem and progenitor cells in skeletal muscle development, maintenance, and therapy.* Mol Ther, 2007. 15(5): p. 867-77.
70. Lazerges, C., et al., *Transplantation of primary satellite cells improves properties of reinnervated skeletal muscles.* Muscle Nerve, 2004. 29(2): p. 218-26.

71. Conconi, M.T., et al., *Homologous muscle acellular matrix seeded with autologous myoblasts as a tissue-engineering approach to abdominal wall-defect repair.* Biomaterials, 2005. 26(15): p. 2567-74.
72. De Coppi, P., et al., *Myoblast-acellular skeletal muscle matrix constructs guarantee a long-term repair of experimental full-thickness abdominal wall defects.* Tissue Eng, 2006. 12(7): p. 1929-36.
73. Marzaro, M., et al., *Autologous satellite cell seeding improves in vivo biocompatibility of homologous muscle acellular matrix implants.* Int J Mol Med, 2002. 10(2): p. 177-82.
74. Ke, Q., et al., *Embryonic stem cells cultured in biodegradable scaffold repair infarcted myocardium in mice.* Sheng Li Xue Bao, 2005. 57(6): p. 673-681.
75. Palermo, A.T., et al., *Bone marrow contribution to skeletal muscle: a physiological response to stress.* Dev Biol, 2005. 279(2): p. 336-44.
76. Devine, S.M., *Mesenchymal stem cells: will they have a role in the clinic?* J Cell Biochem Suppl, 2002. 38: p. 73-9.
77. Friedenstein, A.J., J.F. Gorskaja, and N.N. Kulagina, *Fibroblast precursors in normal and irradiated mouse hematopoietic organs.* Exp Hematol, 1976. 4(5): p. 267-74.
78. Pittenger, M.F., et al., *Multilineage potential of adult human mesenchymal stem cells.* Science, 1999. 284(5411): p. 143-7.
79. Pereira, R.F., et al., *Cultured adherent cells from marrow can serve as long-lasting precursor cells for bone, cartilage, and lung in irradiated mice.* Proc Natl Acad Sci U S A, 1995. 92(11): p. 4857-61.
80. Wakitani, S., T. Saito, and A.I. Caplan, *Myogenic cells derived from rat bone marrow mesenchymal stem cells exposed to 5-azacytidine.* Muscle Nerve, 1995. 18(12): p. 1417-26.
81. Petersen, B.E., et al., *Bone marrow as a potential source of hepatic oval cells.* Science, 1999. 284(5417): p. 1168-70.
82. Woodbury, D., et al., *Adult rat and human bone marrow stromal cells differentiate into neurons.* J Neurosci Res, 2000. 61(4): p. 364-70.
83. Jiang, Y., et al., *Pluripotency of mesenchymal stem cells derived from adult marrow.* Nature, 2002. 418(6893): p. 41-9.
84. Ferrari, G., et al., *Muscle regeneration by bone marrow-derived myogenic progenitors.* Science, 1998. 279(5356): p. 1528-30.
85. Dezawa, M., et al., *Bone marrow stromal cells generate muscle cells and repair muscle degeneration.* Science, 2005. 309(5732): p. 314-7.
86. Muguruma, Y., et al., *In vivo and in vitro differentiation of myocytes from human bone marrow-derived multipotent progenitor cells.* Exp Hematol, 2003. 31(12): p. 1323-30.
87. Matziolis, G., et al., *Autologous bone marrow-derived cells enhance muscle strength following skeletal muscle crush injury in rats.* Tissue Eng, 2006. 12(2): p. 361-7.
88. Natsu, K., et al., *Allogeneic bone marrow-derived mesenchymal stromal cells promote the regeneration of injured skeletal muscle without differentiation into myofibers.* Tissue Eng, 2004. 10(7-8): p. 1093-112.

89. Wei, H.J., et al., *Porous acellular bovine pericardia seeded with mesenchymal stem cells as a patch to repair a myocardial defect in a syngeneic rat model.* Biomaterials, 2006. 27(31): p. 5409-19.
90. Bartlett, C.S., et al., *Ballistics and gunshot wounds: effects on musculoskeletal tissues.* J Am Acad Orthop Surg, 2000. 8(1): p. 21-36.
91. Meddings, R.N., et al., *A new bioprosthesis in large abdominal wall defects.* J Pediatr Surg, 1993. 28(5): p. 660-3.
92. Engler, A.J., et al., *Matrix elasticity directs stem cell lineage specification.* Cell, 2006. 126(4): p. 677-89.
93. Valentin, J.E., et al., *Macrophage Participation in the Degradation and Remodeling of ECM Scaffolds.* Tissue Eng Part A, 2009.
94. Badylak, S.F., *The extracellular matrix as a biologic scaffold material.* Biomaterials, 2007. 28(25): p. 3587-93.
95. Arand, M., T. Friedberg, and F. Oesch, *Colorimetric quantitation of trace amounts of sodium lauryl sulfate in the presence of nucleic acids and proteins.* Anal Biochem, 1992. 207(1): p. 73-5.
96. Kragh, J.F., Jr., et al., *Epimysium and perimysium in suturing in skeletal muscle lacerations.* J Trauma, 2005. 59(1): p. 209-12.
97. Crow, B.D., et al., *Evaluation of a novel biomaterial for intrasubstance muscle laceration repair.* J Orthop Res, 2007. 25(3): p. 396-403.
98. Hwang, J.H., et al., *Therapeutic effect of passive mobilization exercise on improvement of muscle regeneration and prevention of fibrosis after laceration injury of rat.* Arch Phys Med Rehabil, 2006. 87(1): p. 20-6.
99. Hill, M., A. Wernig, and G. Goldspink, *Muscle satellite (stem) cell activation during local tissue injury and repair.* J Anat, 2003. 203(1): p. 89-99.
100. Bach, A.D., et al., *Skeletal muscle tissue engineering.* J Cell Mol Med, 2004. 8(4): p. 413-22.
101. Fansa, H., et al., *Acellular muscle with Schwann-cell implantation: an alternative biologic nerve conduit.* J Reconstr Microsurg, 1999. 15(7): p. 531-7.
102. Ott, H.C., et al., *Perfusion-decellularized matrix: using nature's platform to engineer a bioartificial heart.* Nat Med, 2008. 14(2): p. 213-21.
103. Dufrane, D., et al., *Regeneration of abdominal wall musculofascial defects by a human acellular collagen matrix.* Biomaterials, 2008. 29(14): p. 2237-48.
104. Friedenstein, A.J., et al., *Stromal cells responsible for transferring the microenvironment of the hemopoietic tissues. Cloning in vitro and retransplantation in vivo.* Transplantation, 1974. 17(4): p. 331-40.
105. Prockop, D.J., *Marrow stromal cells as stem cells for nonhematopoietic tissues.* Science, 1997. 276(5309): p. 71-4.
106. Chang, Y., et al., *Tissue regeneration observed in a basic fibroblast growth factor-loaded porous acellular bovine pericardium populated with mesenchymal stem cells.* J Thorac Cardiovasc Surg, 2007. 134(1): p. 65-73, 73 e1-4.
107. Lamb, D.W. and K.M. Chan, *Surgical reconstruction of the upper limb in traumatic tetraplegia. A review of 41 patients.* J Bone Joint Surg Br, 1983. 65(3): p. 291-8.

108. Brinchmann, J.E., *Expanding autologous multipotent mesenchymal bone marrow stromal cells.* J Neurol Sci, 2008. 265(1-2): p. 127-30.
109. Falanga, V., et al., *Autologous bone marrow-derived cultured mesenchymal stem cells delivered in a fibrin spray accelerate healing in murine and human cutaneous wounds.* Tissue Eng, 2007. 13(6): p. 1299-312.
110. Rose, R.A., et al., *Bone marrow-derived mesenchymal stromal cells express cardiac-specific markers, retain the stromal phenotype, and do not become functional cardiomyocytes in vitro.* Stem Cells, 2008. 26(11): p. 2884-92.
111. Rossignol, J., et al., *Mesenchymal stem cells induce a weak immune response in the rat striatum after allo or xenotransplantation.* J Cell Mol Med, 2009.
112. Chen, S.L., et al., *Effect on left ventricular function of intracoronary transplantation of autologous bone marrow mesenchymal stem cell in patients with acute myocardial infarction.* Am J Cardiol, 2004. 94(1): p. 92-5.
113. Dreyfus, P.A., et al., *Adult bone marrow-derived stem cells in muscle connective tissue and satellite cell niches.* Am J Pathol, 2004. 164(3): p. 773-9.
114. De Bari, C., et al., *Skeletal muscle repair by adult human mesenchymal stem cells from synovial membrane.* J Cell Biol, 2003. 160(6): p. 909-18.
115. Corti, S., et al., *A subpopulation of murine bone marrow cells fully differentiates along the myogenic pathway and participates in muscle repair in the mdx dystrophic mouse.* Exp Cell Res, 2002. 277(1): p. 74-85.
116. Goncalves, M.A., et al., *Human mesenchymal stem cells ectopically expressing full-length dystrophin can complement Duchenne muscular dystrophy myotubes by cell fusion.* Hum Mol Genet, 2006. 15(2): p. 213-21.
117. Abedi, M., et al., *Robust conversion of marrow cells to skeletal muscle with formation of marrow-derived muscle cell colonies: a multifactorial process.* Exp Hematol, 2004. 32(5): p. 426-34.
118. Winkler, T., et al., *Dose-Response Relationship of Mesenchymal Stem Cell Transplantation and Functional Regeneration after Severe Skeletal Muscle Injury in Rats.* Tissue Eng Part A, 2008.
119. Kamihata, H., et al., *Implantation of bone marrow mononuclear cells into ischemic myocardium enhances collateral perfusion and regional function via side supply of angioblasts, angiogenic ligands, and cytokines.* Circulation, 2001. 104(9): p. 1046-52.
120. Kinnaird, T., et al., *Local delivery of marrow-derived stromal cells augments collateral perfusion through paracrine mechanisms.* Circulation, 2004. 109(12): p. 1543-9.
121. Gnecchi, M., et al., *Paracrine action accounts for marked protection of ischemic heart by Akt-modified mesenchymal stem cells.* Nat Med, 2005. 11(4): p. 367-8.
122. Shabbir, A., et al., *Heart Failure Therapy Mediated by the Trophic Activities of Bone Marrow Mesenchymal Stem Cells: A Non-invasive Therapeutic Regimen.* Am J Physiol Heart Circ Physiol, 2009.
123. Lien, S.C., P.S. Cederna, and W.M. Kuzon, Jr., *Optimizing skeletal muscle reinnervation with nerve transfer.* Hand Clin, 2008. 24(4): p. 445-54, vii.
124. Dhawan, V., et al., *Neurotization improves contractile forces of tissue-engineered skeletal muscle.* Tissue Eng, 2007. 13(11): p. 2813-21.

125. Winkler, T., et al., *In vivo visualization of locally transplanted mesenchymal stem cells in the severely injured muscle in rats.* Tissue Eng Part A, 2008. 14(7): p. 1149-60.
126. Chang, E.I., et al., *Tissue engineering using autologous microcirculatory beds as vascularized bioscaffolds.* Faseb J, 2009. 23(3): p. 906-15.

Vita

Edward Kelly Merritt, Jr. was born in Charleston, West Virginia on December 28, 1979. He is the son of Kelly and Teri Merritt and has a younger brother, Brandon. He attended South Charleston High School in West Virginia. In high school, Edward successfully competed with the track, cross-country, and baseball teams and was in student government. After graduation from high school in 1998, he attended Virginia Tech in Blacksburg, Virginia. Edward was a member of the Virginia Tech crew team for four years and was president of the club for two years. He graduated Summa Cum Laude in 2002 with a Bachelor of Science degree in Nutrition and Exercise Science and a minor in Chemistry. Upon completion of his studies at Virginia Tech, Edward moved to Austin, to continue his education at the University of Texas at Austin. In 2004, working in the laboratory of Dr. Roger Farrar, Edward received his Master of Arts degree in Kinesiology with an emphasis in Exercise Physiology. For his doctoral studies, he continued in the Muscle Physiology and Plasticity laboratory. Edward has presented his research at conferences such as The Federation of American Societies for Experimental Biology and The American Physiological Society's Integrative Biology of Exercise and contributed to publications appearing in the Journal of Applied Physiology and Experimental Biology and Medicine. Edward will marry Bronwyn Owen in February, 2010.

Permanent Address: 1705B West Ave, Austin, TX 78701

This dissertation was typed by the author.